SOME ELECTRON SPIN RESONANCE

AND INFRA-RED STUDIES OF

IRRADIATED CYANIDES

K. D. J. Root

A thesis submitted for the degree of
Doctor of Philosophy in the Faculty
of Science of the University of
Leicester.

Leicester

May 1967

UMI Number: U296382

UMI®

Dissertation Publishing

UMI U296382

ProQuest®

STATEMENT

The work described in this thesis was carried out
by the author, under Professor M. C. R. Symons, in
the laboratories of the Department of Chemistry of
the University of Leicester between October 1964
and February 1967. The work has not been presented,
and is not being concurrently presented, for any
other degree.

Signed:

Keith D. J. Root.

ACKNOWLEDGEMENTS

It is a great pleasure to thank:

This thesis is dedicated to my parents and my past and present teachers - to all these people I owe a 'ginormous!'[1] debt of gratitude.

1. Pronounced gi-normous. The word is attributed to Dr D. M. Adams

"Change
         and
              decay
                   in
                      all
                         around
                               I
                                    "
                                 see

H. F. Lyte

(Always sung out of context at the Cup Final at Wembley)

ABSTRACT

This thesis reports some electron spin resonance and other spectroscopic studies of radiation damage in ionic cyanides, and in alkali halides doped with simple and complex cyanide ions.

A correlation of electron spin resonance data for F-centres has been obtained which relates the isotropic hyperfine coupling, from the first shell of cations surrounding the F-centre, to the lattice size and the atomic radius of the cations. This correlation has been used to identify the electron spin resonance spectrum of the F-centre in γ-irradiated sodium cyanide. The electron spin resonance spectrum of the V_k-centre in γ-irradiated sodium and potassium cyanide is reported.

The V_k-centre (The cyanogen negative ion $(CN)_2^-$) has also been prepared in γ-irradiated potassium chloride doped with cyanide ions. A single crystal study of this radical has been performed and the structure determined and compared with the HCN^- and H_2CN radicals which were also formed on irradiation of the doped potassium chloride. In all three radicals the unpaired electron is in the plane of the molecule and there is a considerable delocalization of the spin density.

The effect of both γ-irradiation and ultra-violet irradiation on ferrous and ruthenium hexacyanide incorporated into alkali halide lattices has been examined by electron spin resonance, infra-red and electronic spectroscopy. The new spectral bands have been

interpreted in terms of the formation of iron and ruthenium complexes in oxidation state (I). The electron spin resonance spectra indicate a novel distortion of the d^7 transition metal complex which produces a unique ligand. Possible interpretations of the electron spin resonance spectra are discussed.

Finally an infra-red study of γ-irradiated alkali halides doped with simple cyanide ions shows that the major product on irradiation is the cyanate ion. Likely mechanisms for the formation of this ion and the other species reported in this thesis are considered.

CONTENTS

CHAPTER 2. Experimental Methods

CHAPTER 3. Colour Centres in Irradiated Cyanides

Chapter 1

Electron Spin Resonance and Infra-red Spectroscopy

Introduction

To the author's knowledge no electron spin resonance studies and very little optical work on irradiated solid cyanides have been reported. Despite this the cyanide group is a very useful monitor of radiation damage. The simple cyanide ion, for example, has a characteristic infra-red stretching absorption, and if incorporated into a paramagnetic species hyperfine coupling to the magnetic nuclei ^{13}C and ^{14}N can, in principle, be observed in the electron spin resonance spectrum. The cyanide ion forms a number of stable transition metal complexes and the infra-red spectra of these are strongly dependent on the environment of the ion[1]. These complex cyanides are low-spin and thus d^5 and d^7 complexes can often yield relatively simple electron spin resonance spectra[2].

The first part of this thesis deals with the theory of the spectroscopic techniques used in this work. Further details of the theory can be obtained from the books and articles given in the bibliography at the end of the thesis. Chapter 2 deals with the experimental techniques used, with a description of the spectrometers and the radiation sources. The remaining chapters describe and discuss the radiation damage in pure ionic cyanides, alkali halides doped with the simple cyanide ion and transition metal cyanide complexes. Chapters 3, 4 and 5 are mainly concerned with the spectra and structures of the species formed on irradiation, while in the last chapter the effects of radiation in these systems is summarised.

A. Electron Spin Resonance Spectroscopy (e.s.r.)

Electron spin resonance spectra measure energy differences between different spin states in a paramagnetic system. In the simplest case the species contains one unpaired electron $(S=\frac{1}{2})$, and hence the possible magnetic spin states are $m_s = \pm \frac{1}{2}$. In the absence of a magnetic field these two m_s states are degenerate (A Kramers' Doublet[3]). A magnetic field lifts this degeneracy, and transitions between the two states can be induced by applying electromagnetic radiation of suitable energy. For most commercial spectrometers the magnetic field is about 3,000 gauss and the energy difference then requires a microwave frequency of about 9,000 Mc/s

Apart from the applied magnetic field there are a number of other factors which determine the energies of the different states, and it is these interactions which make e.s.r. such a valuable tool for examining paramagnetic species. We will now consider the effects of these interactions on the energies of the spin states. No attempt will be made to treat this fully, further details can be found in the articles tabulated in the bibliography at the end of this thesis.

I. The Spin Hamiltonian

In the e.s.r. experiment we are only interested in the energy levels associated with the lifting of the degeneracy of the Kramers' doublet, and so we need only consider the electron spin part of the state function, and the corresponding part of the Hamiltonian. This truncated Hamiltonian is known as the spin Hamiltonian (H_{spin}) and is of the form[4]:

$$H_{spin} = g_e \beta \underline{H} \cdot \underline{S} + \sum_i \left[\underline{I}(a_i + \underline{B}_i) \cdot \underline{S} + \underline{I}_i \cdot \underline{Q}_i \cdot \underline{I}_i - g_{I_i} \beta_n \underline{H} \cdot \underline{I}_i \right]$$

(1)

where g_e is the electronic 'g'-factor for a free electron.

g_{I_i} is the nuclear g-factor for nucleus i.

β and β_n the Bohr and nuclear magnetons.

$\underline{H}$ the applied field.

$\underline{S}$ the electron spin.

$\underline{I}_i$ the nuclear spin for nucleus i.

a_i the isotropic hyperfine interaction for nucleus i.

$\underline{B}_i$ the anisotropic hyperfine interaction for nucleus i.

$\underline{Q}_i$ the quadrupole tensor for nucleus i.

The last term of (1) does not affect the differences between the energy levels monitored in an e.s.r. experiment, and so can be neglected to first order. The quadrupole term will not be required either, and so the Hamiltonian reduces to:

$$H_{spin} = g_e \beta \underline{H} \cdot \underline{S} + \sum_i \underline{I}(a_i + \underline{B}_i) \cdot \underline{S}$$

(2)

This Hamiltonian can act on the spin state $| m_s, m_I \rangle$ to yield the

energy levels required. We will now consider the two terms in

(2) and examine the effect which each has on the energy transitions

observed in the spectra.

i. The Spin Hamiltonian in the Absence of Interaction with Magnetic Nuclei

a. Orbital Angular Momentum and g-values

In the absence of magnetic nuclei the Hamiltonian reduces to:

$$H_{spin} = g_e \beta \underline{H} \cdot \underline{S} \qquad (3)$$

This assumes that the orbital angular momentum has been completely

quenched, the degeneracy of the atomic orbitals being lifted by

either a crystal field or by bonding. In the case where there is

still some angular momentum two further terms have to be considered,

these are:

$$\beta \underline{H} \cdot \underline{L} + \lambda \underline{L} \cdot \underline{S}$$

where $\underline{L}$ is the angular momentum operator

λ is the spin orbit interaction parameter

In actual practice the spin orbit interaction $\lambda \underline{L} \cdot \underline{S}$ induces some

residual angular momentum, even when the degeneracy of the orbitals

has been completely lifted. This orbital angular momentum can be

considered to affect the energy levels in one of two ways:

1. The angular momentum of the electron causes a local field which

adds or subtracts from the applied field. This is a useful

picture in practice for deciding qualitatively the effect of

orbital angular momentum.

2. The angular momentum $(\underline{L})$ can be considered to couple with the

spin $(\underline{S})$ which is then replaced by the resultant $- \underline{J}$, where $\underline{J} = \underline{S} + \underline{L}$

In practice the effect of the angular momentum is taken into account by replacing the constant g_e in the Hamiltonian by a experimental g-value of the form:

$$\underline{g} = g_e \cdot \underline{E} + \Delta g_{ij}$$

where $\underline{E}$ is the unit matrix

Δg_{ij} is the amount the g-value obtained by putting the experimental results in the Hamiltonian $H_{spin} = \underline{H} \cdot \underline{g} \cdot \underline{S}$ varies from the free spin value of 2.002319....

$\underline{g}$ is a tensor of the form:

$$\begin{vmatrix} g_{xx} & & \\ & g_{yy} & \\ & & g_{zz} \end{vmatrix}$$

A theoretical calculation of g-values is difficult, but it is usually possible to determine the signs and approximate magnitude of Δg_{ij}. The effect of mixing in excited states of the system is considered as a perturbation on the ground state. The admixture coefficients of these higher states are calculated from first order perturbation theory. Thus $\lambda \underline{L} \cdot \underline{S}$ perturbs the state $|0,\frac{1}{2}\rangle$ by mixing in other states $|m_L,m_s\rangle$ in the following form:

$$\sum_{m_L} \sum_{m_s} |m_L,m_s\rangle \frac{\langle m_L, m_s | \lambda \underline{L} \cdot \underline{S} | 0, \frac{1}{2} \rangle}{|E_{0,\frac{1}{2}} - E_{m_L,m_s}|}$$

Using the components L_z, S_z and the L_+, L_-, S_+, S_- forms of L_x, L_y, S_x and S_y the allowed $|m_L,m_s\rangle$ states can be found and the new state is of the form:

$$|0, \frac{1}{2}\rangle + c_1 |m_L, m_s\rangle + c_2 |m_L', m_s'\rangle \cdots\cdots = |0, \frac{1}{2}\rangle' \quad (3)$$

the values of c_i depend upon λ and the energy difference between the state $|\ 0,\ \frac{1}{2}\rangle$ and the excited state.

Now if we operate on this state with the Hamiltonian the effect of the perturbing states will depend on the direction of the field $\underline{H}$, which determines the direction of the angular momentum $\underline{L}$. For a species having axial symmetry, where H_z is directed along the axis of the orbital containing the unpaired electron, there will be two principal values of g. These are $g_{//}$ when the field is along z, and $g_\perp$ when the field is in the x,y plane. The Hamiltonian can be written in the component form:

$$\beta\underline{H}\cdot\underline{g}\cdot\underline{S} = \beta g_{//} H_z S_z + \beta g_\perp (H_x S_x + H_y S_y) \qquad (8)$$

b. The Use of Group Theory to Determine the Angular Dependence of the g-tensor

When the state $|\ 0,\ \frac{1}{2}\rangle'$ has been determined, group theory can be used to decide which of the components of $|0,\ \frac{1}{2}\rangle'$ will be important when the field is along the three principal directions x, y, and z. This is because the g-tensor depends on matrix elements of the form: $\langle \psi_n |\ L_i\ |\psi_o\rangle$

where ψ_o is the state $|0,\ \frac{1}{2}\rangle$, ψ_n is the possible perturbing orbital, and L_i the component of the angular momentum operator along the ith. direction. For this to be non-zero the matrix element must form a basis for the totally symmetric representation of the group 'G' to which the species belongs.

Therefore the symmetrised direct product of the irreducible

representations for which ψ_n and ψ_o form a basis must contain

the irreducible representation for which L_i forms a basis. The

former product can be found using product tables, examples of

which are given in appendix B. The irreducible representation

for which L_i forms a basis can be obtained direct from character

tables, as it transforms as a rotation R_i (See appendix A).

c. Direction of g-Shifts

The sign of Δg depends on the sign of λ, which in turn

depends on whether the orbital which is mixed with ψ_o is filled

or empty. If there is mixing with an empty orbital, the orbital

motion of the electron will be such that the induced magnetic

field will tend to oppose the applied field. The absorption line

will thus move to high field, since the microwave frequency is

held constant. This displacement to high field will cause a

negative g-shift. If there is mixing with a filled orbital then

the resultant angular momentum will be of an electron hole. This

will tend to enhance the applied field and so such mixing will

cause a positive g-shift.

d. Simple Molecular Radicals

In simple molecular species where there is low symmetry, the

g-shifts can be discussed qualitatively without the use of character

tables. Consider, for example, the molecular fragment $A \rightleftharpoons B$

having the unpaired electron in the π_y-system. The degeneracy of the π-orbitals can be lifted either by a crystal field or by bending. Two simple cases will now be considered.

1. _The_Unpaired_ Electron_in_ the_ π _-bonding_Orbital_

The orbital scheme is shown in fig. 1;2a. When the magnetic field is along the z-axis (Fig. 1;1) orbital angular momentum can only occur in the x,y plane and hence only coupling with the π_x orbitals has any effect on the g-shift. The π_x-bonding orbital is filled and so coupling with this orbital will lead to a positive shift in g_{zz}. The π_x-antibonding orbital is empty and so coupling to this orbital will lead to a negative g-shift. The amount of the coupling depends on the energy differences between the orbital containing the unpaired electron and the orbital to which it is excited. The net shift in g_{zz} is thus positive.

When the field is along the x-axis the $\sigma_{n.b.}$-orbital can be used for orbital motion, and since this is empty there will be a negative shift in g_{xx}. The A-B σ-bonding orbital could also be used for coupling, but this will be of smaller effect, and the net shift in g_{xx} will be negative.

When the magnetic field is along the y-axis no orbitals are available for orbital angular momentum and so g_{yy} will be very close to the free spin value.

2. _One_Electron_ in_the_ π-antibonding Orbitals_

This situation is shown in fig. 1;2b. As before Δg_{yy} is
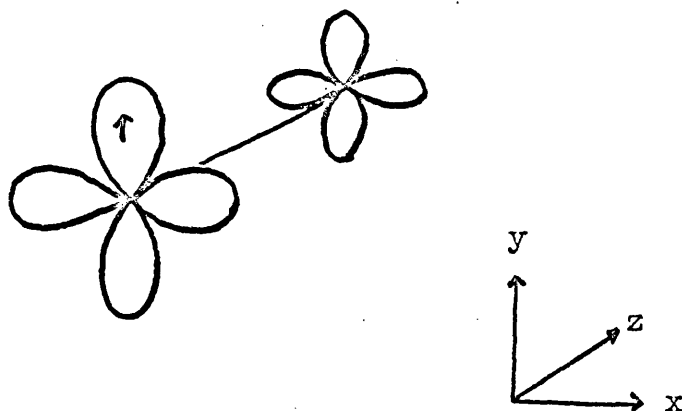
Fig 1;1

The Molecular Orbitals in the A≡B- fragment
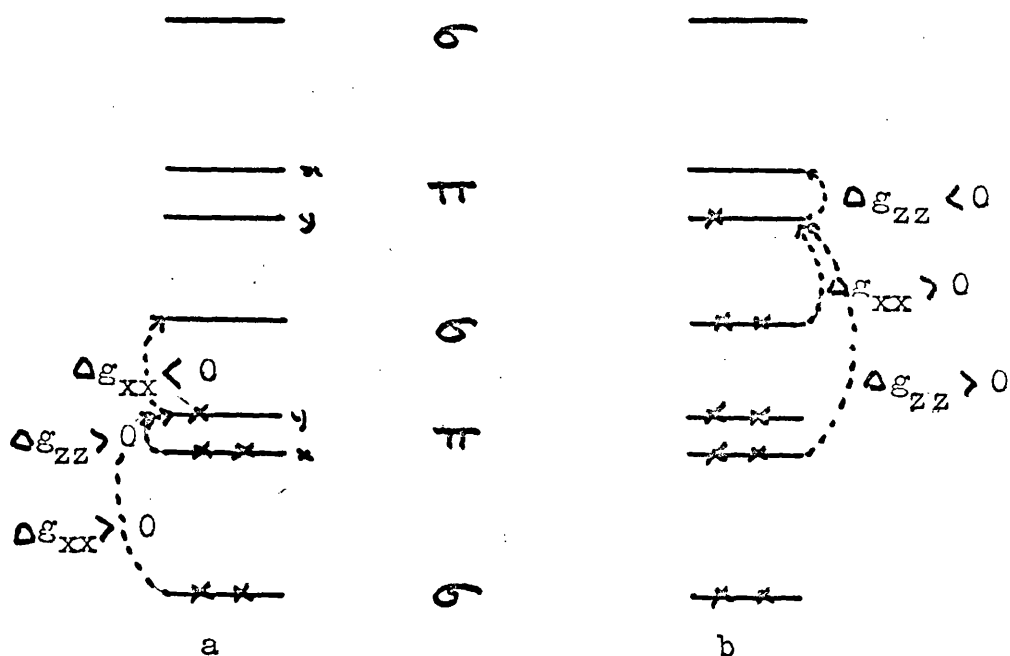
Fig 1;2

The Energy Levels of the Molecular Orbitals in the

A≡B- fragment and Possible Orbital Coupling

Contributing to the g-shifts

zero since when the field is along the y-axis there are no orbitals which can mix with the ground state and allow orbital angular momentum. Further, Δg_{xx} will be positive as the main interaction will be with the filled non-bonding orbital on A, and Δg_{zz} will be negative as the main interaction will be with the other empty π_x-orbital.

ii. The Spin Hamiltonian in the Presence of Interaction with Magnetic Nuclei

a. The Hyperfine Coupling Terms

A magnetic nucleus will affect the electron energy levels, and the spin Hamiltonian then has the form:

$$H_{spin} = \beta \underline{H} \cdot \underline{g} \cdot \underline{S} + \underline{S} \cdot \underline{A} \cdot \underline{I} \qquad (9)$$

The effect of the nuclear spin $\underline{I}$ can be considered in an analogous manner to that for including the orbital angular momentum contribution. For an axially symmetric system the spin Hamiltonian has the component form:

$$(10)$$

$$H_{spin} = \beta g_{/\!/} H_z S_z + \beta g_{\perp}(H_x S_x + H_y S_y) + A_{/\!/} S_z I_z + A_{\perp}(S_x I_x + S_y I_y)$$

Here $\underline{A}$ is a coupling tensor with components A_{xx}, A_{yy} and A_{zz}, assuming that $\underline{g}$ and $\underline{A}$ have the same principal axis system.

The $\underline{A}$ tensor consists of two terms, an isotropic part 'a' and an anisotropic part 'B'.

$$\underline{A} = a \cdot \underline{E} + \underline{B}$$

The anisotropic part $\underline{B}$ is due to coupling via a dipole-dipole mechanism between the electron and the nuclear spin and

is of the form:

$$\underline{B} = g_n \beta_n g_e \left\langle r^{-3} \right\rangle (1 - 3\cos^2\theta) \ \underline{I} \cdot \underline{S} \qquad (11)$$

where r^{-3} is a function of the electron distribution relative

to the nucleus in question integrated over all space. θ is the

angle between the mean position of the electron and the magnetic

field. Now $\left\langle r^{-3} \right\rangle$ is non-zero only if the electron is in a p-

d- or f-orbital, for in an s-orbital integration over all space

gives a value of $\underline{B}$ equal to zero.

The isotropic term arises from the Fermi contact term[4], this

requires actual unpaired electron density at the nucleus. Thus

only electrons in s-orbitals can cause this coupling directly.

The coupling operator a is:

$$a = \frac{8}{3} \ g_n \beta_n g_e \beta \left(\psi(0) \right)^2 \ \underline{I} \cdot \underline{S} \qquad (12)$$

The experimental A-tensor only contains contributions from

spin density actually interacting with the nucleus, while the

experimental g-tensor contains contributions from spin density

over the whole of the radical. It is possible, therefore, for

the principal axes of the two tensors to be non-coincident.

b. The Energy Levels

Once we have obtained the spin Hamiltonian it is then possible

to calculate the energies of the different states, by operating on

the states $|m_s, m_I \rangle$. If the field $\underline{H}$ is along the z-direction

(10) reduces to:

$$H_{spin} = g\ \beta H_z S_z + A\ S_z I_z + \tfrac{1}{2}A_- (S_+ I_- + S_- I_+) \quad (13)$$

where $I_+ = I_x + i I_y$; $I_- = I_x - i I_y$ etc.

For the case $S = \tfrac{1}{2}$ and $I = \tfrac{1}{2}$ we have the matrix:

	$\lvert \tfrac{1}{2}, \tfrac{1}{2} \rangle$	$\lvert \tfrac{1}{2}, -\tfrac{1}{2} \rangle$	$\lvert -\tfrac{1}{2}, \tfrac{1}{2} \rangle$	$\lvert -\tfrac{1}{2}, -\tfrac{1}{2} \rangle$
$\langle \tfrac{1}{2}, \tfrac{1}{2} \rvert$	$\tfrac{1}{2}g_{/\!/}\beta H_z + \tfrac{1}{4}A_{/\!/}$	0	0	0
$\langle \tfrac{1}{2}, -\tfrac{1}{2} \rvert$	0	$\tfrac{1}{2}g_{/\!/}\beta H_z - \tfrac{1}{4}A_{/\!/}$	$\tfrac{1}{2}A_\perp$	0
$\langle -\tfrac{1}{2}, \tfrac{1}{2} \rvert$	0	$\tfrac{1}{2}A_\perp$	$-\tfrac{1}{2}g_{/\!/}\beta H_z - \tfrac{1}{4}A_{/\!/}$	0
$\langle -\tfrac{1}{2}, -\tfrac{1}{2} \rvert$	0	0	0	$-\tfrac{1}{2}g_{/\!/}\beta H_z + \tfrac{1}{4}A_{/\!/}$

The roots of this matrix are:

$$\tfrac{1}{4}A_{/\!/} \pm \tfrac{1}{2}g_{/\!/}\beta H_z \quad \text{and} \quad -\tfrac{1}{4}A_{/\!/} \pm \sqrt{(\tfrac{1}{2}g_{/\!/}\beta H_z)^2 + (\tfrac{1}{2}A_\perp)^2}$$

If A_- is much less than the value of $g\,\beta H_z$

the four eigen values are:

$$\tfrac{1}{2}g_{/\!/}\beta H_z \overset{+}{_-} \tfrac{1}{4}A_{/\!/}$$

$$-\tfrac{1}{2}g_{/\!/}\beta H_z \overset{+}{_-} \tfrac{1}{4}A_{/\!/}$$

The selection rules $m_s = \pm 1$, $m_I = 0$ hold for e.s.r. absorptions

and the possible transitions are shown in fig 1;3 below.

Fig 1;3
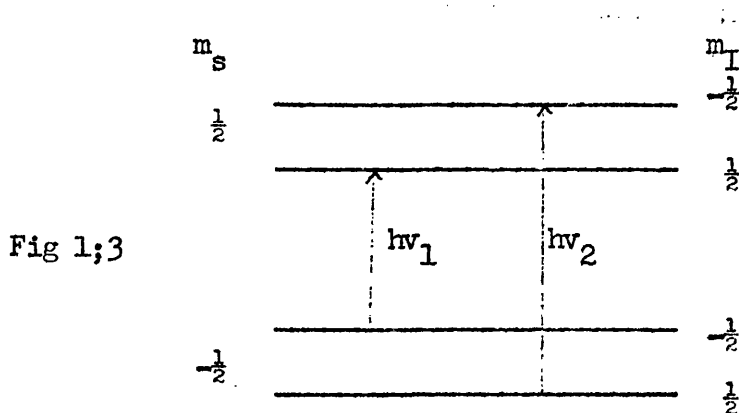
c. The Second Order Correction

If the nuclear hyperfine interaction is not very much less than the $g\beta \underline{H}$ term the off diagonal terms cannot be ignored, and the measured values of $A_{//}$, $A_{\perp}$, $g_{//}$, and $g_{\perp}$ will not correspond to the theoretical coupling and orbital mixing parameters. In order to use the same parameters for small and large splittings the experimental values are 'corrected'. The correction terms can easily be obtained. We will consider, as an example, the correction for $A_{//}$ in some detail, and quote the other corrections.

The energy levels are:

1. $\frac{1}{2}g_{//}\beta H_z + \frac{1}{4}A_{//}$

2. $[(\frac{1}{2}g_{//}\beta H_z)^2 + (\frac{1}{2}A_{\perp})^2]^{\frac{1}{2}} - \frac{1}{4}A_{//}$

3. $-\frac{1}{2}g_{//}\beta H_z + \frac{1}{4}A_{//}$

4. $-[(\frac{1}{2}g_{//}\beta H_z)^2 + (\frac{1}{2}A_{\perp})^2]^{\frac{1}{2}} - \frac{1}{4}A_{//}$

In practice hv is held constant and so the two allowed transitions can be written:

1. $h\nu = \frac{1}{2}g_{//}\beta H_{\perp} + \frac{1}{4}A_{//} + [(\frac{1}{2}g_{//}\beta H_{\perp})^2 + (\frac{1}{2}A_{\perp})^2]^{\frac{1}{2}} + \frac{1}{4}A_{//}$

2. $h\nu = [(\frac{1}{2}g_{//}\beta H_{+})^2 + (\frac{1}{2}A_{\perp})^2]^{\frac{1}{2}} - \frac{1}{4}A_{//} + \frac{1}{2}g_{//}\beta H_{+} - \frac{1}{4}A_{//}$

where H_{-} and H_{+} are the low and high field line positions.

1. $h\nu = \frac{1}{2}A_{//} + \frac{1}{2}g_{//}\beta H_{-} + \frac{1}{2}g_{//}\beta H_{-}[1 + A_{\perp}^2/g_{//}^2\beta^2 H_{-}^2]^{\frac{1}{2}}$

2. $h\nu = -\frac{1}{2}A_{//} + \frac{1}{2}g_{//}\beta H_{+} + \frac{1}{2}g_{//}\beta H_{+}[1 + A_{\perp}^2/g_{//}^2\beta^2 H_{+}^2]^{\frac{1}{2}}$

Dividing through by $g\beta$ to put $\underline{A}$ in gauss. This assumes that

$g_{//} \doteqdot g_{\perp} \doteqdot g_e$.

1. $\dfrac{h\nu}{g\beta} = \frac{1}{2}A_{//} + \frac{1}{2}H_{-} + \frac{1}{2}H_{-}[1 + A_{\perp}^{2}/H_{-}^{2}]^{\frac{1}{2}}$

2. $\dfrac{h\nu}{g\beta} = -\frac{1}{2}A_{//} + \frac{1}{2}H_{+} + \frac{1}{2}H_{+}[1 + A_{\perp}^{2}/H_{+}^{2}]^{\frac{1}{2}}$

Expanding the square root term and neglecting terms over second order.

1. $\dfrac{h\nu}{g\beta} = \frac{1}{2}A_{//} + H_{-} + A_{\perp}^{2}/4H_{-}^{2}$

2. $\dfrac{h\nu}{g\beta} = -\frac{1}{2}A_{//} + H_{+} + A_{\perp}^{2}/4H_{+}^{2}$

Taking 1. from 2.

$A_{//} = H_{+} - H_{-} + A_{\perp}/4H_{+} - A_{\perp}/4H_{-}$

$= [H_{+} - H_{-}][1 - A_{\perp}^{2}/4H_{+}H_{-}]$

Thus if $[H_{+}-H_{-}]$ is the measured value of $A_{//}$ then the true value of $A_{//}$ is given by:

$$A_{//} = [H_{+} - H_{-}].[1-A_{\perp}/4H_{+}H_{-}]$$

Similarly:

$$A_{\perp} = [H_{+} - H_{-}].[1-(A_{//}^{2}+ A_{-}^{2})/8H_{+}H_{-}]$$

$$g_{//} = \dfrac{h\nu}{\beta H_{\pm}} [1 + A_{\perp}/4H_{+}H_{-}]^{-1}$$

$$g_{\perp} = \dfrac{h\nu}{\beta H_{\pm}} [1 + (A_{//}^{2} + A_{\perp}^{2})/8H_{+}H_{-}]$$

where $H_{\pm} = \frac{1}{2}[H_{+} + H_{-}]$

d. Hyperfine Tensors in Radicals

1._The_Unpaired Electron_in a Pure_p-orbital_

An expression for the interaction of the

electron with a magnetic nucleus, when there

is no spin density at the nucleus was given by

equation (11).   For a p-orbital the coupling

tensor has the form:

$$\begin{vmatrix} -B & & \\ & -B & \\ & & 2B \end{vmatrix}$$

Fig 1;4

where $\begin{vmatrix} x \\ y \\ z \end{vmatrix}$ are the principal directions of the B-tensor

(Fig.1;4).   B can be calculated from [4]:

$$B = 2/5 \; g_n \beta_n g_e \beta \left\langle r^{-3} \right\rangle \qquad (14)$$

2._The_Unpaired Electron_in an_s-p_Hybrid Orbital

In this case there is an isotropic coupling due to the electron

in the s-orbital and an anisotropic coupling of the form outlined

above.   The total hyperfine tensor is thus of the form:

$$\begin{vmatrix} a & - & B & \\ & a & - & B \\ & & a & + & 2B \end{vmatrix}$$

The isotropic part is thus the algebraic mean of the three principal

values.   If a is of the same size or smaller than 2B the value

of a and hence also B cannot be found without ambiguity, unless

the signs of the principal values are known.
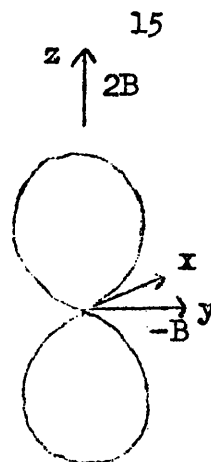
II. Electron Spin Resonance Spectra

In this section we outline the analysis of a recorded e.s.r. spectrum. Generally there will be a g-tensor with different principal values along three orthogonal axes, and also a number of hyperfine coupling tensors · associated with different magnetic nuclei each with three principal directions.

i. Solution Spectra

In solutions radicals will normally be tumbling so fast that the anisotropic coupling will average to zero, and only the isotropic coupling will be observed in the spectrum. The observed g-value is the average value of the g-tensor (g_{iso}). This situation is also observed if the radicals are tumbling freely in a glass or crystal, or if the unpaired electron is entirely in an s-orbital. With only one g-value and isotropic hyperfine coupling the spectrum is considerably simplified. A radical with one magnetic nucleus of spin 3/2 will produce a four line spectrum. If more than one magnetic nucleus is present then the absorption lines will be further split. In the case of a number of magnetically equivalent nuclei a series of lines are obtained of equal splitting. Six sodium nuclei, for example, each of spin 3/2 will yield a 19 line spectrum of intensities:

1; 6; 21; 56; 120; 216; 336; 456; 546; 580; 546; 456; 336; 216...etc.

ii. Single Crystal Spectra

If the radical is fixed in a lattice position in a single crystal then the g-value and hyperfine coupling will depend on the angle between the p- or d- orbital containing the unpaired electron and the magnetic field. In general none of the principal directions of the g- and hyperfine coupling tensors need be coincident. The principal values of the g- and hyperfine coupling tensors can be derived by recording the spectra at different orientations with respect to the applied field about three orthogonal axes. Once the maximum and minimum values of the g- and hyperfine coupling tensors are obtained, and the angle between these features and the chosen three axes, it is possible to obtain both the principal values and the direction cosines of the tensors by diagonalising the tensor matrix. Computer programs are now available for this otherwise tedious calculation. In some cases, the radical lies with its principal g- and hyperfine coupling tensors along the three chosen orthogonal axes. In this case the principal values can be obtained directly. Comparison with powder spectra in some cases simplifies the calculations.

iii. Randomly Orientated Radicals

In this case the radicals are fixed either in a powdered crystal or in a glass, and the spectra obtained are the envelope spectra of all possible single crystal spectra. A number of authors have discussed these line shapes[5-8]. Absorption and

derivative curves in fig. 1;5 follow Kneubuhl[5]. Fig. 1;5a and b

is of radicals with axially symmetric and non-axially symmetric

g-tensors respectively.

If the absorption lines do not overlap, and if the principal

directions of the g- and hyperfine coupling tensors coincide, all

the e.s.r. parameters can be obtained from the powder spectra,

except the direction cosines. Often, however, lines do overlap,

and sometimes the $|a - B|$ term is so small that the hyperfine

coupling is contained in the line width of the perpendicular g-

feature. Even so powder spectra provide a check on the diagonal-

isation results from single crystal studies, and should always be

obtained and compared with the single crystal spectra.

Where lines with different g-value overlap, it may, in some

cases, be possible to resolve the spectra better by increasing the

magnetic field and corresponding microwave frequency. In this case

the splitting (in gauss) between two lines of different g-value

increases, while the separation of lines caused by hyperfine

coupling is independent of the field strength, and so the separation

will not increase.
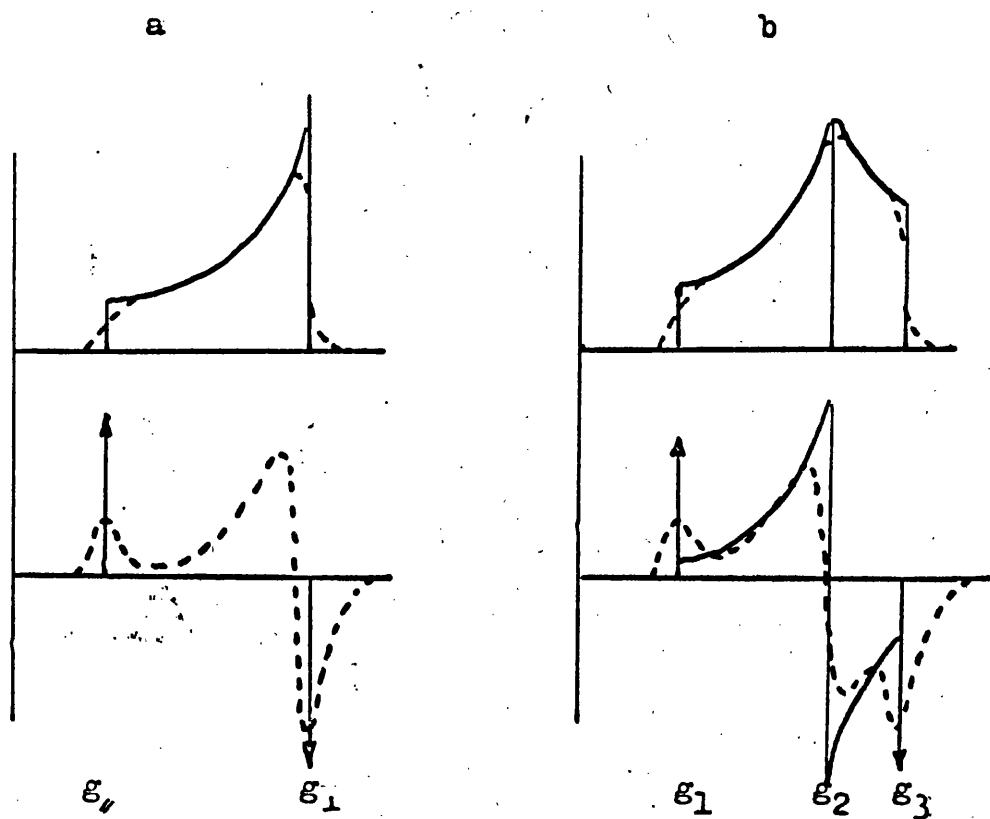
Fig1;5.

Absorption and First Derivative Line Shapes for
Polycrystalline Samples of a Radical with:-

a. Axial symmetry.

b. Non-axial   symmetry.

III. Spin Densities

From the e.s.r. spectrum we can, in favourable cases, obtain values for A_{iso} (a) and B for all the magnetic nuclei which interact with the unpaired electron. To turn these values into parameters which will be of use in discussing the orbital containing the unpaired electron, we introduce the concept of spin density. This is defined as the hyperfine coupling constant divided by the relevant hyperfine constant if the electron were completely in a particular orbital. For example the experimental B value is divided by the value of B if the electron were purely in a pure p-orbital, this is the "atomic" parameter.

In some cases these atomic parameters can be obtained experimentally, from atomic beam results. Table 1;1 gives the experimental results for a few alkali metals and halogens. In other cases the value of $\psi(0)^2$ and $\langle r^{-3} \rangle$ are calculated using Slater or Self-Consistent-Field wavefunctions for the relevant s-, p- and d-orbital. Table 1;2 lists the non-transition metal magnetic nuclei for which these calculations have been performed. Most of the values were calculated by Morton, Rowlands and Whiffen from S.C.F. wave functions. These values have been checked and where necessary corrected using more recent data and a program written by Mr. D. J. A. Tinling. Values for the alkali metals were calculated by Gooding[9] using the unrestricted Hartree-Fock approximation taking into account exchange polarisation. These are much closer to the

experimental values than those of Morton et al, who used normal

restricted Hartree-Fock wave functions. Comparison of tables 1;1

and 1;2 indicates that care has to be taken in considering the

accuracy of the spin densities using the calculated values.

The calculated results for a number of ions are given in table

1;3, and for a number of unpromoted states of nitrogen in table 1;4.

Table 1;1
Experimental Atomic Spin Resonance Data

Isotope	$\langle r^{-3} \rangle$ a	$2B$ b	A_{iso} b	Ref
^{1}H (1s)			506.8	10
(2s)			63.4	10
^{2}H			77.9	10
^{7}Li			143.4	10
^{23}Na	1.703	10.16	316.1	10
^{39}K	2.945	3.10	82.4	10
^{85}Rb			361.1	10
^{133}Cs			820.1	10
^{17}O	31.08	95.1		11
^{19}F	49.88	1059		11
^{35}Cl	49.5	109.45		12
^{79}Br	80.5	455.2		13
^{127}I	94.0	424.41		14

a. Values in $\overset{\circ}{A}{}^{-3}$ b. Values in Gauss

Table 1:2

Calculated Atomic Spin Resonance Data for Nuclei

Isotope	Abund.	Spin	$\langle r^{-3} \rangle$ a	$\Psi(0)^2$ a	2B b	A_{iso} b	Ref.
^{7}Li	99.98	3/2		1.135		139	9
^{9}Be	100	3/2		3.871		130	15
^{11}B	81.2	3/2	5.259	9.554	38	725	15
^{13}C	1.11	1/2	11.481	18.77	66	1130	15
^{14}N	99.64	1	21.043	32.37	34	.552	15
^{17}O	0.04	5/2	33.73	51.83	104	1,660	15
^{19}F	100	1/2	51.91	81.20	1,084	17,200	15
^{23}Na	100	3/2				266	9
^{27}Al	100	5/2	7.159	16.00	42	985	16
^{29}Si	4.70	1/2	13.848	25.833	62	1,220	16
^{31}P	100	1/2	22.520	38.171	206	3,640	16
^{33}S	0.74	3/2	32.667	53.735	56	975	16
^{35}Cl	75.4	3/2	45.530	72.225	100	1,680	16
^{37}Cl	24.6	3/2			84	1,395	16
^{39}K	93.08	3/2				63.5	9
^{43}Ca	0.13	7/2		9.362		149	17
^{67}Zn	4.12	5/2		30.687		376	18
^{69}Ga	60.2	3/2	19.45	47.157	106	2,675	18
^{71}Ga	39.8	3/2			134	3,400	18
^{73}Ge	7.61	9/2	32.469	64.955	26	535	18
^{75}As	100	3/2	47.41	85.234	183	3,430	18
^{77}Se	7.5	1/2	62.623	107.07	270	4,840	18
^{79}Br	50.57	3/2	80.588	131.734	456	7,800	18
^{81}Br	49.3	3/2			564	8,400	18

a. Values in $\overset{o}{A}^{-3}$ b. Values in Gauss.

Table 1:3

Calculated Atomic Spin Resonance Data for Nuclei in Ions

Isotope	State	$\langle r^{-3}\rangle$ a	$\Psi(0)^2$ a	2B b	A_{iso} b	Ref.
$^9Be^+$	^1S		5.4560		181.3	19
$^{11}B^-$	^1S	2.9318	8.7281	21.227	661.8	20
$^{13}C^-$	^2P		17.6413		1,048.3	20
$^{14}N^{2-}$	^2P	11.8299	30.98	19.29	529.1	20
$^{14}N^-$	^1S	15.3073	30.95	24.96	528.5	20
$^{17}O^{2-}$	^1S	22.0843	48.7555	67.56	1,562	20
$^{17}O^-$	^2P	27.2557	48.795	83.39	1,563	20
$^{19}F^-$	^1S	43.1718	73.13	916.57	16,207	20

- - - - - - - - - - - - - -

Table 1:4

Calculated Spin Resonance Data for Different States in Unpromoted Nitrogen Atoms and Ions

Species	State	$\langle r^{-3}\rangle$ a	$\Psi(0)^2$ a	2B b	A_{iso} b	Ref
$^{14}N^-$	^3P	15.90	30.29	25.93	517.2	20
	^1D	15.66	30.54	25.53	521.5	20
	^1S	15.31	30.95	24.96	528.5	20
^{14}N	^4S	20.87	32.18	34.03	549.5	21
	^2D	20.32	32.51	33.14	555.2	21
	^2P	19.96	32.75	32.56	559.2	21
$^{14}N^+$	^3P	25.86		42.17		22
	^1D	25.26		41.18		22
	^1S	24.37		39.74		22

a. Values in $\overset{\circ}{A}^{-3}$ b. Values in Gauss.

i. The Sign of Spin Density

The spin densities calculated as above are a rough guide to the unpaired electron density in the different atomic orbitals. If the spin density is due to actual delocalization of the unpaired electron into the orbital in question, then the spin density is defined as positive. The nucleus will be affected by spin density of the same m_s value as the major part of the spin density. If the spin density is not due to direct delocalization of the unpaired electron, but due to polarisation effects, then the spin of the electron need not be the same as that of the major part of the spin density. If the spin is not the same then the spin density is negative. The possibility of negative spin density, and polarisation mechanisms are discussed further in Chapter 4.

B. Infra-red and Raman Spectroscopy

For a non-linear polyatomic molecule of n-atoms there are 3n-6 degrees of vibrational freedom and 3n-6 fundamental frequencies. Some of these may be degenerate and not all these can be observed in the infra-red or Raman spectra because of the selection rules. The use of group theory greatly aids the interpretation of the spectra as it predicts which transitions will be i.r. or Raman active.

I. Selection Rules of Infra-red and Raman Spectra

For a vibrational mode to couple with the i.r. radiation there must be a change in dipole moment on changing the relative positions of the nuclei. For Raman spectra there must be a change in polarisation. The selection rule for an i.r. absorption is determined by the integral:

$$\mu_{v'v''} = \int \psi_{v'}(Q_a) \, \mu \, \psi_{v''}(Q_a) \, dQ_a \quad (1)$$

where μ is the dipole moment operator.

v' and v'' the vibrational quantum numbers (For fundamental normal modes these are 0 and 1 respectively).

Q_a the normal coordinate of vibration.

This integral can be resolved in three directions and thus depends on μ_x, μ_y, and μ_z. If one of these integrals is non-zero the normal vibration associated with Q_a is i.r. active.

Similarly for the Raman spectra the selection rule is determined by the integral:

$$a_{v'v''} = \int \psi_{v'}(Q_a) \, a \, \psi_{v''}(Q_a) \, dQ_a \quad (2)$$

where α is the electronic polarisability operator of the molecule, and has six components α_{xx}, α_{yy}, α_{zz}, α_{xy}, α_{xz}, and α_{yz}, and hence (2) can be resolved into six components. If one of these integrals is non-zero the normal vibration associated with Q_a is Raman active.

These integrals will only be non-zero if they form a representation which includes the totally symmetric representation. The fundamental normal modes are those from the ground state to one of the excited states in which the vibrational mode has a quantum number of one. $\psi_0(Q_a)$ is invariant under any symmetry operation while the symmetry of $\psi_1(Q_a)$ is the same as that for Q_a. Thus for i.r. transitions the integral (1) does not vanish when the irreducible representation for which μ_x, for example, forms a basis is exactly the same as that for Q_a. Similarly for Raman spectra α_{xx} must be of the same representation as Q_a.

The operators μ_x, μ_y, and μ_z transform in the same way as those of translational motion T_x, T_y and T_z respectively (Usually written x,y, and z in character tables). The polarisability operators α_{xy} etc. transform in the same way as the product xy etc. and these are also listed in the character tables. It is thus possible to read from character tables which normal modes will be active in the i.r. or Raman spectrum.

Two further observations may be made:

i. If the molecule has a centre of symmetry then the i.r. and Raman active bands will be mutually exclusive, the i.r. bands being

anti-symmetric with respect to the centre (u) and the Raman bands symmetric (g).

ii.   The totally symmetric irreducible representation is always Raman active.

Two types of molecules are studied in this work, the linear ABC molecule and the octahedral $M(AB)_6$ molecule.   These will be treated here as examples of the symmetry methods used, the methods of obtaining the actual normal modes are treated in a number of books[22, 23].

i. The Linear ABC Molecule

This molecule has $3n-5$ vibrational degrees of freedom and hence there are four vibrational modes.   The molecule is of the $C_{\infty v}$ symmetry group (See appendix A), and the normal modes are shown in fig 1;6b.   In fig 1;6a the normal modes of the ABA linear molecule $(D_{\infty h})$ are shown for comparison.   From table A;1 all three modes transform in the same way as components of both the polarisation and the dipole moment and hence all three modes are Raman and i.r. active.

ii. The Octahedral $M(AB)_6$ Molecule (O_h)

There are 33 vibrational modes, the 13 normal modes are shown in fig 1;7.   From table A;3 there is a centre of symmetry and thus the i.r. and Raman active bands are mutually exclusive.   Only the normal modes which transform as T_{1u} are i.r. active, while those which transform as A_{1g}, E_g and T_{2g} are Raman active.   From these considerations only one A-B and one M-A stretching transition should be observed in the i.r. spectra.

Fig. 1;6

a. <u>The Normal Modes of Vibration for an ABA Molecule</u>
$(D_{\infty h})$

Σ_g^+

π_u

Σ_u^+
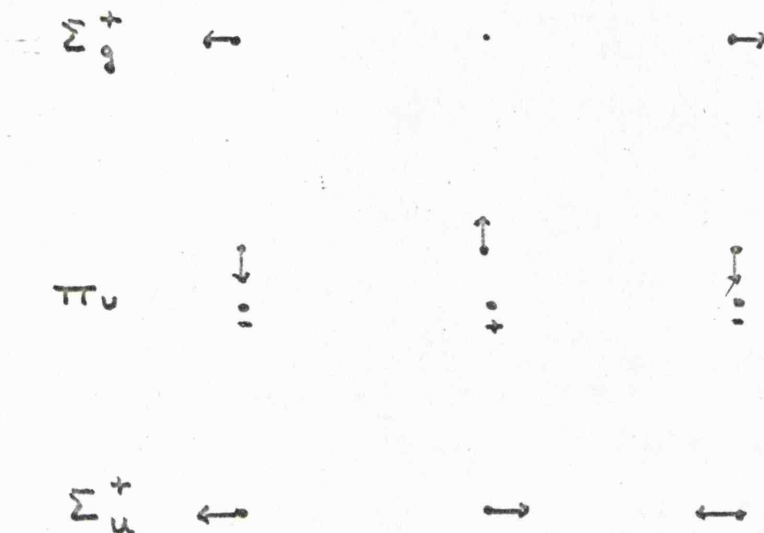
b. <u>The Normal Modes of Vibration for an ABC Molecule</u>
$(C_{\infty v})$

Σ^+

π

Σ^+

$\nu_1 \quad A_{1g}$
$\nu(CN)$

$\nu_2 \quad A_{1g}$
$\nu(MC)$

$\nu_3 \quad E_g$
$\nu(CN)$

$\nu_4 \quad E_g$
$\nu(MC)$

$\nu_5 \quad T_{1g}$
$\delta(MCN)$

$\nu_6 \quad T_{1u}$
$\nu(CN)$

$\nu_7 \quad T_{1u}$
$\nu(MC)$

$\nu_8 \quad T_{1u}$
$\delta(MCN)$

$\nu_9 \quad T_{1u}$
$\delta(CMC)$

$\nu_{10} \quad T_{2g}$
$\delta(MCN)$

$\nu_{11} \quad T_{2g}$
$\delta(CMC)$

$\nu_{12} \quad T_{2u}$
$\delta(MCN)$

$\nu_{13} \quad T_{2u}$
$\delta(CMC)$

The Normal Modes of Vibration of the $M(AB)_6$ Molecule
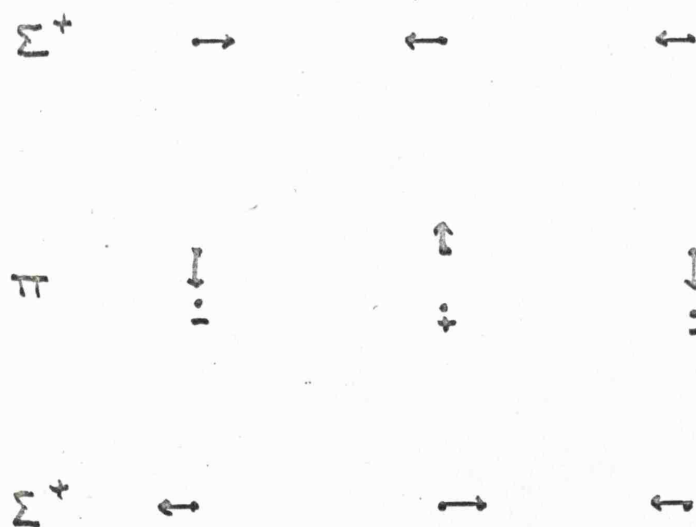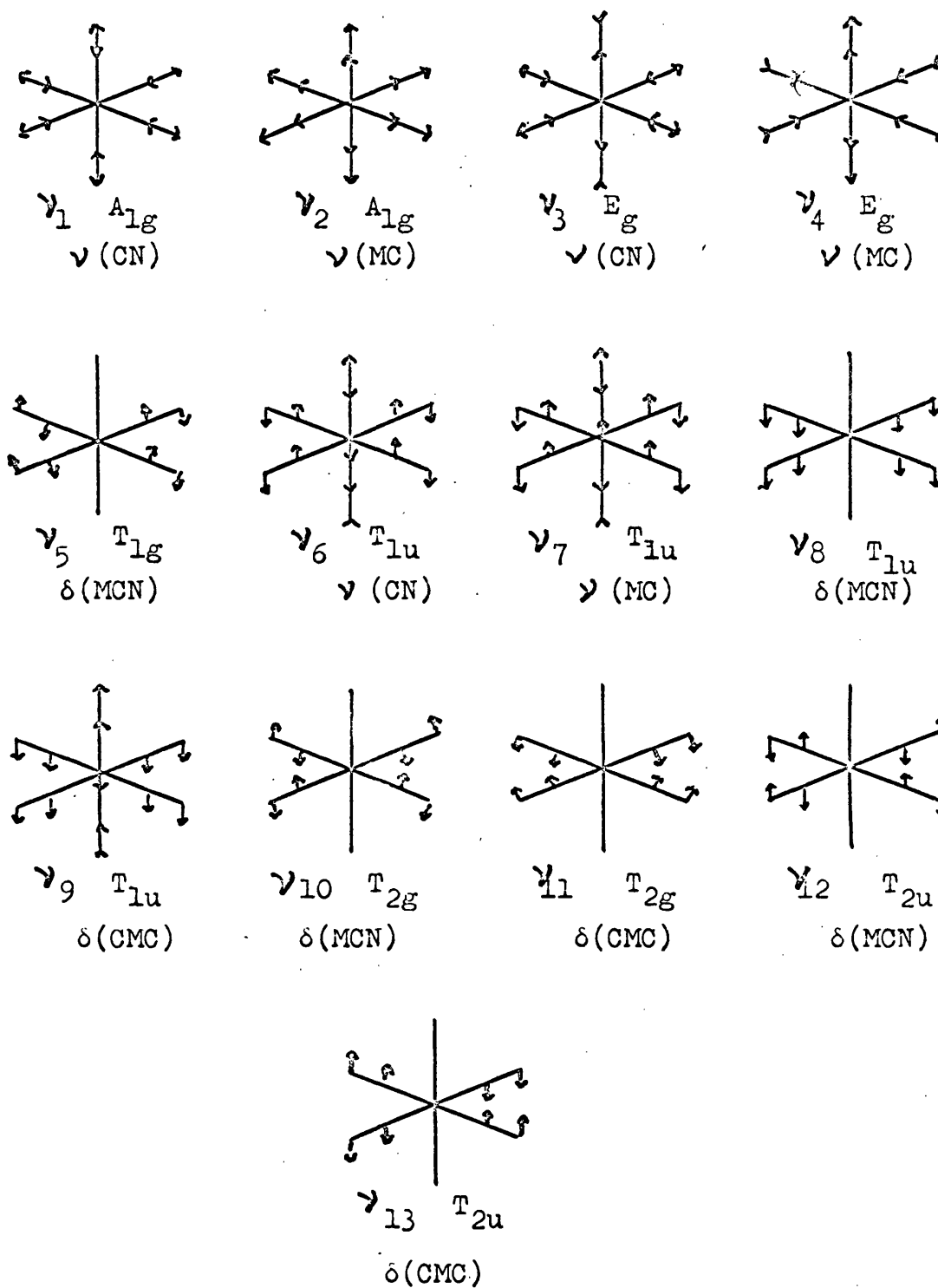
iii. Site Symmetry [25,26]

The symmetry considerations above apply to isolated molecules. If the molecule is in a crystal, the environment may lower the symmetry, and if the crystal is ionic this may have quite a strong effect on the i.r. spectra. In many cases the site symmetry can be treated as a perturbation on the normal modes of the isolated molecule. Normally site symmetry alters the character of each irreducible representation, and in some cases lifts degeneracies. Usually more vibrational transitions become allowed. Correlation tables have been prepared to show how the representations are perturbed by the site symmetry. Table 1;5 is a correlation table for O_h symmetry to a number of lower symmetries.

An $M(AB)_6$ molecule in a cubic lattice has O_h symmetry, but if there is a vacancy or impurity ion near one of the ligands to compensate for a charge unbalance, then the symmetry will be reduced to C_{4v}. The irreducible representations of the O_h group which transform in the same way as the stretching vibrations in $M(AB)_6$ are correlated to a site symmetry of C_{4v} in fig 1;8. From table A;2 (Character table for C_{4v}) the a_1 and e modes will be i.r. active, and the a_1, b_1, b_2 and e will be Raman active. Since there is no centre of symmetry the i.r. and Raman bands are not now necessarily mutually exclusive. Thus instead of only one A-B stretching band there are now four allowed transitions. The intensities of the v_1 and v_3 bands depend, in part, on the strength of the crystal field causing the distortion.

Table 1:5

Correlation Table for the Group O_h

O_h	T_d	D_{4h}	D_{2d}	C_{4v}	C_{2v}	C_{2h}
A_{1g}	A_1	A_{1g}	A_1	A_1	A_1	A_g
A_{2g}	A_2	B_{1g}	B_1	A_2	A_2	B_g
E_g	E	$A_{1g}+B_{1g}$	A_1+B_1	A_1+B_1	A_1+A_2	A_g+B_g
T_{1g}	T_1	$A_{2g}+E_g$	A_2+E	A_2+E	$A_2+B_1+B_2$	A_g+2B_g
T_{2g}	T_2	$B_{2g}+E_g$	B_2+E	B_2+E	$A_1+B_1+B_2$	$2A_g+B_g$
A_{1u}	A_2	A_{1u}	B_1	A_2	A_2	A_u
A_{2u}	A_1	B_{1u}	A_1	B_2	A_1	B_u
E_u	E	$A_{1u}+B_{1u}$	A_1+B_1	A_2+B_2	A_1+A_2	A_u+B_u
T_{1u}	T_2	$A_{2u}+B_{1u}$	B_2+E	A_1+E	$A_1+B_1+B_2$	A_u+2B_u
T_{2u}	T_1	$B_{2u}+E_u$	A_2+E	B_1+E	$A_2+B_1+B_2$	$2A_u+B_u$

— — — — — — — —

Fig 1:8

Correlation Diagram for the A-B Stretching Modes in the $M(AB)_6$
Molecule when the Symmetry is Reduced to C_{4v}

	O_h	C_{4v}
v_1, v_2	a_{1g} (R.A.) ————————	a_1 (R.A. and I.R.)
v_3, v_4	e_g (R.A.)	a_1 (R.A. and I.R.) b_1 (R.A. and I.R.)
v_6, v_7	t_{1u} (I.R)	a_1 (R.A. and I.R.) e (R.A. and I.R.)

(R.A.) Raman active.   (I.R.) Infra-red active.

Chapter 2

Experimental Methods

I. Preparation of Samples

1. Crystal Growing

Crystals of both pure cyanides and alkali halides doped with either cyanide or complex cyanide ions were required in this investigation. These crystals were grown either by slow evaporation of aqueous solution or by slowly cooling the molten compound or mixture.

a. From Solution

Evaporation of an aqueous solution is not suitable for growing pure crystals of the alkali cyanides since there is a tendency to hydrolyse in water, and growing from dried methanol did not yield pure crystals either. We have however used the aqueous solution method to dope alkali halides with both simple and complex cyanide ions. The solution method has the advantage of being relatively simple, but it is difficult both to grow large crystals, and to control the amount of impurity incorporated. In some cases the impurities are incorporated more easily than the required ion. Infra-red spectra showed that all crystals grown by this method contained an appreciable amount of water incorporated into the lattice.

Cyanide ions were incorporated into alkali halides by slow evaporation of a solution containing a ten to one excess of the halide. Infra-red spectra showed that all crystals obtained using potassium cyanide as the dopant contained a high concentration of the ferrous hexacyanide ion. Crystals grown using sodium

cyanide contained no observable amounts of this ion. Crystals
doped with the complex cyanide ions were grown from solutions
containing 1 - 0.001% of the complex.

b. From the Melt

A number of methods have been devised to grow crystals from the
melt. The main features of these methods are the slow reduction of
the temperature from above the melting point to about 20° below and
the seeding of the melt either with a small crystal or some feature
in the crucible. We have used a Stockbarger furnace [27] to prepare
some doped alkali halide crystals. This method uses a furnace with
a temperature gradient through which the crucible is lowered. The
crucible is drawn to a sharp point at the lower end to facilitate
the formation of a single crystal. When attempting to dope with
cyanide ions, unless the crucible is evacuated, the major ion
incorporated is the cyanate ion. In order to reduce to a minimum
the oxidation and hydrolysis of the cyanide ion, a fresh sample
of sodium cyanide was used each time. The reagent bottle was
opened in an oxygen-free dry box, and mixed with the halide which
had previously been dried at $100^\circ C$ for three days and cooled in the
dry box. Before sealing, the crucible was evacuated to about 0.001
mm of Hg and gradually heated to remove as much of the adsorbed gas
as possible. After the crucible had been lowered through the
furnace, a process which took about 36 hours, it was left to anneal
at a temperature about 20° below the melting point. Finally the
temperature was lowered slowly to room temperature, the crystals

cut along cleavage planes and sealed into ampoules before removing from the dry box.

The complex ions all decomposed below the melting point of the halide and so these could not be introduced into the lattice by this method.

The preparation of pure crystals of sodium cyanide was attempted by modifying the Stockbarger furnace so that the crucible could be evacuated during the growing of the crystal. In this case the temperature of the furnace was lowered slowly keeping the higher winding about 15° above the lower one. The constant evacuation was necessary as gases were given off while the cyanide was molten. It was hoped that this method would also roughly zone refine the crystal, but although single crystals were obtained, they were not pure enough for the colour centre experiments.

ii. Pressed Discs

Samples suitable for i.r. were conveniently prepared by compressing the finely powdered halide in a steel die at about 20 tons per square inch and about 2 mm of Hg pressure[28]. The preparation of the potassium chloride and bromide discs was straightforward, but sodium salts, because of their higher melting point, did not form good discs. In this case a disc was formed by adding potassium bromide to the sample, followed by careful mixing in an agate ball mill.

When using the pressed disc technique there is a chance that halide ions may be incorporated into the complex ions, or the lattice may affect the site symmetry. Therefore the spectra of all the

different species examined were also run as Nujol mulls.

The main advantage of these pressed discs is that they can be irradiated easily and a series of spectra can be run of the same sample after different irradiation times.

II. The Spectrometers

1. The Electron Spin Resonance Spectrometers

Three e.s.r. spectrometers were used in this investigation, two at X-band and one at Q-band frequencies. The two X-band machines were a Varian V 4502-03 with 100 kc/s modulation, and a machine constructed by Mr J. A. Brivati[29]. The Q-band machine, unlike the X-band spectrometers which have crystal detection, has a super-heterodyne detection system. This latter system has the advantage of requiring very little incident microwave power, and hence the spectra of samples which saturate easily can be recorded. This is especially useful for Q-band spectra at low temperature where samples saturate very easily.

The Varian spectrometer has a variable temperature attachment which enables sample temperatures between 100°K and 378°K to be obtained. The temperature could be controlled to within $2-3^{\circ}$. In the other X-band machine the sample cavity is mounted in an insulating bath. Using a suitable coolant, such as liquid nitrogen solid carbon dioxide/methanol or ice/water, the sample could be kept at a constant temperature. This instrument was ideal for single crystal specta, and runs as long as 15 hours at 77°K have been performed, the microwave frequency and the temperature remaining

stable. The Q-band cavity could be cooled by placing a copper extension of the cavity in a bath of coolant, and temperatures down to about 100°K could be reached.

Powdered samples were contained in quartz sample tubes, which were free of paramagnetic impurities. Single crystal samples were mounted on the end of a perspex rod. The end of this rod was detachable and a number of different ends were prepared so that the crystal could be rotated about axes perpendicular to I00, II0 and III planes. In the instrument used for the single crystal spectra the crystal was rotated and the angle could be read to within 0.5°.

The g-values quoted in this thesis are all corrected with an external reference, "charred dextrose", which has a sharp absorption at 2.0023, this reference being run at the beginning and end of each series of spectra. Thus errors due to the field probe being in a slightly different position from the sample are eliminated. All g-values in this thesis are subject to an experimental error of about $\pm$ 0.0004, for broad lines the error may be much greater than this. The error in the hyperfine splitting also depends on the width of the lines. All hyperfine coupling constants in this thesis are in gauss, unless otherwise stated.

ii. Infra-red Spectrometer

All the i.r. spectra were recorded on a Perkin Elmer 225 double beam instrument. A low temperature attachment of the cold finger type[28] was used to record spectra down to about 100°K. On slow and expanded scans the spectra were reproducible to 1 cm^{-1}.

iii. Visible and Ultra-violet Spectrometer

All spectra were recorded on a Beckman DK 2A. Thin slices of crystals were used for transmission spectra, and both pressed discs and finely ground powders for diffuse reflectance.

III. Radiation Sources

i. Gamma Radiation Source

All γ-irradiation was carried out in a "Gamma Cell 200", with a Cobalt-60 isotope. Cobalt-60 emits about equal numbers of γ-photons of energy 1.332 and 1.173. The dose rate fell from 2.20 $\times 10^5$ to 1.69 $\times 10^5$ rads/hour during the course of this work.

A Dewar flask placed in the cavity of the cell enabled irradiation at temperatures between ambient and $77^{\circ}K$. Light sensitive samples were irradiated in ampoules enclosed in aluminium foil, and pressed discs were irradiated in the holders used to mount them in the i.r. spectrometer.

ii. Ultra-violet Irradiation Source

A medium pressure mercury lamp was used in all photolytic experiments. This has high energy radiation bands at 254, 265, 280, 296, 302 and 313 mμ . Quartz containers were used in all photolysis experiments, and for low temperature work a Quartz Dewar flask was used which enabled temperatures down to 77° to be reached.

IV. The Chemicals Used and their Purity

The main chemicals used in this investigation are tabulated

below. The alkali halides were dried at $100^\circ C$ for 1-3 days and

then cooled in a dry-box. The alkali cyanides were kept in a

dry-box and a new reagent bottle used to prepare about twenty

sealed ampoules of the powdered cyanide at a time.

Chemical	Grade	Min % Purity	% NO_3	% Fe
KCl	Analar	99.8	0.002	0.0005 ?
KBr	Analar	99.0		0.001
NaCl	Analar	99.9	0.002	0.0003
NaBr	Reagent	99.0		0.001
KCN	Analar	96		0.02
NaCN	Reagent	96		
$K_4Fe(CN)_6$	Reagent	99		
$K_3Fe(CN)_6$	Reagent	99		

Chapter 3

Colour Centres in Irradiated Cyanides

Colour Centres

Two paramagnetic species have been studied extensively in
irradiated alkali halides, these are the F- and V_k-centres.
Centres analogous to these have been identified and studied in
γ-irradiated sodium cyanides. Two other paramagnetic centres have
been observed, one of which has been tentatively assigned to the
F_2^+-centre.

In this chapter the e.s.r. data for F- and V_k-centres in the
alkali halides is reviewed. To facilitate assignments of e.s.r.
spectra to F-centres a general correlation has been found which
relates the isotropic coupling of the first shell of cations
surrounding the F-centre to physical parameters of the ions and the
lattice. The use of this correlation is discussed for F-centres in
non-alkali halides and used to identify the F-centre spectrum in
sodium cyanide.

I. The F-centre

If an alkali halide crystal is γ-irradiated, it soon becomes
coloured, and a number of absorption bands appear in the visible
and ultra-violet region. The major absorption band is known as the
F-band. This band is also observed if the crystal is heated in the
presence of alkali metal vapour. The method of formation indicates
an electron excess centre, and the accepted model of the F-centre is
an electron trapped at an anion vacancy[30]. This model of de Boer
did not however define the state of the electron or the extent of
delocalization in the crystal. This information was not forth-
coming from optical studies, but using magnetic resonance methods it

has been possible to obtain a partial picture of the F-electron

distribution.

<u>i. Optical Work on the F-centre and Related Electron Excess Centres</u>

The energy of the F-band depends on the size of the lattice and

Mollwo[31] found that λ_{max} was given very closely by:

$$\lambda_{max} = 600 \, d^2$$

where λ_{max} and d (The lattice constant) are in $\overset{o}{A}$.   Ivey refined

this relation and obtained[32]:

$$\lambda_{max} = 703 \, d^{1.84}$$

A number of other absorption bands in irradiated alkali halides

have been attributed to electron excess centres, where the electrons

are trapped at aggregates of vacancies.   The absorption band energy

of these centres also varies with lattice size.   Models for many of

these centres are still uncertain, but the M-band has been shown to

be two adjacent F-centres[33].

<u>ii. Magnetic Resonance Work on the F-centre</u>

The e.s.r. spectrum of an F-centre is usually a broad line of

50-700 gauss from points of maximum slope, with g-values slightly

less than the free spin value.   The line widths and g-values of

F-centres in the alkali halides are listed in table 3;1.   The

origin of the broad line was first satisfactorily explained by Kip,

Kittel, Levy and Portis[34], who attributed it to unresolved hyperfine

coupling to the surrounding shells of ions.   For a number of alkali

halides the hyperfine interactions have been resolved, e.g. those for

sodium fluoride[35] and lithium fluoride[36].

Table 3:1

The E.S.R. Line Widths and g-values for F-centres in Alkali Halides

Halide	Line Width (gauss)	g-value (38)	No of Shells Resolved	Ref
LiF	150	2.0018	1;2	37
LiCl	57	2.0018	0	37
LiBr		1.9997	0	38
NaF	220	2.0001	1;2	37,39
NaCl	140	1.9978	0	37
NaBr	300	1.9846	0	37
KF	100	1.9964	0	35
KCl	46	1.9958	0	34
KBr	125	1.9829	0	34,36
KI	210	1.9649	0	36
RbCl	420	1.9804	0	40,41
RbBr	380	1.9673	0	40
RbI	640	1.9494	0	44
CsCl	700	1.968	1	42
CsBr		1.9586		38
CsI		1.958		38

‒ ‒ ‒ ‒ ‒ ‒ ‒ ‒ ‒ ‒

E.S.R. spectra of F-centres have also been reported in the alkaline earth fluorides[43], sodium hydride[44] and sodium azide[45].

The use of E.N.D.O.R.[46] enables the resolution of the F-centre spectra to be improved, and coupling to up to eight shells surrounding the centre have been observed. Table 3;2 lists the coupling to the first few shells of ions, for F-centres in alkali halides with the sodium chloride structure.

Table 3:2

Hyperfine Interactions of the Shells of Ions Surrounding F-centres

Halide	Temp. °K	Hyperfine Coupling to the Ions (Gauss)						Ref.
		Cations			Anions			
		Shell	a	2B	Shell	a	2B	
LiF	1.3	1	13.94	2.28	2	37.80	10.67	37
		3	0.18	0.48	4	0.17	0.89	
		5	0.10	0.18	6	0.62	0.49	
LiCl	1.3	1	6.8	1.22	2	4.01	0.64	37
		3	0.74	1.48	4	0.18	0.04	
		5	0.07		6	0.07		
NaF	4	1	38.18	2.98	2	34.28	0.64	39
		3	1.07	0.21	4	2.32	0.85	
		5	0.25	0.14	6	0.53	0.36	
NaCl	90	1	22.27	2.1	2	4.46	0.76	35
		3	0.12	0.12	4	0.16	0.04	
		5	0.22		6	0.09	0.04	
KF	90	1	12.24	1.14	2	12.67	2.93	35
KCl	90	1	7.39	0.67	2	2.46	0.35	35
		3	0.11	0.02	4	0.38	0.08	
KBr	90	1	6.54	0.55	2	15.29	1.93	35
		3	0.96	0.02	4	2.03	0.29	
		5	0.06	0.01	6	0.30	0.01	
KI	20	1	5.34	0.44	2	17.66	2.14	35
RbCl	90	1	35.04	3.57	2	2.06	0.27	40
		3	2.21	0.17	4	0.57	0.11	
RbBr	90	1	31.33	2.85	2	13.69	1.43	40
		3	2.00	0.07	4	3.25	0.13	
		5	0.91	0.07	6	0.26	0.05	

iii. General Correlation of F-centres

The correlations of F-centre data by Mollwo[31] and Ivey[32] have

been of great value in assigning colour centre optical bands to

this centre. It was thus decided to look for a similar correlation

which would used in interpreting e.s.r. data of colour centres.

The most characteristic feature of the magnetic resonance data for

F-centres is the isotropic coupling to the first shell of cations,

and hence possible correlations involving this quantity were examined.

To map the electron density in an F-centre from e.s.r. coupling

constants spin densities for the s-orbitals of the first shell of

cations were calculated using the 'atomic' isotropic values for the

alkali metals. These are known from atomic beam measurements

(Table 1;1). Table 3;3 lists the calculated total spin densities

$\rho_{M^+_s}$ in the s-orbital of the cations, for the F-centres in Table 3;2.

This will not be the absolute value since we have used gaseous

atomic values, while the atoms in the crystal are charged and

surrounded by other ions. Since, however, the effects of charge

and the surrounding ions should be similar in all cases it does allow

comparisons to be made. As will be shown later the spin density on

the second and subsequent shells of ions is probably due to spin

polarisation, rather than actual delocalization. The hyperfine

coupling to these outer shells is small in most cases and so in this

model we neglect it. Even the large hyperfine coupling to the

fluoride ion in lithium fluoride does not indicate a large spin-

density, because of the large magnetic moment of the ^{19}F nucleus.

Table 3:3

Spin Densities in the s-orbital of the First Shell of Cations around the F-centre in Alkali Halides

	Crystal	$\rho_{M^+}\%_s$	r_M (Å)	L.P. (Å)	$4\pi r_M^3/(\text{L.P.})^3$
1.	LiF	58.3	1.45	4.017	0.5910
2.	LiCl	28.6		5.13	0.2838
3.	NaF	71.4	1.80	4.62	0.7432
4.	NaCl	41.7		5.628	0.4111
5.	KF	89.2	2.20	5.33	0.8845
6.	KCl	53.4		6.28	0.5408
7.	KBr	48.9		6.59	0.4680
8.	KI	39.0		7.05	0.3822
9.	RbCl	58.2	2.35	6.54	0.5830
10.	RbBr	52.0		6.85	0.5074

Atomic radii (r_M) from J.C. Slater 1964 J. Chem. Phys. **41** 3199
Lattice parameters (L.P.) from Landolt-Bornstein Tables Vol 1
part 4, Springer, Berlin, 1955.

— — — — — — — — — —

We then assign the electron density not in the s-orbital of the cations either to the cavity or to the p-orbitals of the cations. Since unpaired spin density in the p-orbitals will place a significant amount of spin density in the cavity, these two pictures need not be different. The energy of an electron in a p-orbital on the cation which is orientated such that it would place spin density in the vacancy will be strongly dependent on the crystal fields in the cavity. To a first approximation the wave function of the F-electron can be described:

$$\psi_F = x\,\psi_{cav.} + y\,\psi_{M_s^+}$$

$$x^2 + y^2 = 1$$

The relative sizes of x and y are determined by a large number of

factors. Two possibly important factors are: 1. The electron

affinity of the cation and 2. The electron affinity of the cavity.

1. The electron affinity of the s-orbitals on the cation decreases

from lithium to rubidium, but the value of $\rho_{M^+_s}$ increases from

lithium to rubidium (Table 3;3). The value of $\rho_{M^+_s}$ increases with

increasing size of the s-orbital on the cation relative to the

lattice size, which may indicate that the hyperfine coupling depends

on the volume of s-orbital available to contain the unpaired electron.

2. The electron affinity of the vacancy depends on the opposing

factors of potential and kinetic energy. The larger the cavity the

lower the kinetic energy of the electron and hence the higher the

electron affinity of the cavity. However, the larger the cavity,

the lower the potential energy and this reduces the electron

affinity of the cavity. A plot of $\rho_{M^+_s}$ against lattice parameter

(Fig. 3;1) shows that the spin density in the s-orbitals of the

cation falls with increasing size of cavity. This may indicate

that the spin density in the s-orbitals of the cation falls with

increasing size of cavity, and hence that the kinetic

energy effect predominates over the potential energy and also,

perhaps, the electron affinity of the s-orbitals on the cations.

Fig. 3;1 as it stands can be used as a correlation for F-centres,

centres with the same cation falling on straight lines, which are

roughly parallel to the lines for other cations. A better

correlation has been found, however, for when $\rho_{M^+_s}$ is plotted

Fig 3;1

Plot of Percentage Apparent s-character (ρ_{M_s}) on the Cations against the Lattice Parameter
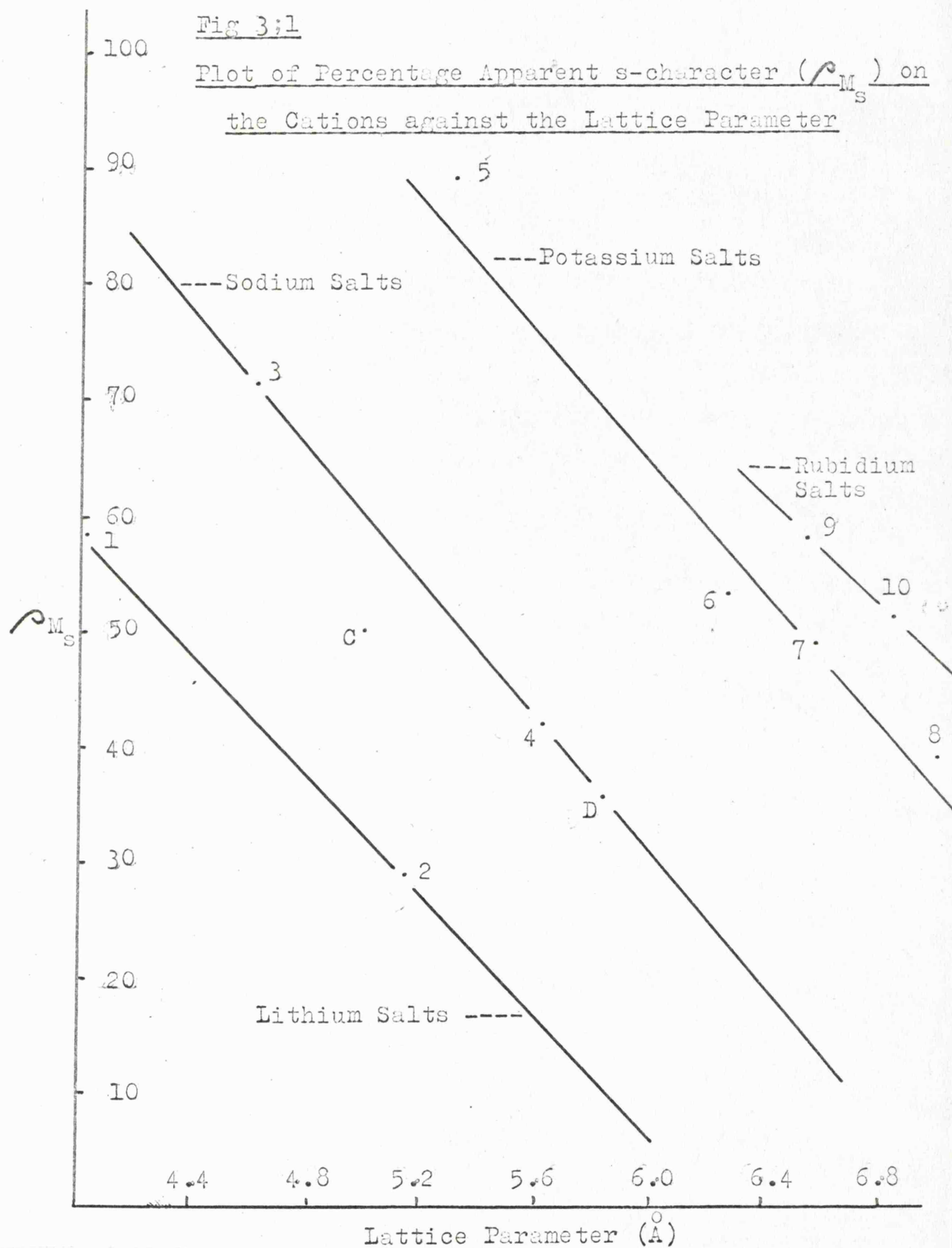
against the cube of the ratio of the atomic radius (r_M) of the cation to the lattice parameter (L.P.) (i.e. $r^3_M/_{(L.P.)^3}$) all the F-centre results fall on a straight line. Since this ratio is proportional to that of the volume occupied by the outer s-orbitals of the cations to the volume of the unit cell, we have plotted in fig. 3;2 $\rho_{M_s^+}$ against $4\pi r^3_M/_{(L.P.)^3}$. It is interesting to note that this plot passes through the origin, and when $\rho_{M_s^+}$ = 100% the volume ratio is unity. This again suggests that the size of the outer s-orbital is important. Further the electron is distributed in such a manner that increasing the size of the s-orbital relative to the volume of the unit cell has the effect of incorporating more of the electron in the s-orbital and hence increasing the hyperfine coupling.

The use of this correlation (Fig. 3;2) will be discussed . further when F-centres in non-alkali halides are considered. It is found that this correlation is satisfactory for crystals which have the sodium chloride structure, but only approximately true if the structure differs markedly from this.

iv. The Effect of Temperature and Pressure on the Isotropic Coupling to the First Shell of Anions

Cooling the crystal or applying a hydrostatic pressure decreases the lattice size and it follows from the above discussion that the isotropic coupling to the cation would be expected to increase. Table 3;4 lists the isotropic coupling of the cations, at a number of temperatures, for F-centres in four alkali halides.

APPARENT S CHARACTER ON CATION AGAINST $\frac{4\pi r^3}{(LP)3}$

$\frac{4\pi r^3}{(LP)3}$

$\alpha(M_s)$ %

48
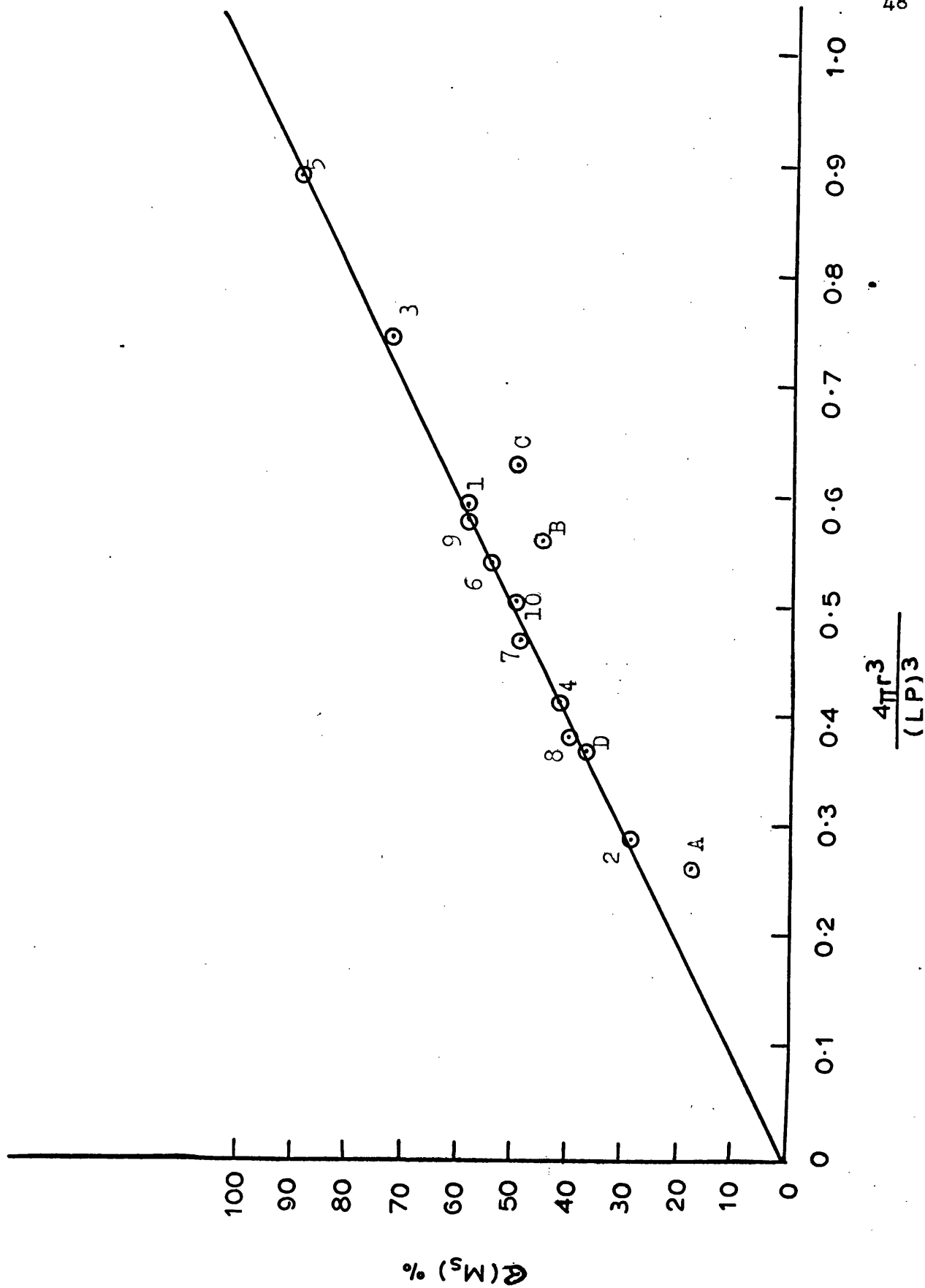
In all cases the hyperfine interaction decreases on cooling. On

inrease in pressure, however, the coupling does increase slightly[47].

A cation in the first shell surrounding the F-centre is

surrounded by five anions. These anions will decrease the electron

affinity of the outer s-orbital of the cation, and this coordination

effect will increase as the lattice is compressed. This effect

will oppose the other effects mentioned above which would otherwise

have produced a larger increase in coupling. In the case of cooling

the lattice this will further increase the effect of coordination

by reducing ionic movement.

<div align="center">Table 3:4</div>

Hyperfine Coupling to the First Shell of Cations at Various
<div align="center">Temperatures</div>

Temperature	NaCl	KCl	KBr	KI	Refs.
1.3°K	21.95	7.35			37
20°				5.32	35
90°	22.27	7.41	6.53	5.39	35
300°		7.49	6.71		35

— — — — — — — — —

v. Anisotropic Coupling in F-centre E.S.R. Spectra

The model of Kip et al[34], assumed that the electron could be

described by a molecular orbital of the form:

$$\psi \ = \ ^1\!/\!\sqrt{6} \ \sum_i c_i \phi_i$$

where ϕ_i is an s-atomic orbital on the ith cation, which in the

crystal will be polarised by the asymmetric crystal field which

exists near the vacancy. This can be taken into account by an admixture of p-orbital character. Inui and Uemura[48] and Kojima[49] have made quantitative calculations for the F-centre in lithium fluoride using linear combinations of s- and p-orbitals, and obtained good agreement with parameters obtained from the optical spectrum.

For a typical anion vacancy, e.g. in potassium chloride (Fig 3;3) the potential in the vacancy is not spherically symmetrical, but the chloride ions repel the F-electron and the potassium ions attract it. The shape of the orbital is thus defined by the crystal parameters. The spatial distribution of the electron can, in principle, be determined from the experimental anisotropic coupling to the anions. Although such calculations involve a number of approximations, they should allow some qualitative conclusions to be drawn.

One simple model of the F-centre places the electron either in cation s-orbitals or in the cavity[50], with the electron density spherically symmetrical in the cavity. In this case the spin density not on the cations can be considered acting from the centre of the cavity so long as the charge is considered to be contained in the cavity and not beyond. A point-dipole approximation can then be used to calculate the anisotropic 2B term, using the anisotropic part of the spin Hamiltonian:

$$\underline{B} = g_e \beta \, g_n \beta \, n \, \frac{(3\cos^2\theta - 1)}{r^3}$$

The value of 2B was found by summing the effect of the electron at the centre of the cavity, and the electron density, considered as a point

Fig. 3;3
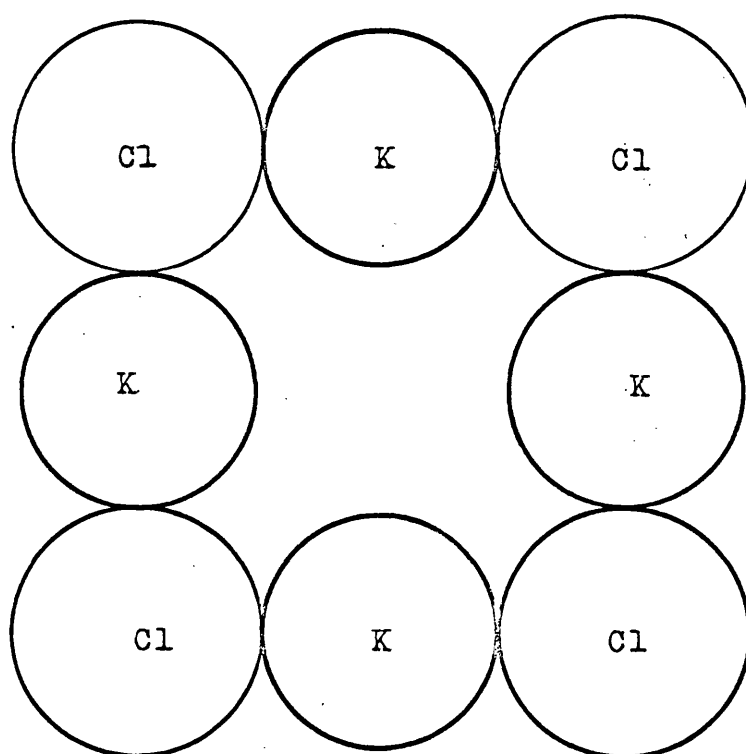
An Anion Vacancy in a Potassium Chloride Lattice

Assuming no Distortion of the Lattice

charge on each of the other five cations. The values obtained as a percentage of the experimentally measured 2B term are shown plotted in fig. 3;4. The choice of the anion radius as abscissa is purely arbitrary and no significance should be attached to the straight lines drawn through the points. From this fig. it is clear that the simple model is inadequate.

If we now lift the restriction of spherical symmetry we can include spin density in p-orbitals on the cation. Unfortunately the 2B terms for alkali metals, although known from gas phase work (Table 1;1), are possibly inappropriate since the spatial distribution of the p-orbitals will be affected by the lattice more than that of the s-orbitals. Using the 2B values for atomic sodium and potassium we get the percentage p-character on the metal given in table 3;5. Also tabulated are the p/s ratios from the p- and s- character both calculated from gas phase results (+) and also the p/s ratio calculated only from the experimental isotropic values (x). The values for the p-character are obviously too high if the gas phase 2B terms are used.

Table 3;5

The Spin Density in the Cation p-orbitals and p/s Ratios

Halides	2B (gauss)	$\dfrac{\rho_M(+)}{p}$	$\dfrac{\rho_M(x)}{p}$	$p/s^{(+)}$	$p/s^{(x)}$
NaF	3.78	227	29	3.2	0.40
NaCl	2.22	132	58	3.2	1.39
KF	1.14	221	11	2.36	0.121
KCl	0.64	124	47	2.32	0.872
KBr	0.54	105	51	2.15	1.04
KI	0.22	85	61	2.19	1.56

+ Using gas phase r^{-3} and $\psi(0)^2$ values
x Using gas phase $\psi(0)^2$ values only.

Plot of $\frac{2B_{calc.}}{2B_{exp.}}$ X 100% against anion radius

Fig 3;4
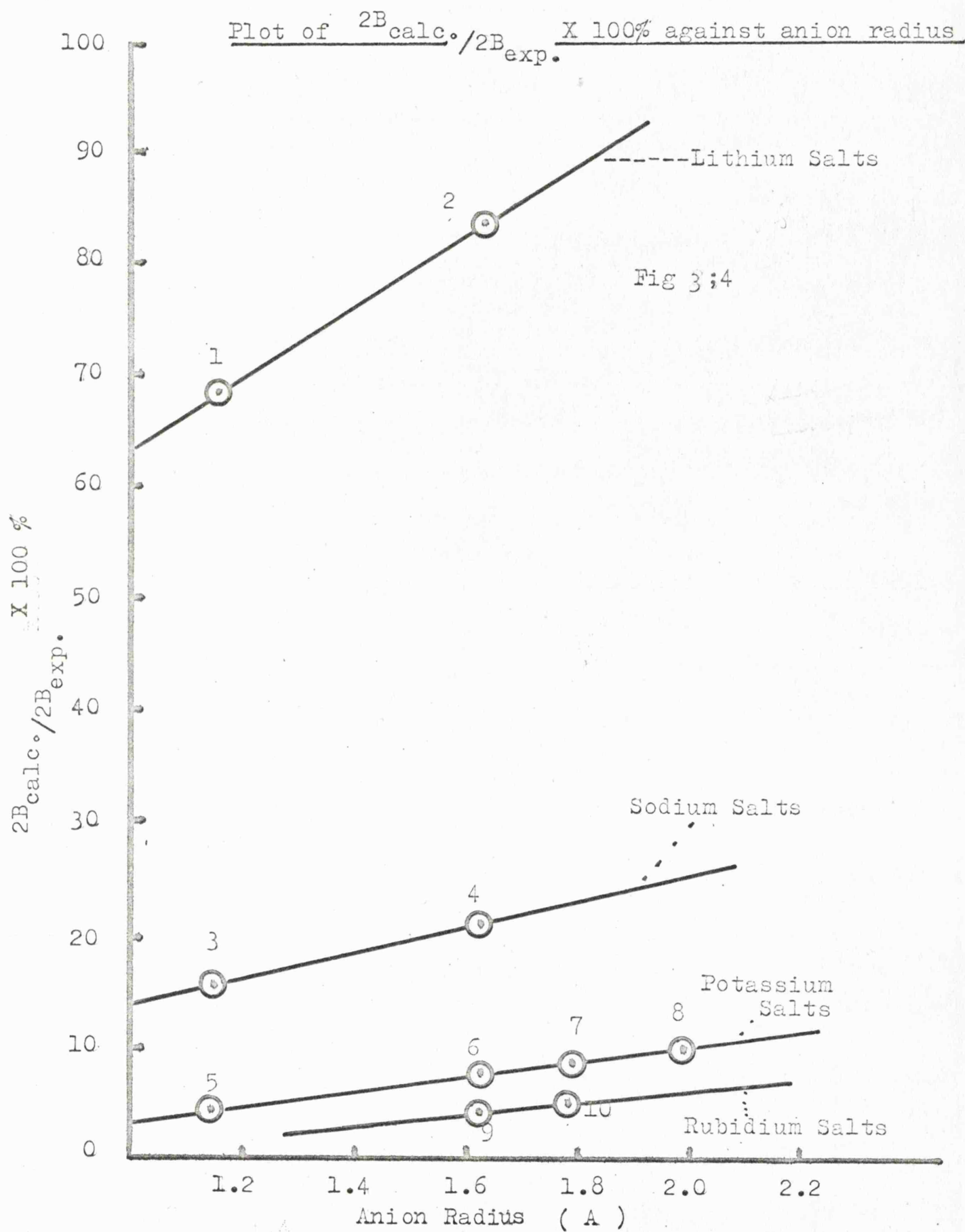
To examine the anisotropic coupling further, we have used orthogonalised Slater orbitals, together with the parameters given by Clementi and Raimondi[51] for all orbitals except the outer np-orbitals, which we have used as our only variable. From the experimental value of the anisotropic coupling and having made a correction for the effect of the electron density on the other cations in the first shell, we have calculated the exponent necessary to produce the correct anisotropic coupling. The results are given in table 3;6. Also given are the exponents expected for the outer s-level of the atom (those for the p-level are expected to be slightly smaller, but were not given by Clementi and Raimondi[51]). Significantly, perhaps, in every case the p-orbitals are contracted relative to the free atom.

<u>Table 3:6</u>

<u>Calculated Exponents for the Outer p-orbitals of the First Shell</u>
<u>of Cations</u>

Halide	LiF	LiCl	NaF	NaCl	KF	KCl	KBr	KI
Exponent Calculated	1.12	0.76	1.48	1.10	1.93	1.23	1.17	1.08
Clementi[51] Exponent(a)	0.64	0.64	0.836	0.836	0.874	0.874	0.874	0.874

a. For the outer ns-orbital

— — — — — — — — — — —

The Clementi-Raimondi parameters apply strictly to an isolated atom, and we have applied them to an ion having a formal charge of + 5/6. However the s-character was also calculated from gas phase values and so we are consistent if not correct in an absolute sense.

From the above considerations it would seem that the F-electron is localized in an orbital which consists of a combination of the s- and p-orbitals of the cations. The p-orbitals are contracted relative to these in the gas phase, which explains the high p-character obtained if the gas phase atomic 2B terms are used. The s-orbitals are also probably contracted, and so in the first part of this discussion we would have over-estimated the s-character. The effect of charge on the s-orbitals, however, should be less than on the p-orbitals.

In view of the many different, but interrelated factors determining the hyperfine coupling, the explanation of the isotropic correlation will be very complicated. At present, therefore, we merely wish to confine attention to its practical use, a point which will be discussed later when the F-centres in non-alkali halides are considered.

vi. Coupling to Other Shells Around an F-centre

Around the F-centre there are six nearest neighbour neighbour cations and twelve anions. The anions also form part of the walls of the cavity (Fig. 3;3), and in fact if the cation is small they may form a major part. They will not, however, have a high electron affinity an so a high spin density on these atoms is not expected. The hyperfine interaction with the second shell of cations is much smaller than with the first (Table 3;2) and so can be neglected to a first approximation. The experimental hyperfine interaction is known also for the anions (Table 3;2), but we have to decide which

of the halide s-orbitals contains the spin density. If it is in

the valence ns-orbital then the hyperfine coupling occurs by a spin

polarisation mechanism. For this orbital the 'atomic' values have

been calculated (Table 1;2). If on the other hand there is actual

delocalization of the unpaired electron, then the unpaired electron

has to go into an outer (n+1)s-orbital and the 'atomic' values are

unknown. However, if the wave function of the corresponding alkali

metal is taken, an approximation to the required value can be

obtained[50]. Using a value of $A_{iso}^{(n+1)s}$ calculated by this method

the spin density in the n+1 s-orbitals of the first shell of halide

ions has been calculated (Table 3;7). The spin densities calculated

using the n+1 parameters are far too large if the earlier discussion

is even qualitatively correct. The spin densities calculated

using the ns-parameters give a more reasonable result, and give some

weight to the assumption that the hyperfine interaction with outer

shells is a spin polarisation effect.

Table 3:7

Coupling to the First Shell of Anions and Spin Densities in the ns- or n+1 s-orbitals

Halide	a	2B	$\rho_{hal}^{(1)}$	$\rho_{hal}^{(2)}$
LiF	37.8	10.67	40	2.7
LiCl	4.0	0.64	28	2.9
NaF	34.28	6.98	37	1.5
NaCl	4.46	0.76	31	3.2
KF	12.67	2.93	13	0.9
KCl	2.46	0.37	18	1.8
KBr	15.29	1.93	21	2.4

(1). The spin densities calc. using A_{iso} for n+1 orbital.

(2) The spin densities calc. using A_{iso} for ns-orbital.

vii. F-centres in Non-alkali Halides

F-centres have been observed in alkaline earth oxides[52], and fluorides[43], in lithium and sodium hydride and sodium azide. In the last three cases the structure is similar to the sodium chloride lattice. The e.s.r. parameters for sodium hydride[44] and azide[45] are given in table 3;8. In the case of lithium hydride only a broad line was observed, but Lewis and Pretzel[53] have obtained the spin densities on the first shell of cations by comparing the line widths of the F-centre in ^{6}LiH and ^{7}LiH. The spin density $\rho_{M_s^+}$ has been calculated and also the factor $4\pi r^3/_{(L.P.)^3}$. Data for these three crystals has been incorporated in fig. 3;2, as points A, B, and C (see table 3;8). These points all fall below the correlation line. Thus in all cases the correlation has over-estimated the hyperfine coupling to the cations. In all these crystals it is possible that there could be more distortion of the lattice around the vacancy than with the alkali halides.

Table 3;8

Spin Densities ($\rho_{M_s^+}$) and other Parameters of F-centres in Non-Alkali Halides

	NaN$_3$ (A)	LiH (B)	NaH (C)
g-value	2.003	2.004	1.9979
a(M) exp. (gauss)	9.1		26.5
a(M) calc. (gauss)	14.3		33.5
$\rho_{M_s^+}$ %	17	45	50
r$_m$ (Å)	1.80	1.45	1.80
L.P. (Å)	6.56	4.085	4.88
$4\pi r^3/_{(L.P.)^3}$	0.2596	0.5620	0.6306

II. The V_k-centre in Alkali Halides and other Lattices

If an alkali halide is γ-irradiated at 77°K one of the species

which can be observed in the e.s.r. spectrum is a Hal_2^- radical.

This radical is known as the V_k-centre. The yield of this centre

increases if there are electron traps incorporated into the halide

lattice. This centre is thus an electron deficient centre. It is

oriented along the 110 axis of the crystal, which is the expected

orientation if the formation of this radical involves the formation

of a halogen atom which attacks a neighbouring anion, both atoms

staying close to their normal lattice positions. In fact the

formation of the chemical bond reduces slightly the distance

between the nuclei.

The first reported work on this centre was by Castner and

Kanzig[54]. The effect of the lattice size was studied by Bailey[55]

who examined the F_2^- centre in lithium, sodium, potassium,

rubidium and caesium fluorides. He showed that the isotropic

coupling to the fluorine nucleus, and the g-values, decreased with

lattice size, while the anisotropic coupling increased slightly.

This behaviour was attributed to changes in the F-F bond distance.

It has also been possible to obtain Cl_2^- and Br_2^- in irradiated

ammonium halides[56]. These matrices yielded similar hyperfine

coupling data to that of the radicals in alkali halide crystals,

but the e.s.r. lines were broader. The ultra-violet bands

associated with the V_k-centre are similar in all lattices showing

that unlike the F-centre the matrix has only a second order effect

on the energy levels of the radical. The experimental results
for the V_k-centres in their respective halides are given in table
3;9.

Mixed V_k-centres, such as FCl^-, FBr^-, and $ClBr^-$ have been
prepared. In the case of FCl^-, FBr^- and FI^-, the radicals are
oriented along the 111 directions[58], the radical occupying one
anion and one interstitial site. Schoemaker has calculated the
spin densities on the nuclei in F_2^-, FCl^-, FBr^- and FI^- (Table 3;9).
The total spin density is about 125%, which he attributes
to neglect of overlap terms in the normalisation. There is in
fact a sign ambiguity in the experimental results and other workers
using the other sign combination of the experimental coupling
tensor have obtained a total spin density of about 100%. Bailey[55]
and Schoemaker[58] argue that for the same species trapped in
different crystals, if $A_\perp$ and $A_{//}$ vary in the same sense then they
have the same sign, but if they vary in the opposite sense then they
have opposite sign. Bailey showed that $(A_{//}, A_\perp)$ for F_2^- varies
from (887, 58) to (908, 28) going from lithium to potassium fluoride,
and hence he claims the signs are opposite.

The molecular orbital structure of the bonding shell in these
centres can be written:

$$(\sigma_g)^2 (\pi_u)^4 (\pi_g)^4 (\sigma_u)^1$$

the subscripts u and g are only applicable to the homonuclear
species, but the general form of the orbital is unchanged. The

Table 3;9

Experimental Results for X_2^- and FX^- species

a. Coupling Constants and Spin Densities in X_2^- Species

Lattice	X_2^-	$A_{//}$	$A_\perp$	$c^2_{F(s)}$	$c^2_{F(p)}$	Σc_i	Ref
KF	F_2^-	908	-28	0.016	0.586	1.204	54
KCl	Cl_2^-	101	12.5	0.024	0.582	1.212	54
KBr	Br_2^-	450	79	0.019	0.586	1.210	54
KI	I_2^-	387	100	0.020	0.563	1.166	57

b. Coupling Constants and Spin Densities of FX^- in KCl Lattice[58]

Species	$c^2_{F(s)}$	$c^2_{F(p)}$	$c^2_{X(s)}$	$c^2_{X(p)}$	Σc_i
FCl	0.011	0.562	0.032	0.700	1.305
FBr	0.008	0.538	0.030	0.720	1.297
FI	0.006	0.498	0.035	0.703	1.242

c. g-values for the Species X_2^- and FX^-

Lattice	Species	$g_{//}$	$g_\perp$	g_{iso}	Ref.
KF	F_2^-	2.0020	2.0218	2.0155	54
KCl	Cl_2^-	2.0012	2.0426	2.0284	54
KBr	Br_2^-	1.9833	2.169	2.1071	54
KI	I_2^-	1.913			57
KCl	FCl	2.0018	2.030	2.0206	58
KCl	FBr	1.9891	2.125	2.0797	58
KCl	FI	1.9363			58

All A values in gauss.

— — — — — — — — — — — — — — —

unpaired electron is in an antibonding σ-orbital. This is

consistent with the instability of these species. Indeed only

FI⁻ is stable at room temperature.

The decrease in the spin density on fluorine down the series

FCl⁻, FBr⁻, FI⁻ is characteristic of the unpaired electron in an

antibonding orbital[59].

The g-values given in table 3;9 show that there is coupling

with filled orbitals when the magnetic field is perpendicular to

the radical, but, when it is parallel, coupling is not possible

unless there are empty d-orbitals available. Hence only with the

bromide and iodide species is $g_{//}$ much less than the free spin value.

These results are consistent with a radical having the unpaired

electron in an orbital along the bond axis.

III. Colour Centres in Sodium Cyanide

i. The Structure of the Sodium Cyanide Crystal

At room temperature sodium cyanide has an averaged sodium

chloride lattice, with a cubic lattice constant of 5.83 ± 0.005 Å [60].

Specific heat measurements exhibit two regions of anomalous heat

capacity with maxima at $172^{\circ}K$ and $288^{\circ}K$ [61]. The upper transition

is related to the change from the low temperature orthorhombic form

to the high temperature cubic form. The low temperature ortho-

rhombic form is a distorted sodium chloride lattice with four

rectangular faces 6.01 by 5.61 Å, and two rhombic faces with edges

6.01 and angle 76.9°. Cyanide ions are oriented with their axes

in the direction of the major axes of the rhombic faces.

Wells [62] suggests that at room temperature the cyanide ions

are randomly oriented along the four body diagonals of the unit

cube, free rotation being unlikely for steric reasons. A similar

situation occurs with potassium cyanide, but the phase transition

between the cubic and orthorhombic forms occurs at about $167^{\circ}K$.

In the cubic form the cyanide ions cannot remain parallel to each

other, but there is disagreement as to whether there is free

rotation. Pauling [63] favoured free rotation, while Frenkel [64]

proposed that above the phase transition temperature the cyanide

ions still behave as torsional oscillators, but are free to take

up one of several equivalent positions. A nuclear magnetic

resonance study of the effect of reorientation of the cyanide ion

on the field gradient near the sodium ions in sodium cyanide, by

Coogan and Gutowsky[65] gave some evidence for partially free rotation

of the ions above the phase transition temperature. The activation

energy for the reorientation is of the order of 6 Kcal/mol. From

this they calculated that the orientation jump frequency was about

$5x10^8$ sec^{-1} at the phase change.

It would seem therefore that at room temperature the ions

although not rotating freely are nonetheless reorientating themselves

rapidly. The short transition times for ultra-violet and e.s.r.

spectroscopy, however, are such that these techniques will probably

monitor random, but fixed ions.

ii. Experimental Results

The presence of an F-centre in X-irradiated sodium cyanide was

reported by Isetti and Neubert[66]. The only other cyanide which

has been examined is potassium cyanide where an F-centre was also

produced on X-irradiation[67]. In both cases the centres were

identified by their characteristic ultra-violet spectrum. Using

the ionic cyanides without further purification, we have found

that only sodium cyanide colours on γ-irradiation. Potassium

cyanide was found to contain an appreciable amount of iron impurity

and did not colour even after prolonged irradiation. As suitable

methods of purification were not available, and also since

the small magnetic moment of the ^{39}K nucleus would make observation

of the hyperfine interaction to the cations unlikely, only the

F-centre in sodium cyanide has been studied.

a. The Optical Spectrum of Irradiated Sodium Cyanide

Isetti and Neubert[66] found three absorption bands in X-irradiated sodium cyanide at 530 mµ , 360 mµ .and '285 mµ , with a shoulder at 251 mµ . The colouration was unstable and bleached with a half-life of about 30 minutes. On bleaching the band at 530 mµ shifted and there was evidence for two bands, one at 540 mµ and the other at 457 mµ . The λ_{max} for an F-centre in sodium cyanide calculated from Ivey's rule[32] is 505 mµ . They concluded that the band at 457 mµ was the F-band and that the band at 540 mµ might be the Z_1 band, although the evidence for the latter assignment was very poor. We have repeated the optical work using γ-irradiation to produce the colour centres in powdered sodium cyanide. Measuring the diffuse reflectance absorption broader bands than those of Isetti and Neubert were obtained, but there were well defined maxima at 520 mµ and at 360 mµ and on bleaching the bands did not shift. The ultra-violet spectra data for irradiated sodium cyanide, together with Susman's results[67] for potassium cyanide are given in table 3;10. The λ_{max} for the F-band in these two cyanides calculated from Ivey's rule are also given.

Irradiation at 77°K reduces the intensity of both the F-band and the band at 360 mµ compared with the intensity of the bands when the irradiation of the sample was carried out for the same time, but at room temperature.

Table 3;10

Optical Band Wavelengths for F-centres in Sodium and Potassium Cyanide

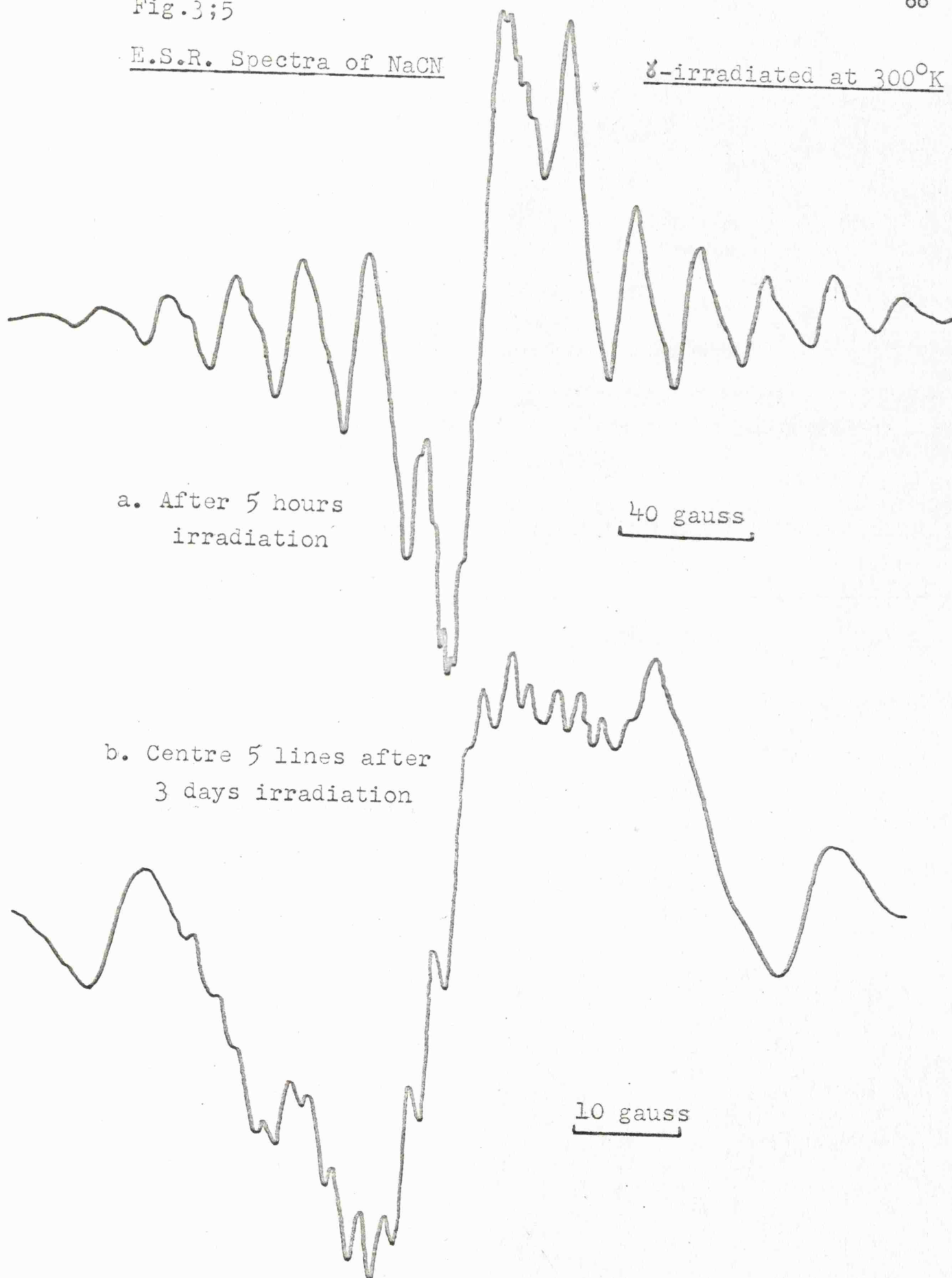|		NaCN	KCN
λ_{max}	a. This Work	520mμ	
	b. Ref 66, 67	457mμ	589mμ
λ_{max} (Calc.)		505mμ	619mμ

b. Electron Spin Resonance Spectra of Irradiated Sodium Cyanide

Powdered sodium cyanide was irradiated for varying lengths of time and the e.s.r. spectra recorded. With low irradiation times the spectrum consists of a series of lines 19.5 gauss apart with fine structure on the central three lines (Fig 3;5a) On further irradiation the central lines become less well resolved and the super-hyperfine structure can be seen more easily (Fig 3;5b). The time required to produce a particular spectrum was strongly sample dependent. For example the spectrum shown in fig 3;5b was observed for some samples which had been irradiated for only 10 hours. To eliminate such effects all comparison experiments were performed with samples from sealed ampoules filled at the same time.

The two sets of hyperfine coupling are not caused by the same species, since the relative intensities of the two signals are dependent on both irradiation time and the sample used. The species causing the larger splitting (Species A) has a hyperfine coupling of 19.5 gauss with a central g-value, when corrected to second order in the spin Hamiltonian, of 2.0019. The second species (Species B) is the dominant species after 10 days

Fig.3;5

E.S.R. Spectra of NaCN   γ-irradiated at 300°K

a. After 5 hours
   irradiation   40 gauss

b. Centre 5 lines after
   3 days irradiation

                                  10 gauss

irradiation (Fig.3;6). The hyperfine coupling is about 2.6 gauss, but varies from 2.0 to 2.8 gauss. The central g-value for the species "B" varies with irradiation time, but at all times is greater than the free spin value (2.0023).

The e.s.r. spectrum alters markedly on cooling. At $16^{\circ}C$ both sets of hyperfine lines become less well resolved and on further cooling the broad central line becomes resolved into a set of lines with an average splitting of 8.1 gauss, and central g-value of 2.0035 (Species C). The splitting was not constant (Fig.3;7) varying from 7.3 gauss between the centre two lines to 9.0 gauss between some of the outer ones. On further cooling this spectrum is again broadened out, and at temperatures below about $100^{\circ}K$ the spectrum is as shown in fig.3;8, and for reasons discussed in the next chapter this spectrum was assigned to the V_k centre $(CN)_2^-$. This species can also be observed in irradiated potassium cyanide. The experimental coupling constants and g-values for species A, B and C are given in table 3;11.

Table 3;11

Experimental E.S.R. Data for Species A, B, and C in NaCN

Species	A_{iso}(gauss)	g_{iso}
A	19.5 ± 0.5	2.0019
B	2.5 ± 0.5	> 2.0023
C	8^+ ± 2	2.0035

+ Not isotropic.

Central Part of the E.S.R. Spectrum of Sodium Cyanide γ-irradiated for 10 Days

10 gauss
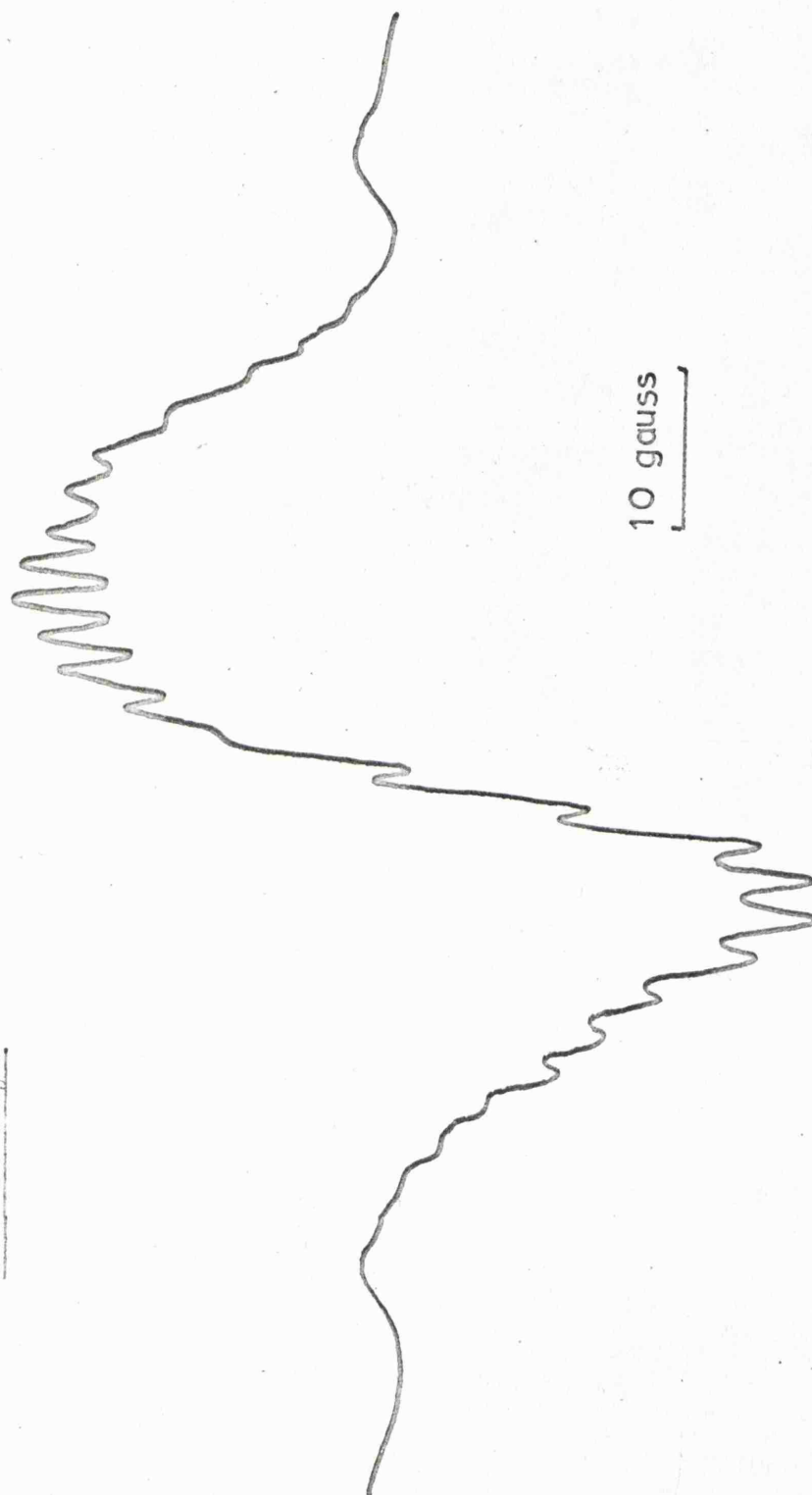
FIG. 3 ; 6

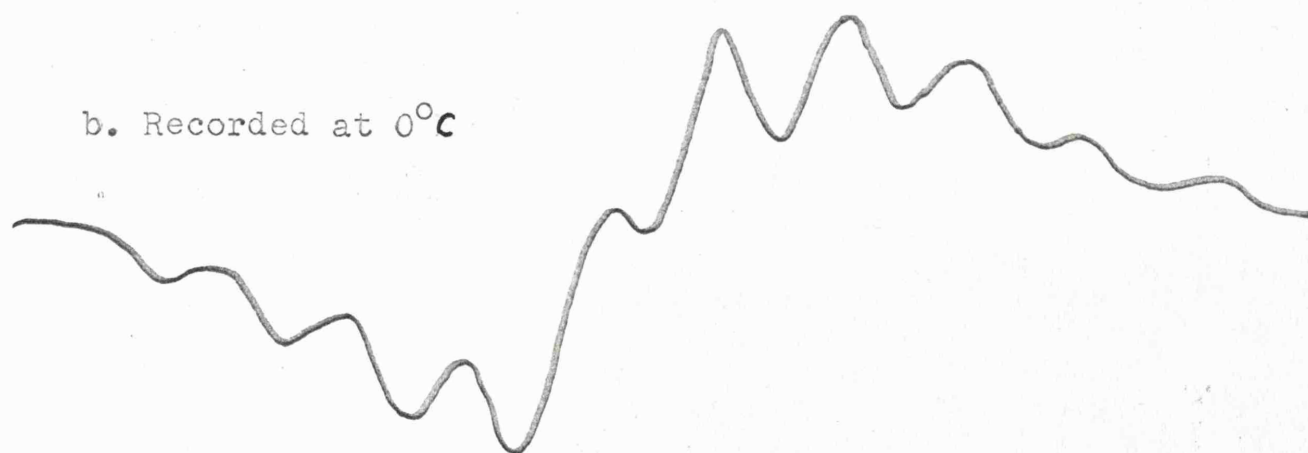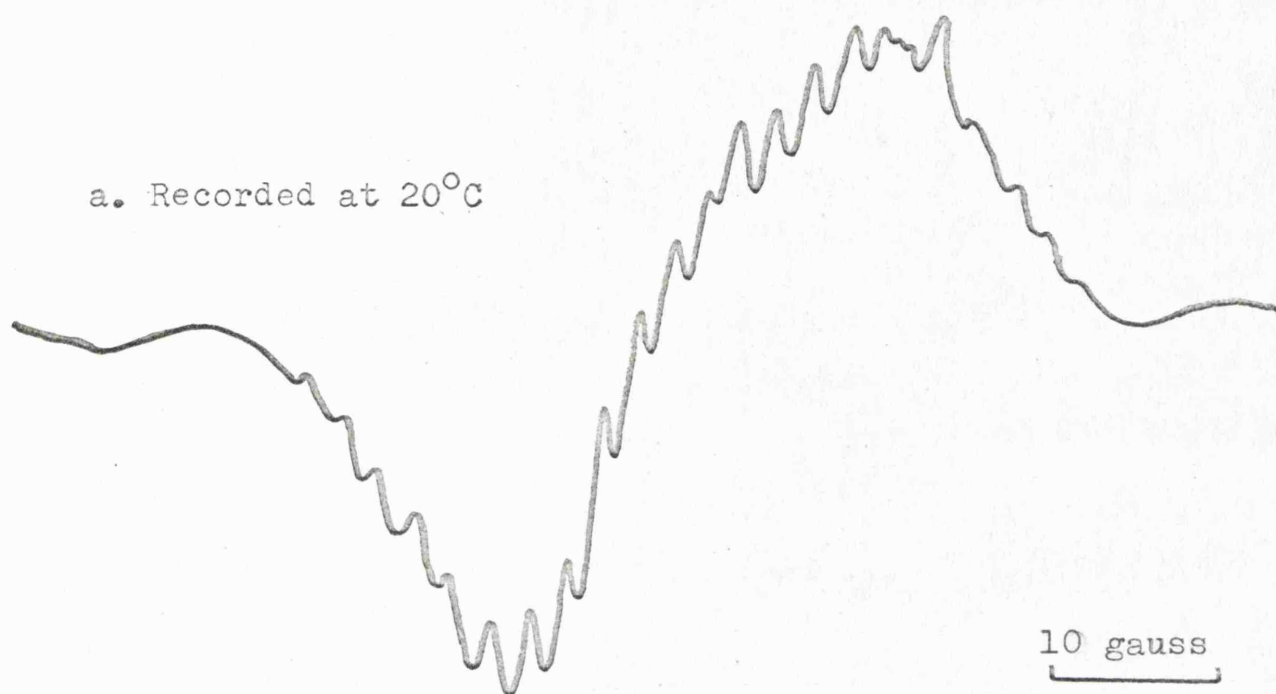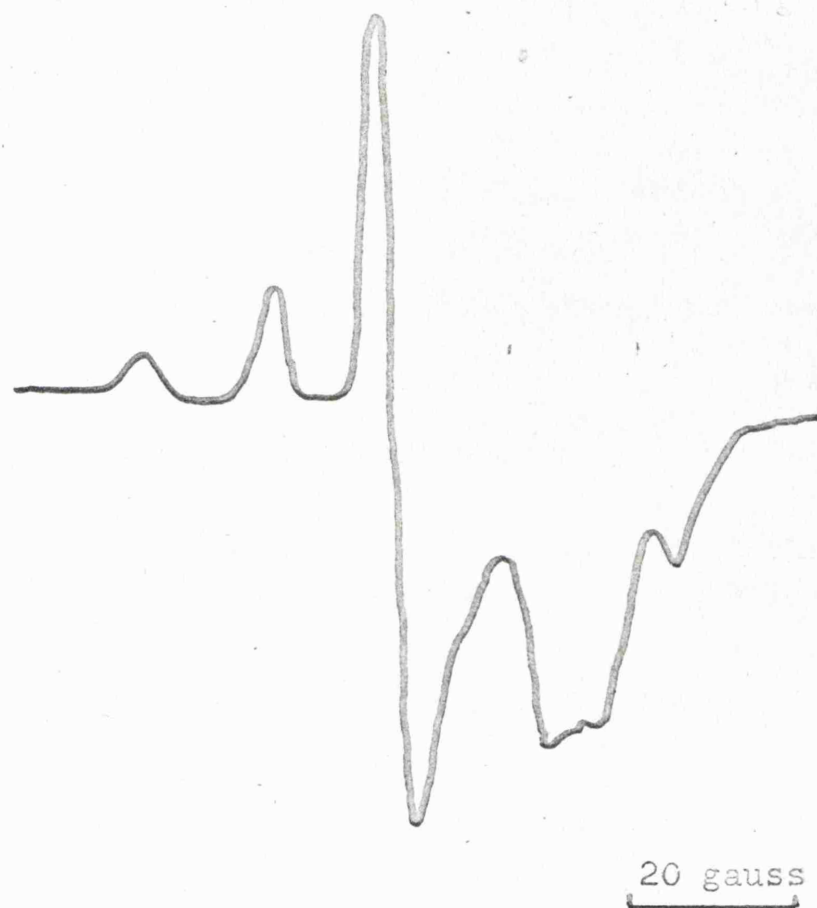E.S.R. Spectrum of NaCN γ-irradiated for 40 hours
at Room Temperature

a. Recorded at 20°C

10 gauss

b. Recorded at 0°C

Fig 3;8

20 gauss

E.S.R. Spectrum of Sodium Cyanide δ-irradiated for
10 hours at $300^{O}K$ Recorded at $77^{O}K$

When sodium cyanide is irradiated at 77°K and warmed to room temperature the e.s.r. spectrum is almost entirely that of species A, (Fig.3;9). On cooling the sample the spectrum becomes less well resolved until at about 5°C the spectrum is identical to that of the room temperature irradiated samples at this temperature.

If the sample is irradiated at 77°K and the spectrum recorded without warming, the spectrum is identical to that shown in fig.3;8. On warming to room temperature and then recooling to 77°K the spectrum is again identical to that in fig.3;8.

On cooling the sample down below room temperature the strength of the absorption decreases markedly, for the low temperature irradiated samples, and so species C which was observed at about 5°C is probably not associated with species A. In the room temperature irradiated samples the signal strength did not fall so much on cooling.

The low temperature irradiated samples luminesced when warmed above 77°K. The light given off appeared blueish, but was not strong enough to observe in an optical spectrometer. This luminescence would indicate that there was some chemical reaction taking place when the irradiated crystal was warmed. Since the e.s.r. spectrum was essentially the same before and after warming neither the initial or the final products of the reaction causing the luminescence were observed in the e.s.r. spectrum.

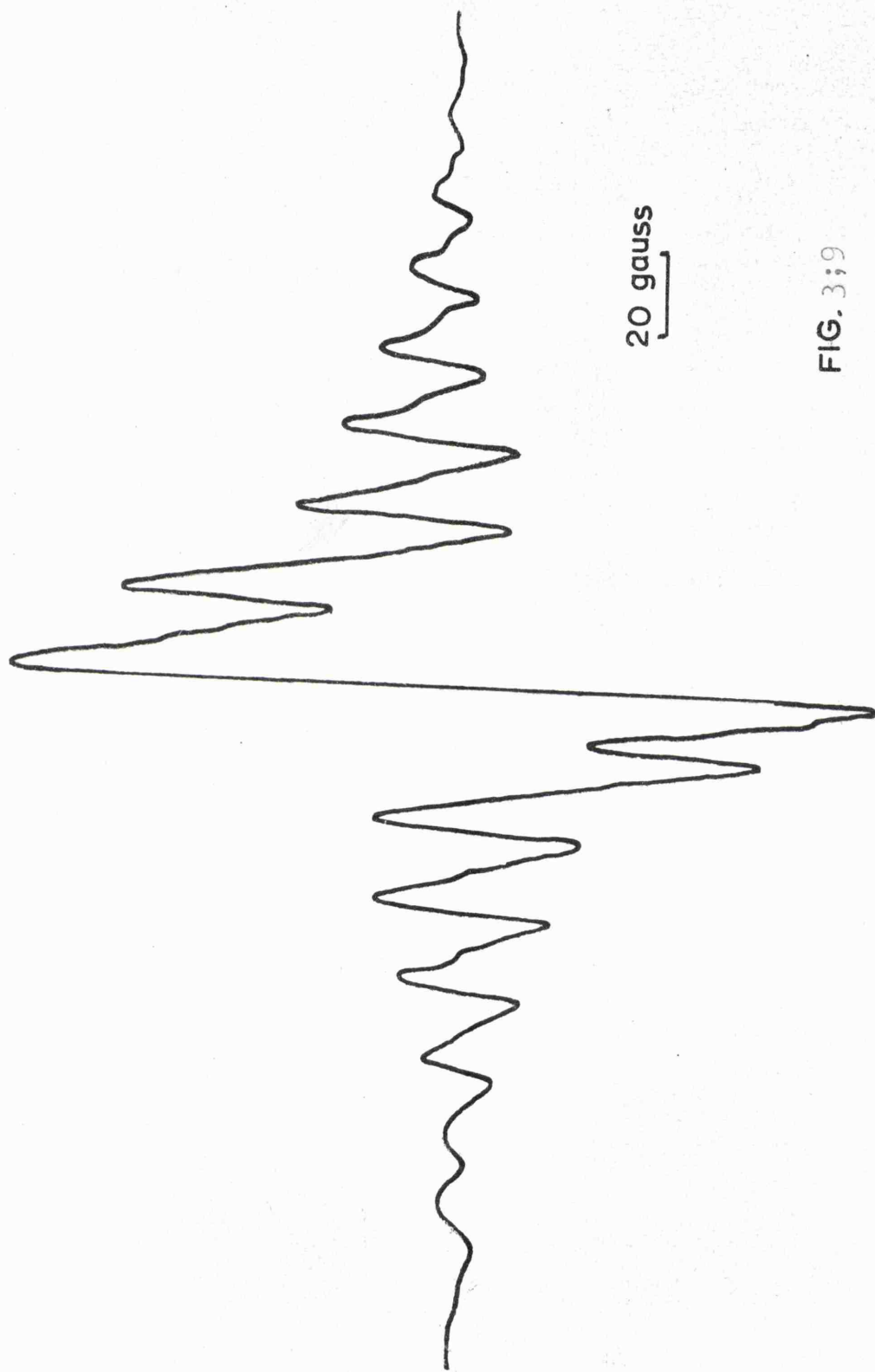E.S.R. Spectrum of NaCN after -irradiation at 77°K for 10 hrs.

20 gauss

FIG. 3;9

The F-centre in NaCN recorded at 300°K

c. The Effect of Impurities

The samples used in the foregoing experiments were all prepared in an oxygen free dry box to prevent the hydrolysis or oxidation of the cyanide. If the cyanide is handled in the atmosphere, especially as a powder, it fails to colour on irradiation or yield the normal room temperature e.s.r. spectrum. Pressed discs of sodium cyanide also failed to colour on irradiation.

If the exposure to the atmosphere is only slight the e.s.r. spectra of species B is predominant even in the samples irradiated at $77^{\circ}K$. However, on prolonged exposure to the atmosphere only a broad featureless e.s.r. line is detected after irradiation.

This contamination of the samples was a very serious problem, even for samples which had been prepared in a dry-box. Different results were obtained for each batch of samples which were made up, and further investigations should employ zone-refined samples. In the absence of a suitable zone-refining apparatus a single crystal was grown in the Stockbarger furnace, as explained in chapter 2. The resulting crystal cleaved well for a soft crystal, but despite all precautions in handling, the compound still did not give on irradiation one e.s.r. signal when the sample was at room temperature. Species A was present, and also a further broad line around the free spin region. The wing lines of species A could easily be seen, but were not strong enough to enable the anisotropic values to be obtained. Despite the lack of sucess in preparing a pure single crystal the crystal obtained did show

that species A gave apparently isotropic wing lines of the same
splitting as the powdered sodium cyanide.

iii. Discussion

a.Identification of the F-centre in Sodium Cyanide

The visible spectrum of irradiated sodium cyanide showed that
there was probably an F-centre in the crystal.   The e.s.r. spectrum
showed two sets of isotropic lines (Species A and B), and also
probably a further species causing a broad line underneath the
central lines.

For an F-centre in sodium cyanide nineteen lines would be
expected from interaction with six nearest neighbour sodium ions.
A g-value below that of the free spin value is expected, and since
sodium cyanide has the sodium chloride lattice we would expect the
e.s.r. data for the F-centre to fit the previous correlation (Fig 3;2)
For species B up to thirty lines have been observed, the central
g-value shifting with irradiation time, which makes the measurement
of the central g-value difficult.   The g-value is however likely
to be higher than that of free spin.   The hyperfine splitting of
2.6 gauss would give a spin density of 5% in the s-orbitals of the
sodium ions, which when placed on the general correlation line,
with the correct value for the abscissa of 0.3698, is well off the
line.   Species A on the other hand has a central g-value of 2.0019
and the total spin density in the s-orbitals of the sodium ions is
37%, which fits very well on the correlation line (Fig.3;2 point D).
Species A is thus assigned to the F-centre.

The change in the spectrum recorded when the sample is below $16^{\circ}C$ can be attributed to the effect of the phase change at $16^{\circ}C$[61]. This change occurs rapidly when the temperature is lowered, and is reversible.

b. The Structure of the F-centre

The experimental parameters of the F-centre are given in table 3;12. The exact fitting of the data to the general correlation indicates the similarity between the alkali halide lattices and the high temperature form of the sodium cyanide lattice.

Table 3;12

E.S.R. Data for the F-centre and Species B in Irradiated NaCN

Species	A_{iso}(Gauss)	$\left(\dfrac{\rho_{M^{+}}}{s}\right)$ a	$\left(\dfrac{\rho_{M^{+}}}{s}\right)$ b
A. F-centre	19.5	37	
B. (F_2^{+}? centre)	2.6	5	8.2

$r_M = 1.80$ Å   L.P. $= 5.83$ Å $4\pi r_M^3/(\text{L.P.})^3 = 0.3698$

a. For six equivalent cations.   b. For ten equivalent cations.

— — — — — — — — — —

We have attempted to obtain a half life for the bleaching of the F-centre, from the e.s.r. data, using low temperature irradiated samples. The bleaching was, however, strongly sample dependent, and only a rough estimate of the half life could be determined. Isetti and Neubert quote a half life of 27 minutes[66], but our value was of the order of 4 ± 2 hours. The optical band in our samples also bleached with a half life of the same order. This

difference may be due to the difference in energy of the radiation used, but it is more probable that the half life is highly dependent on the purity of the sample, and until very pure samples are available reliable half lives cannot be obtained.

c. The Species B and C

The species B and C remain to be assigned, and there is good reason to consider these two as related. We have tentatively assigned B to the F_2^+-centre, which is an electron trapped at two anion vacancies, for the following reasons:

1. The many lines which are not all equally spaced, but which appear roughly isotropic in the powder, must come from a centre where there is a large number of nuclei of relatively high spin.

2. This species is formed much more readily by irradiation at room temperature, than at 77°K. This is a characteristic of a multiple vacancy centre[68].

3. A similar species has been suggested to explain a similar e.s.r. spectrum in irradiated sodium azide[69],

With an F_2^+-centre there will be ten sodium nuclei which if they were all equivalent would yield thirty-one lines. Work on the triplet M-centre (F_2-centre) in alkali halides showed that two cations had a coupling twice as large as the rest[70]. This may explain why the lines are not exactly equally spaced in this species.

The species C can then be a related centre which can form in the low temperature form of sodium cyanide. The number of lines given by species C is uncertain and the hyperfine coupling is not

constant. Further work on this and the other species will require a single crystal study.

d. The V_k-centre

The V_k-centre in sodium and potassium cyanide $(CN)_2^-$ is a molecular species rather than a physical defect and so discussion of the structure is left until the next chapter, where a single crystal e.s.r. study of the radical trapped in a potassium chloride lattice is reported. The main difference between $(CN)_2^-$ and the halogen V_k-centres is that in the former the unpaired electron is in a π-antibonding orbital and in the latter a σ-antibonding orbital.

Chapter 4

Simple Inorganic Radicals

A. Introduction

Three simple inorganic molecular species have been identified in irradiated alkali cyanides or alkali halides doped with the cyanide ion. These are the methylene imino radical (H_2CN), the hydrogen cyanide negative ion (HCN^-) and the cyanogen negative ion ($CN)_2^-$. These radicals have related structures which can be discussed using Walsh's one-electron molecular orbital schemes[71].

In this chapter the following topics are briefly discussed. I. Simple molecular orbital theory, conjugation, hyperconjugation and the Walsh diagrams. II. The mechanisms for delocalization of spin density and a brief review of the evidence for a hyperconjugative mechanism of delocalization of spin density in radicals with β-protons. Finally the electron spin resonance data for the three radicals mentioned above is described, and the structures of these radicals compared with those of related radicals.

I. Bonding Theory in Simple Radicals

i. Simple Molecular Orbital Theory

Molecular orbitals (m.o's) can be obtained by taking a linear combination of a basic set of atomic orbitals, the nuclei being considered fixed (the Born-Oppenheimer approximation[72]). Each m.o. is thus of the form:

$$\psi_m = \sum_i a_i \phi_i$$

where ϕ_i is the i th atomic orbital

a_i is the coefficient determining the contribution of ϕ_i to the m.o.

The energies of the eigenstates of the molecule are given by
the i th dimensional secular determinant $\left| H_{kl} - ES_{kl} \right| = 0$.
This can often be factorised by symmetry considerations, and a set
of 'symmetrised' m.o's is obtained (ψ_j), which transform as an
irreducible representation of the symmetry group. These 'canonical'
m.o's are useful in discussing the total energy of the system, but
are not individually useful for discussing the many bond additive
properties of the molecule, e.g. bond energies. These orbitals
can, however, be transformed into an entirely equivalent set by
taking combinations of ψ_j's to obtain another set of m.o's χ :

$$\chi_m = \sum_j b_j \, \psi_j$$

These non-canonical m.o's or equivalent orbitals form only a basis
for a reducible representation, like a set of atomic orbitals.
The only restriction on the combination being that a symmetry
operation on one member of the set must transform it into another
member of the set.

The energy of the electrons in a set of m.o's is the sum of
the energy of the electrons in the isolated m.o's and the inter-
action energy of the electrons. If a set of two centre m.o's is
obtained such that the energy of interaction between the electrons
in the different orbitals is weak, then the bonds can be regarded
as localized. If the energy of interaction of electrons in these
two centre m.o's is not negligible, then delocalized orbitals must
be used, or the localized picture corrected to take into account
the delocalization.

Four important factors determine the extent of interaction of localized orbitals; these are symmetry, distance and energy differences between the possible interacting orbitals, and electron correlation effects. The first three factors can be identified with the necessity of overlap between the interacting orbitals. The final factor has two effects[73]; charge correlation, and spin correlation. Thus localized orbitals of the same symmetry interact if they are of similar energy and near each other. In the case of π-systems this interaction can be transmitted along a π-bond, i.e. conjugation.

ii. The Energies of Molecular Orbitals and the Effects of their
Interactions

By solving the secular equation a set of m.o. eigenstates with their corresponding energies can be obtained. If two or more of these m.o's interact their energies are modified. This is shown in fig 4;1 for a simplified case of two bonding orbitals of the same symmetry, ψ_a and ψ_b, and two associated antibonding orbitals ψ_a' and ψ_b'. These orbitals have energies such that $E_a < E_b$ and $E_a' > E_b'$. In this case the bonding orbitals are completely filled and the antibonding orbitals empty. There are two possible interactions:-

a._Interaction_between_the_two_bonding_orbitals.

A linear combination of ψ_a and ψ_b is taken and two new orbitals are obtained one of energy δ below E_a and the other δ above E_b (Fig 4;1). Since both ψ_a and ψ_b were filled both these two new orbitals are filled and there is no net gain or loss of

Fig. 4;1
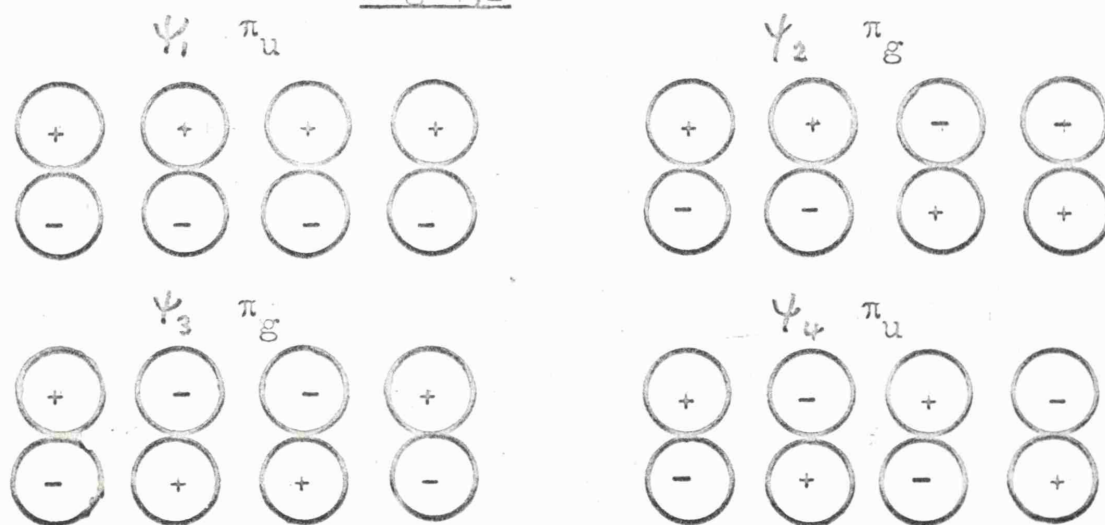

a   b
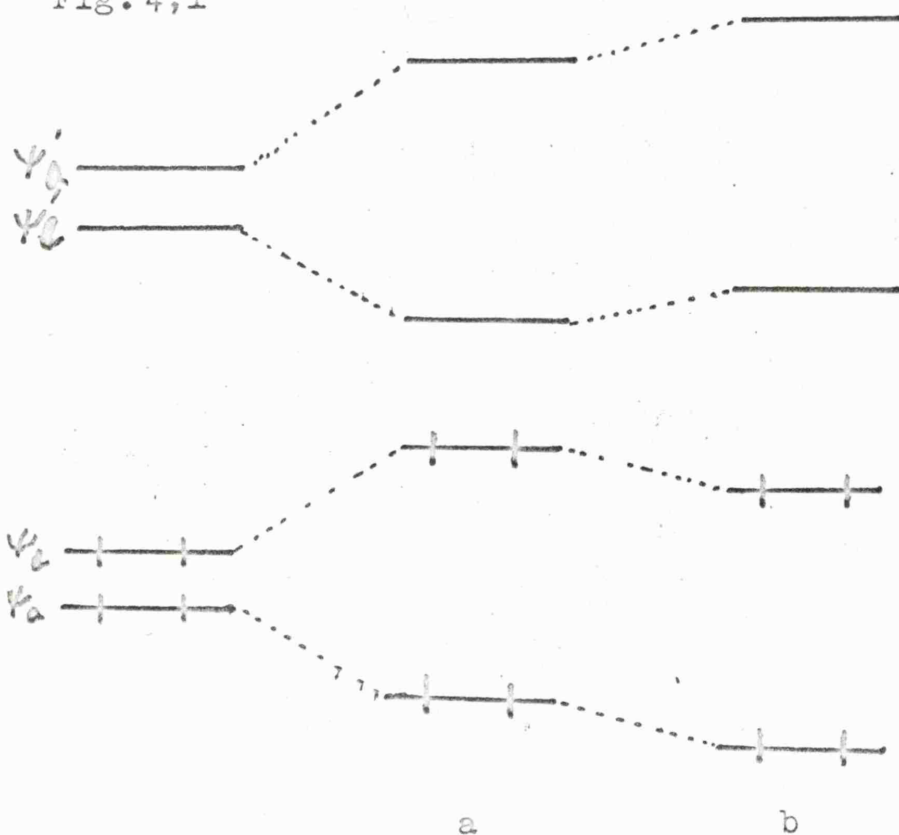
Effect of Of Interactions of Orbitals on their Energy

a. Interaction between two bonding orbitals.
b. Interaction between the bonding and the
   corresponding antibonding orbitals.

- - - -

Fig 4;2

π-Molecular Orbitals in Butadiene

energy of the system as a whole. The energy displacement δ is

given from first order perturbation theory by:

$$\delta = \frac{\langle \Psi_a | V | \Psi_b \rangle}{| E_a - E_b |}$$

where V is the interaction operator.

The energy of the interaction depends inversely on the energy

difference between the two orbitals.

b. _Interaction_between_the_bonding_and_antibonding_orbitals

In this case (Fig 4;1b) there are four valence electrons and

the interaction does not affect the total energy of the system.

The energy of interaction is smaller in this case, however, because

of the larger energy difference.

In radicals where there is an unpaired electron, interaction

of bonding orbitals can affect the total energy of the system.

In these cases interactions can affect the energy and electron

distribution in the system considerably.

iii. Conjugation

An example of a conjugated molecule is butadiene, $CH_2=CH-CH=CH_2$,

where the two π-bonds can be considered delocalized over the

whole system. This delocalization is due to the fact that all

the p-orbitals, of the correct symmetry, on the carbon atoms can

overlap and hence the centre bond can have some double bond character.

The two delocalized Ψ_1 and Ψ_2 bonding and the Ψ_3 and Ψ_4

antibonding m.o's are shown in fig 4;2. In the ground state,

electron correlation will tend to localize the π-electrons in the

terminal C-C region. This simple m.o. model thus over-emphasises

the amount of delocalization, and this is true for all similar

systems where only one valence-bond structure can be written down[74].

iv. Hyperconjugation

In some respects a $-CH_3$ group acts as if it were an unsaturated

group. In 1934 Wheland[75] noted that the replacement of hydrogen

atoms in ethane by methyl groups tends to weaken the central C-C

bond and suggested that alkyl substituents could stabilize free

radicals:

$$H-\underset{\underset{H}{|}}{\overset{\overset{H}{|}}{C}}-CH_2 \cdot \qquad H \cdot \underset{\underset{H}{|}}{\overset{\overset{H}{|}}{C}}=CH_2$$
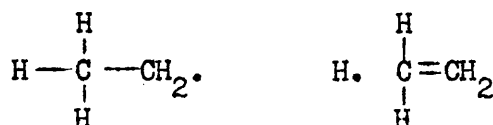
Pauling[76] pointed out that the shortening of the $H_2C-C \cdot$ bond in

methyl-acetylene relative to the single bonds in ethane was similar

to that found in conjugated molecules. This was explained in terms

of a similar mechanism to that of Wheland. Mulliken[77] used the

term hyperconjugation to describe this phenomenon.

Chemical evidence for hyperconjugation had already been found

by Baker and Nathan[78]. They proposed a new mechanism for electron

release which acted in the opposite sense to the inductive mechanism[74]

and was pictured as: $H-CH_2-C=C-C=C$
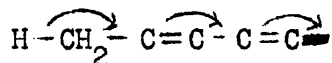
Dewar concludes his review of the evidence for hyperconjugation[74]

by saying that although qualitatively the effects quoted as evidence

for this mechanism can be explained without recourse to hyper-

conjugation, the size of the effects are such that hyperconjugation

may be important.

As with conjugation, hyperperconjugation is likely to be more

more important in free radical than in classical molecules.

v. The Walsh Diagrams

Many authors have pointed out that the structure of a large number of simple molecules seems to the governed by quite simple numerical rules[71, 79-81]. For example all known AB_2 molecules with up to sixteen valence electrons are linear (e.g. CO_2), while those with seventeen to twenty valence electrons are bent in their ground state (e.g. CO_2^-, NO_2).

In 1942 Mulliken[81] published a correlation diagram for the AB_2 molecule. This work was extended in 1953 by Walsh[71] who gave a new correlation diagram for AB_2 and also for AH_2, AH_3, AB_3, HAB and H_2AB. The last two will be required later and are reproduced in figs 4;3 and 4;4. These diagrams have been very useful in discussing the electronic structure of simple molecules and radicals[82, 83], and predicting whether a molecule would be linear or bent. Using these schemes it has been possible to predict m.o. schemes for bent molecules which would otherwise have been tedious to obtain.

Walsh[71] used a linear combination of atomic orbitals treatment for linear molecules and considered the effects of bending on the energies of these m.o's. He used symmetry considerations and a mixture of localised and non-localised orbitals, sometimes in the same diagram. For example in the H_2A diagram (Fig 4;5a) he used the fully localized m.o's for the linear case, but for the bent case the upper a_1 m.o. is the localized 2s lone-pair and the lower a_1 m.o. the delocalized in-phase combination of the two localised m.o's which
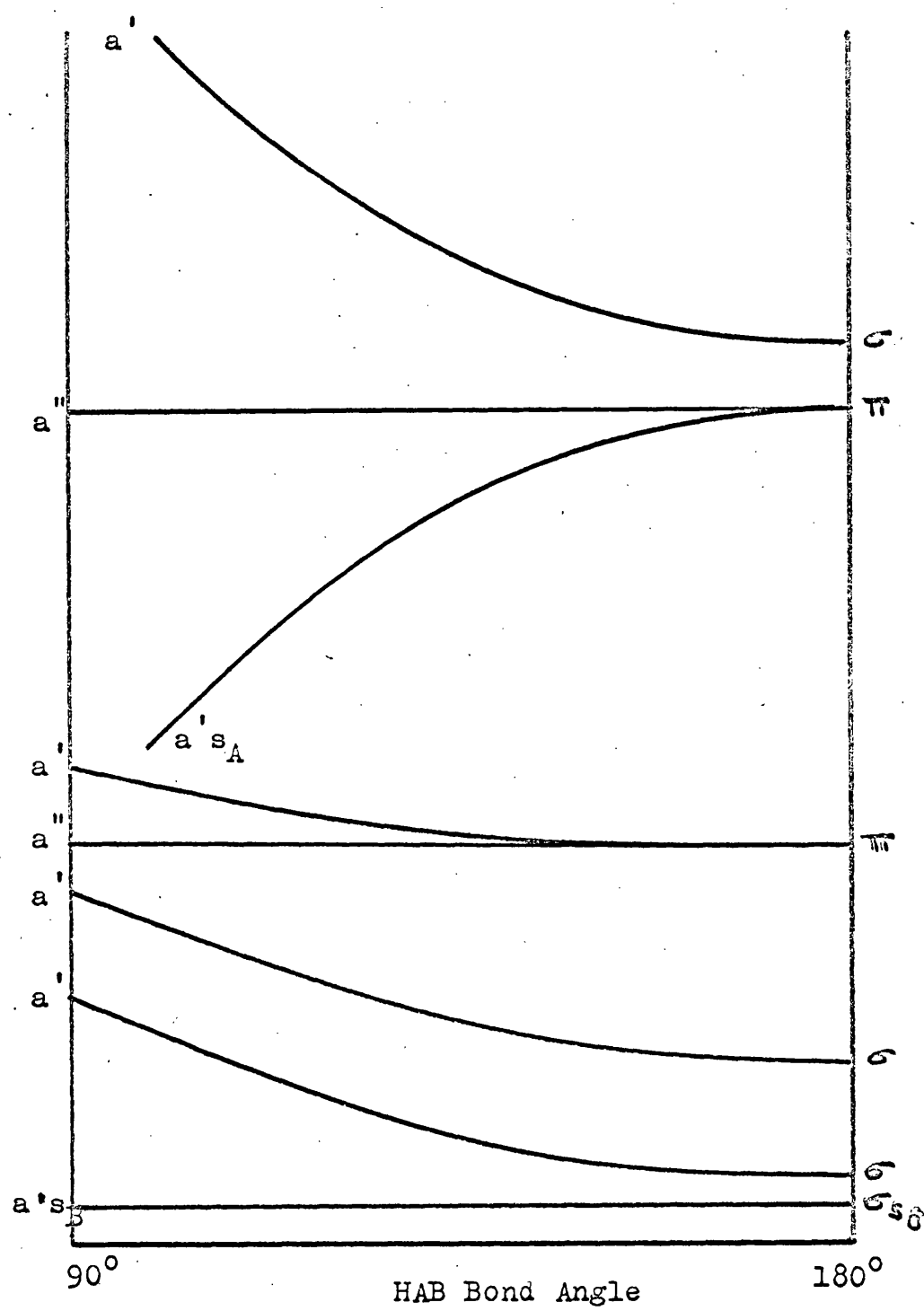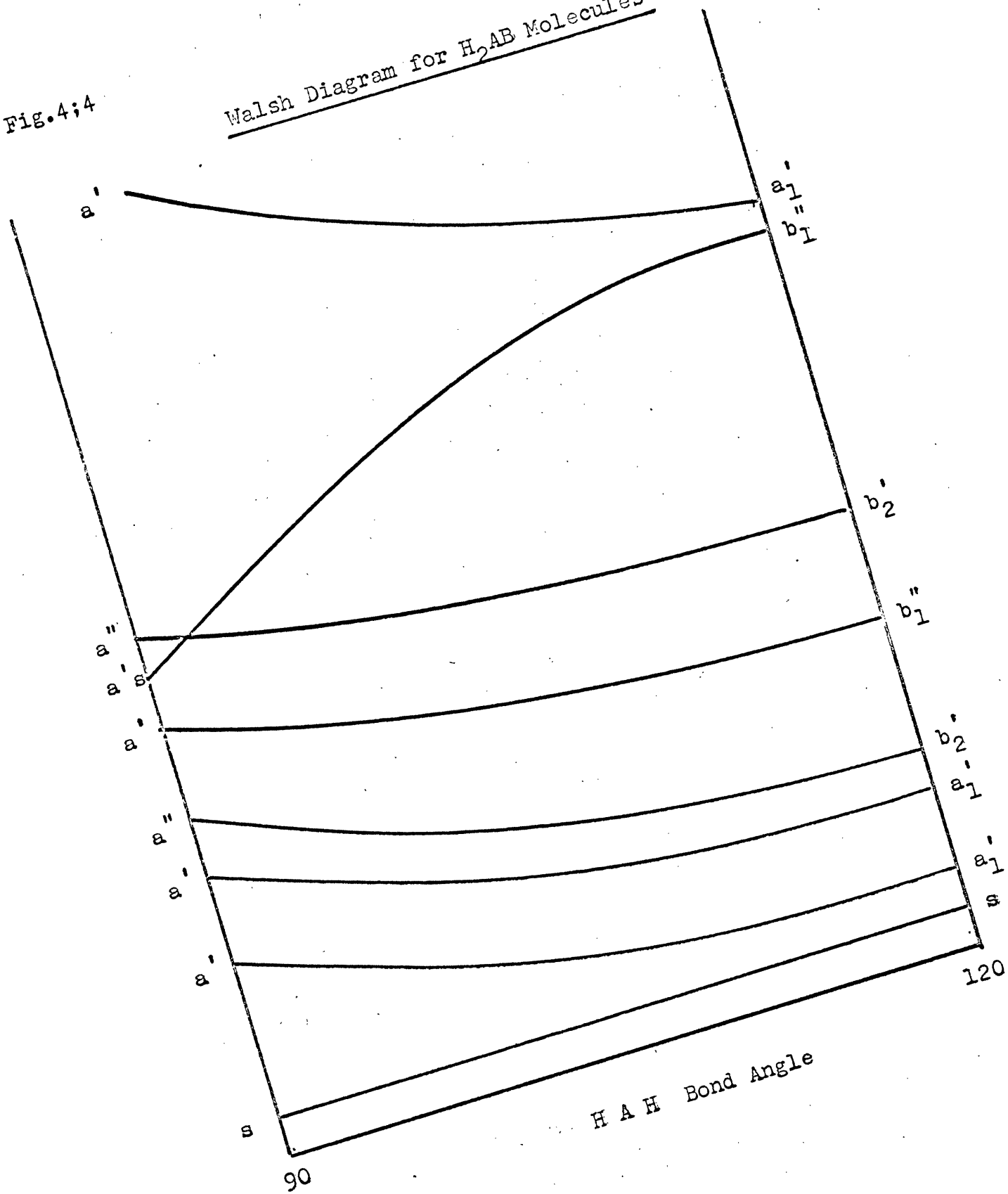
Fig.4;3

Walsh Diagram for HAB Molecules

a'

a"

a's_A

a'

a"

a'

a'

a's_B

90°   HAB Bond Angle   180°

Fig.4;4

Walsh Diagram for H_2AB Molecules

H A H Bond Angle

90

120

describe the bonds. Walsh was, however,,able to obtain a consistent

scheme by making the following assumptions:

1. In the 90° AB_2 molecule the s-orbital on A does not contribute

to the m.o's, but acts as a lone pair.

2. If a m.o. changes, with change in bond angle, from being built

from a p-orbital on A to being built from an s-orbital on A the

orbital becomes more tightly bound and more confined to A.

3. If the valence state of A does not change when the bond angle is

changed the following subsidiary effects determine whether the

orbital becomes more, or less, tightly bound:

i. If the orbital is antibonding between the end atoms a

linear molecule is favoured.

ii. If the orbital is bonding between the end atoms, a bent

molecule is favoured.

Since Walsh's paper there has been much discussion on the

significance of the binding energy referred to, whether it was in

fact equivalent to the ionisation potential of the orbitals, and

also whether it contains the internuclear Coulomb repulsions.

The first assumption has also been challenged[84].

The essential idea implied in these curves is that of a one

electron model, in which the effect of changes of valence angle on

the energy of each electron is considered. Coulson and Neilson[85]

criticize the suggestion that the binding energy is the ionisation

energy, since a sum of the ionisation energy includes all inter-

electron and exchange energies twice, and will hence not yield the

correct total energy, as these will vary considerably with angle.

They also point out that the nuclear-nuclear interactions have not

been included and that these are important.

Schmidtke and Preuss[86] reproduced the diagrams quite well

(Fig 4;5b) by making the levels eigenvalues of a pseudo-Hamiltonian

containing no inter-electronic or nuclear operators, but the nuclear

charge on the central atom had to be given an arbitrary value. The

total energy was simply the sum of the separate one-electron energies.

Coulson and Neilson[85] defined a partition of energies into

nuclear repulsion and electronic energies in the form:

$$E = 2 \sum_i e_i + V_n$$

where $e_i = E_i + \sum_j (J_{ij} - \tfrac{1}{2}K_{ij}) = \tfrac{1}{2}(E_i + \mathcal{E}_i)$

E_i is the core energy for orbital ϕ_i

$\mathcal{E}$ is the ionisation energy

J is the Coulomb integral

K is the Exchange integral

V_n is the internuclear Coulomb repulsions.

A plot of e_i against valence angle was thus attempted, but this

does not take into account nuclear repulsions, and the diagrams are

different from those of Walsh in a number of respects (Fig 4;5a and

c.). The most noticeable difference is the behaviour of the highest

a_1 orbital which increases in energy on bending rather than decreasing

as in the Walsh scheme. Krauss[87] used a more sophisticated self-

consistent-wave function and qualitatively changed their results.

He concluded that there was little evidence for a one electron

Fig.4;5
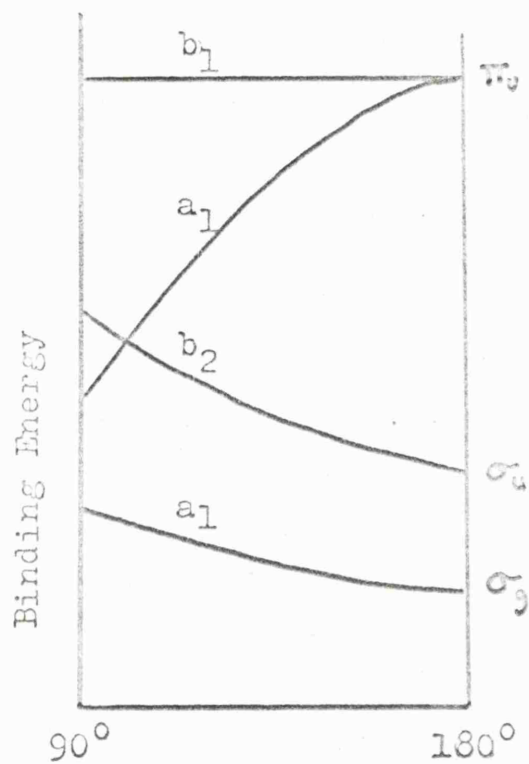
a. Walsh
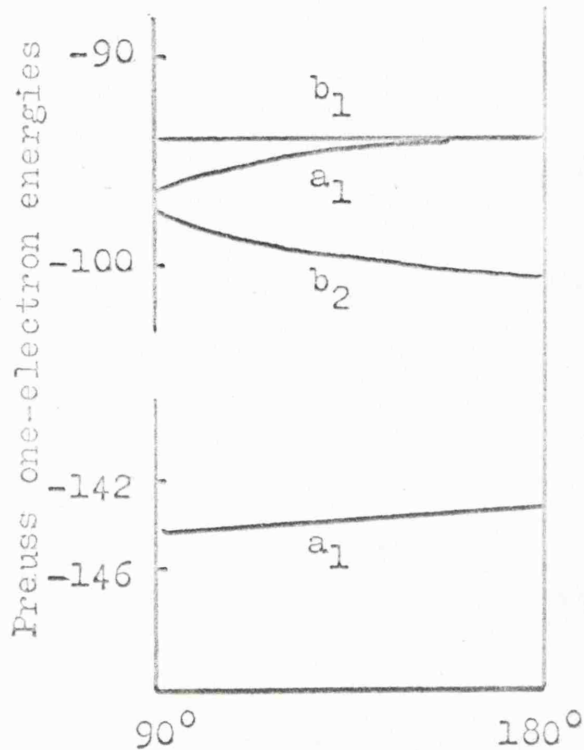
b. Preuss
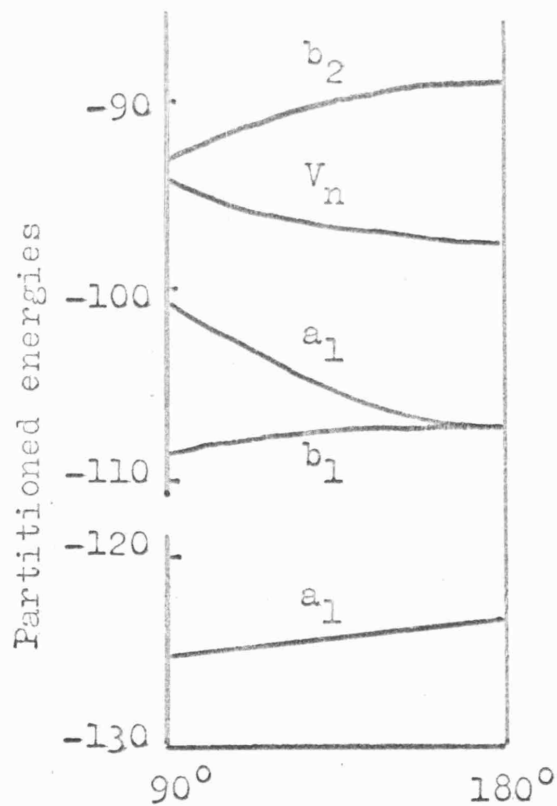
c. Coulson and Neilson

Energy Scale
in E.V.

type partition of the total energy.

Recently Boer et al[88] have shown that, in the framework of the S.C.F. theory, the "atomisation" energy (A) of a molecule is given approximately by the difference in energy of the orbitals in the molecule and the dissociated atoms. The total energy thus varies as a function of the geometry of the molecule in the same way as the energy of the orbitals in the molecules, and so the two errors pointed out by Coulson and Neilson cancel each other.

Leclerc and Lorquet[89] used an extended Huckel approximation which approximates the total energy to the sum of one electron energies, to obtain Walsh diagrams for H_2N, H_2O and H_2C (Fig 4;6b, c, and d). The order of occupation of the prbitals depends on the nature of the central atom, but the rise or fall of the curves corresponding to the first occupied orbitals agrees remarkably well with Walsh's predictions, although the symmetry labelling does not. This is particularly noticeable in the relative weights of the 2s and 2p orbitals used. The s/p ratio is relatively insensitive to the changes in the valence angle, which is contrary to Walsh's first assumption. Mulliken[84] has questioned this first assumption, and the S.C.F. m.o. calculations for H_2O of Ellison and Schull[90] indicates that the s-orbital on the central atom is used in bonding orbitals for the 90° molecule.

Leclerc and Lorquet conclude their paper[89], "Walsh's method is a simulation of an S.C.F. calculation, which is itself an approximation to the exact solution of the Schrodinger equation.

<u>Leclerc and Lorquet Simulation of the</u>
<u>Walsh Diagrams</u>

a. Walsh AH_2

b. Lorquet CH_2

c. Lorquet NH_2

d. Lorquet OH_2
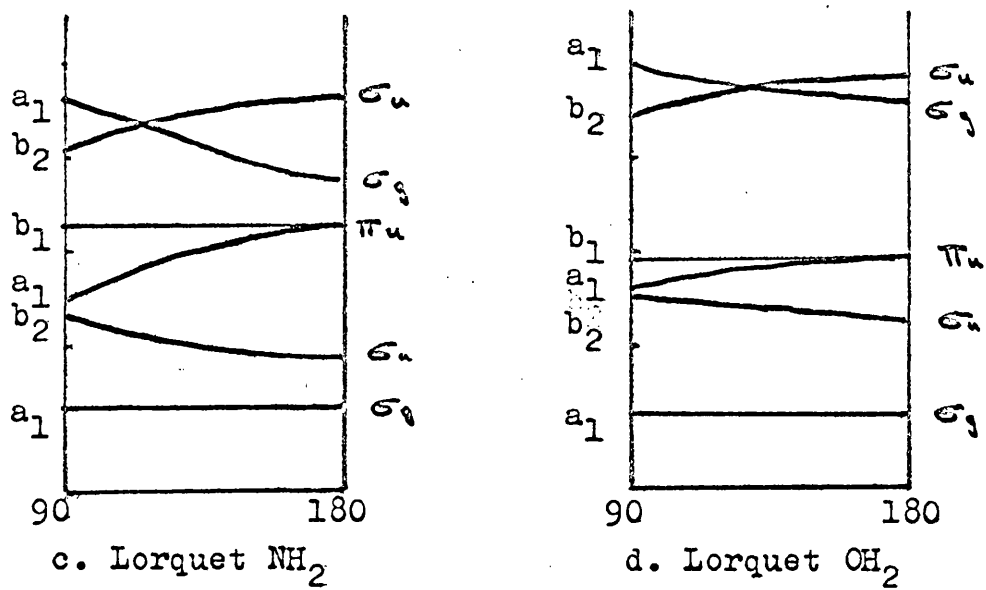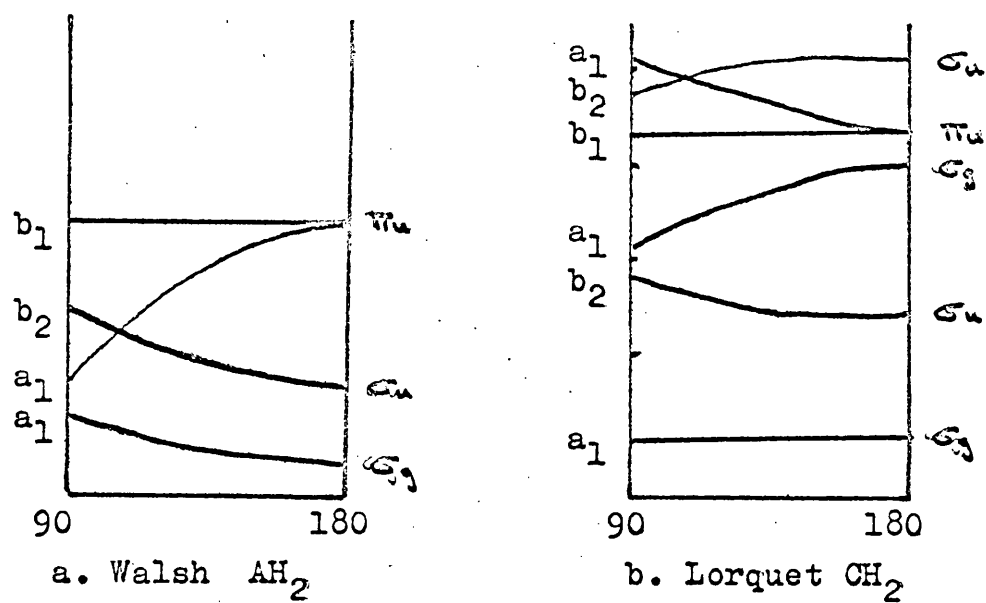
The errors in all stages cancel out in an intricate way".

To summarise, although no-one is absolutely clear as to what Walsh's binding energy entails, or whether his assumptions can be accepted as correct, these diagrams are nevertheless extremely useful as a guide to the way the energies of m.o's are affected by bending the molecule.

II. Electron Spin Resonance of Simple Radicals

i. The Use of Spin Densities in Simple Radicals

If an m.o. is constructed from a linear combination of an s- and . p-orbitals (ψ_1^A and ψ_2^A respectively) on atom A, and a number of other atomic orbitals on other atoms ψ_i^X

i.e. $\qquad \Psi = c_1 \psi_1^A + c_2 \psi_2^A + \sum_{i=3}^{n} c_i \psi_i^X$

The spin densities defined in chapter 1 are equated to the relevant c_i^2's, the coefficient determining the contribution of each atomic orbital to the m.o. If overlap terms are neglected:

$$\sum c_i^2 = 1$$

Thus the total spin density should be unity. Recently, Schoemaker[58] has shown that overlap contributions may be important in certain cases. There will also be errors due to the assumptions used in the calculation of the spin densities.

We will now consider three model systems that will be used in later discussions. These are the α and β coupling in alkyl radicals, and the allyl radical.

ii. The α-proton Hyperfine Coupling in the π C-H Fragment

The hyperfine coupling of the α-protons in the C-H fragment, and in the related π-radical ions has been treated by a number of authors[91-96]. The problem is to explain the isotropic splitting due to the proton when the unpaired electron density is in a pure p-orbital on the carbon atom with zero electron density at the proton. A number of quantitative models have been proposed, using both the valence bond[91, 92, 94] and molecular orbital[93] approximations. Here we will describe briefly the m.o. treatment of Weissman[93].

The ground state of the C-H fragment can be written :

$(\sigma_b)^2 (\pi)^1$, where σ_b is the C-H bond. With this configuration can be mixed other excited states. Excitation of the electron from the π-orbital to another π-orbital will not yield spin density at the proton. An electron in a π-orbital cannot be mixed with a π σ-orbital because of the difference in symmetry, nor a σ with a π and so the only excitation which need be considered in this connection is the σ bonding to σ antibonding.

$$(\sigma_b)^2 (\pi)^1 \longrightarrow (\sigma_a)^1 (\pi)^1 (\sigma_a)^1$$
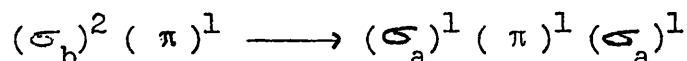
The ground state can be written:

$$\phi = \frac{1}{\sqrt{6}} \begin{vmatrix} \sigma_b(1) & \sigma_b(2) & \sigma_b(3) \\ \sigma_b(1) & \sigma_b(2) & \sigma_b(3) \\ \pi(1) & \pi(2) & \pi(3) \end{vmatrix} \alpha\beta\alpha \quad = \frac{1}{\sqrt{6}} \left\| \sigma_b(1) \sigma_b(2) \pi(3) \right\| \alpha\beta\alpha$$

and corresponding to the excited state there are three state functions with eigenvalue $S_z = \frac{1}{2}$;

$$D_1 = \frac{1}{\sqrt{6}} \left\| \; \mathcal{S}_b(1) \quad \mathcal{S}_a(2) \quad \pi \; (3) \; \right\| \quad \alpha\alpha\beta$$

$$D_2 = \frac{1}{\sqrt{6}} \left\| \; \mathcal{S}_b(1) \quad \mathcal{S}_a(2) \quad \pi \; (3) \; \right\| \quad \alpha\beta\alpha$$

$$D_3 = \frac{1}{\sqrt{6}} \left\| \; \mathcal{S}_b(1) \quad \mathcal{S}_a(2) \quad \pi \; (3) \; \right\| \quad \beta\alpha\alpha$$

We have to find a linear combination of D_1, D_2 and D_3 to obtain the improved wave function. One combination will be a quartet state and the other two will be doublets. We are only interested in doublet states which are;

$$\phi_1 = \frac{1}{\sqrt{6}} (2D_1 - D_2 - D_3) \quad ; \quad \phi_2 = \frac{1}{\sqrt{2}} (D_2 - D_3)$$

ϕ_2 can be thought of as a combination of the singlet σ state $(\mathcal{S}_b) \, \alpha \, (\mathcal{S}_a) \, \beta$ with π, so will not introduce spin density in the σ-orbitals. ϕ_1 with the inclusion of D_1 is the only function which will produce unpaired spin in the σ orbitals. The total wave function is thus: $\quad \chi = \phi + \lambda\phi_1$

This treatment predicts negative spin density at the proton, as has been shown experimentally[97].

iii. The Allyl Radical

This radical is a good example of one in which two valence-bond structures can be written for the ground state. In such a system a large amount of delocalization will be expected[94]. This molecule will be discussed in terms of both the valence bond and molecular orbital theories[98]. The simple theories yield different results, although refinements tend to reduce the differences.

The two valence bond structures can be written:

Ψ_1 $\cdot CH_2 - CH = CH_2$ Ψ_2 $CH_2 = CH - CH_2 \cdot$

     a   b   c   a   b   c

The valence bond function for the ground state is:

$$\emptyset = \frac{1}{\sqrt{3}} (\Psi_1 + \Psi_2) = \frac{1}{\sqrt{6}} \left\| a(1) \; b(2) \; c(3) \right\| \frac{1}{\sqrt{6}} (2\alpha\beta\alpha - \alpha\alpha\beta - \beta\alpha\alpha)$$

If we consider solely the spin wave function and calculate the total

spin in each atomic orbital, we obtain $\frac{2}{3}\alpha$ on a and c and $\frac{1}{3}\beta$ on the

central atom b. Thus there is $\frac{2}{3}$ positive spin on the end atoms and

$\frac{1}{3}$ negative spin on the central atom. The total is normalised

correctly to unity.

Using a simple molecular orbital picture the two paired π -

electrons are in an orbital over the whole of the molecule of the

form: $\psi_1 = \frac{1}{2} (a + \sqrt{2} b + c)$

and the unpaired electron is in an orbital with a node at the

central atom, the orbital being of the form:

$$\psi_2 = \frac{1}{\sqrt{2}} (a - c)$$

Thus one would predict 50% of the unpaired electron on the terminal

carbon atoms and zero density on the central atom. If however,

spatial correlation of electrons of opposite spin is taken into

account by configurational interaction[98], negative spin density at

the central carbon atom is obtained. If refinements to the valence

bond picture are considered the amount of negative spin density on

the central atom is reduced.

Fessendon et al[99] calculated from the proton coupling that the

spin density on the central carbon atom was 16% and on the end

carbon atom 58%. The signs were not obtained experimentally, but
an allyl type radical identified by Heller et al[100] was shown to
have 19% negative spin density on the central atom. Some
experimental evidence for negative spin densities in related
systems was given by Hanna and McConnell[101].

iv. The Hyperfine Coupling to the β-protons in the Ethyl Radical

The coupling to the α-protons in π radicals is due to a spin
polarisation effect. The size of the effect can be taken as a
measure of the degree to which Hund's rule is broken down by chemical
bonding[91]. This mechanism is thus unlikely to cause a high spin
density at the β-proton. The coupling due to the β-proton is in
fact 26.9 gauss compared with the α-proton coupling of only 22.38
gauss. Colpa and de Boer[102] have considered the spin polarisation
mechanism in a $C'' - C' \diagdown^{H}$ fragment and showed that it was possible to
distinguish between two distinct polarisation mechanisms. These
are direct spin polarisation and consecutive polarisation. The
first arises from a direct polarisation of the $C' - H$ bond by the
unpaired electron on C'', and this contributes a calculated coupling
of -1.76 gauss. The consecutive polarisation mechanism arises
from the unpaired π-electron on C'' polarising the $C'' - C'$ bond which
consecutively polarises the $C' - H$ bond. This gave a contribution
of the opposite sign (+0.65 gauss) and so the total coupling was
only -1.1 gauss. These authors concluded that the spin density
on the β-protons arises from direct overlap between the π-electron
and the $C' - H$ bond. This is a hyperconjugative mechanism.

This hyperconjugative mechanism had been postulated by

Bersohn[92] and Chesnut[103] who used an m.o. treatment to explain

the hyperfine coupling. A valence bond treatment was carried out

by McLachlan[104]. In most treatments the methyl protons are

considered using a pseudo hetero atom approach similar to the

earlier work of Coulson[105]. In this

way, orbitals are obtained which can

overlap with the unpaired electron in

the π -orbital. For example the

combination shown in fig 4;7 has the
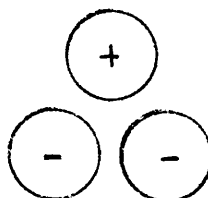
Fig 4;7

same symmetry as a p-orbital and the situation is thus similar to

the allyl radical, and a similar treatment will place spin density

on the protons, and a small negative spin density on the β -carbon

atom.

The valence bond and m.o. treatments are fundamentally

different. In the valence bond mechanism the π-electron spin

delocalization is entirely produced by exchange polarisation, while

in the Huckel m.o. treatments the delocalization is entirely due to

electron transfer. Lazdins and Karplus[106] have considered both the

allyl and the ethyl radicals by a treatment that includes both

exchange polarisation and electron transfer to find out the relative

weights of these effects. They used a configurational interaction

m.o. method with semi-empirical parameters, and found that 60% of

the delocalisation was contributed by exchange polarisation and 40%

from electron transfer. Thus neither the simple m.o. nor the

simple valence bond treatments provide, by themselves, a completely satisfactory description of the spin delocalization in these systems. The apparently good results which were obtained by these simple treatments being due to the empirical nature of these calculations.

The pseudo-hetero atom technique neglects a contribution from the antibonding orbital in the methyl group[102]. This leads to errors in the calculation of spin densities on the aliphatic protons in, for example, 9, 10-dimethylanthracene, which were a factor of four too low[102]. How far this can be explained in terms of this error or the errors pointed out by Lazdins et al[106] is not, however, clear.

Some features of hyperconjugation are obscured by the pseudo-hetero atom method. One of these is the dependence of the coupling on the orientation of the $C' - H$ bond to the p-electron on the α-carbon atom. It has been suggested that the β-coupling constant Q is related to the angle θ between the C'' π-orbital and the $C'' - C' \diagdown^H$ plane by the following relation[107-111].

$$Q\ (\theta)\ =\ B_o\ +\ B_1\ \cos^2\theta$$

where B_o = spin polarisation coupling

B_1 = coupling due to hyperconjugation mechanism when θ = 0.

Experimental evidence from radicals trapped in single crystals seems to support this relationship[111]. In the ethyl case the methyl group is rotating and the only coupling observed is the averaged coupling which is one half of B_1.

B. The Methylene Imino Radical

I. Experimental Results

A sample of potassium chloride doped with cyanide ions was prepared by growing from aqueous solution. On χ-irradiation, for 24 hours, of the powdered sample the e.s.r. spectrum showed amongst other signals a doublet of triplets. The doublet splitting is 180 gauss. A similar spectrum was observed when the sample was cooled to 77°K. The crystals obtained by fusing potassium chloride with potassium cyanide did not yield this doublet on irradiation, but if the dopant was potassium thiocyanate a very strong signal was obtained on irradiation. Infra-red spectra showed that the latter sample contained appreciable quantities of cyanide, but the former did not give an absorption peak at all. The e.s.r. spectrum of the irradiated thiocyanate doped sample is shown in fig 4;9.

Deuteration confirmed that the doublet was due to coupling to protons, but the hyperfine coupling of about 180 gauss is very high for coupling to only one proton. More probably it is a 'triplet' caused by two equivalent protons, with the central:triplet always obscured by other species. The hyperfine coupling is thus about 90 gauss, which agrees well with the spectrum of the methylene imino radical (H_2CN) observed by Cochran et al[112]. The central g-value of 2.0031 agrees well with that of 2.0024 for the H_2CN radical. The radical observed by Cochran[112] was stationary, and so they were not able to obtain the isotropic parameters, and one of their ^{14}N anisotropic features was contained in their line width. Our results

Fig.4;8

E.S.R. Spectrum of KCl Doped with Thiocyanate Ion
after 20 hours Irradiation

9.5 gauss

←------------------180 gauss ------------------→
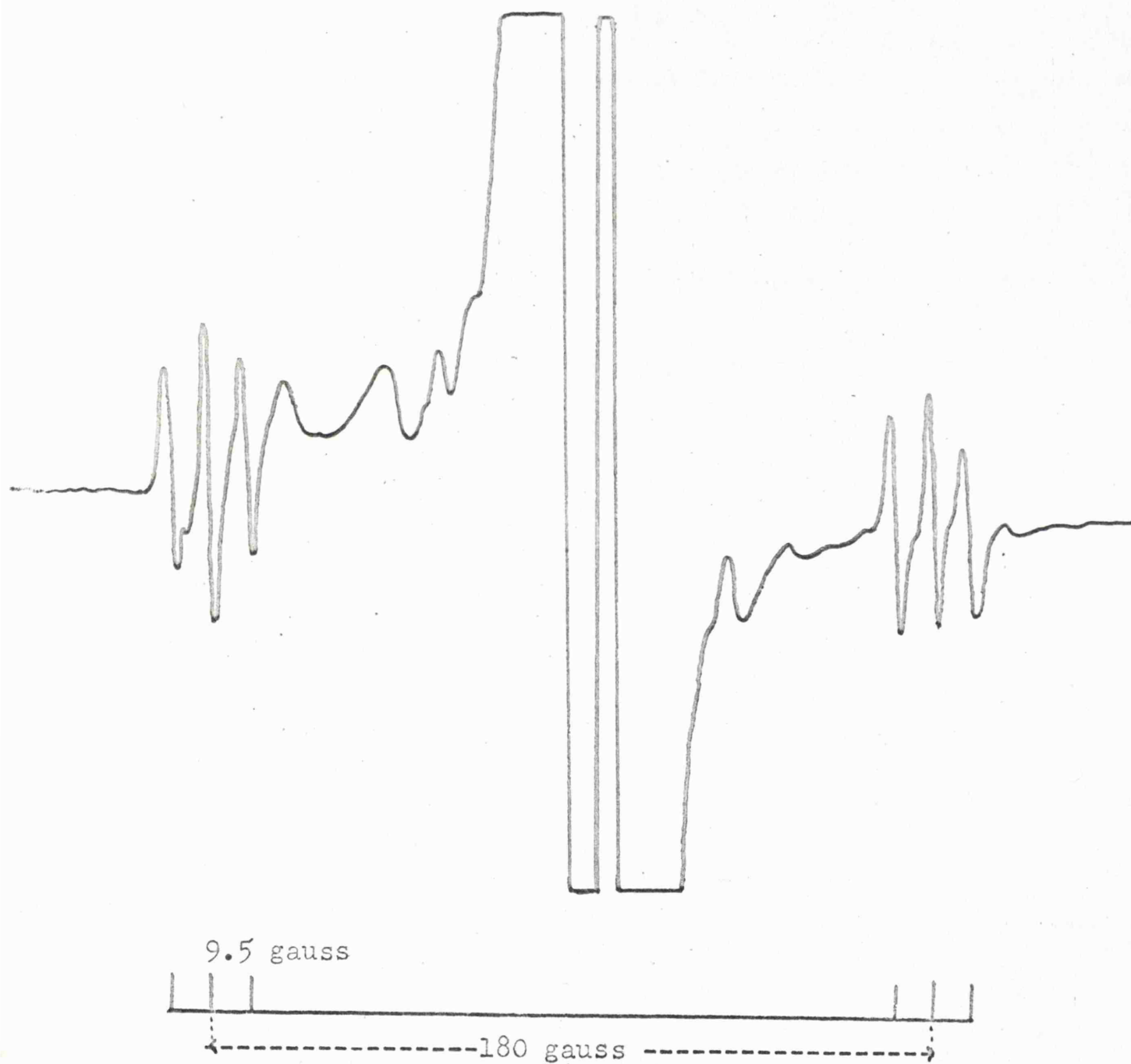
together with those of Cochran allow evaluation of the total spin density. We have confirmed that the | a - B | term would have been contained in their line width. The experimental results, together with those of Cochran[112] are given in table 4;1. Also included in the table are the calculated spin densities.

Table 4;1

E.S.R. Data and Spin Densities for the H_2CN Radical

	$A_{iso}(H)$	$A_{iso}(^{14}N)$	$2B(^{14}N)$	c_H^2	$c_{N(s)}^2$	$c_{N(p)}^2$	Total
This Work	91.4	⁻ 9.5	(25)	36	1.7	73.3	111
Ref 112	87.4	(11.5)	22.9	34.4	2.1	67.2	103.7

g = 2.0031   corrected to second order in the spin Hamiltonian.
( ) indicates e.s.r. data not observed experimentally.

— — — — — — — — — — — — —

II. The Electronic Structure of H_2CN

From Walsh's diagram for an H_2AB molecule (Fig 4;4) the m.o's can be written:

$$(1a_1')^2 \ (2a_1')^2 \ (3a_1')^2 \ (1b_2')^2 \ (1b_1'')^2 \ (2b_2')^1$$

where $(1a_1')$ is an s-orbital on B

$(2a_1')$ is a C-N σ-orbital

$(3a_1')$ is a C-H σ-orbital)
)=(hydrogen group orbitals)
$(1b_2')$ is a C-H π-orbital)

$(1b_1')$ is a C-N π-orbital

$(2b_2')$ is a π-antibonding C-N orbital in the plane of the molecule and formally on the nitrogen atom.

The unpaired electron is in the $(2b_2')$ orbital formally on the

nitrogen atom and so the coupling to the other nuclei should be small.

There is, however, approximately 36% of the total spin density on the

hydrogen atoms (Table 4;1). This can only have occurred by the

mixing of the $2b_2'$ orbital with the only other orbital of the

correct symmetry, the out-of-phase hydrogen group orbital. This

hyperconjugation leads to large coupling because of the short C-N

bond and also because the hydrogen atoms are held in the plane of

the molecule, which also contains the $2b_2'$ orbital.

The orbitals which can be used to discuss the mechanism of

placing unpaired electron density on the proton are shown in fig 4;9.

Fig 4;9
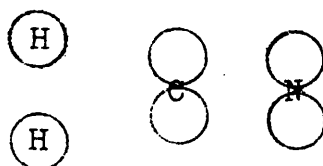
These orbitals are the antisymmetrical hydrogen group orbital ($1b_2'$)

and the in-plane p-orbitals on the nitrogen and carbon atoms.

This situation is very similar to that in the allyl radical discussed

earlier. With the allyl radical simple valence bond treatments

predicted negative spin densities on the central atom, and high

positive spin density at the terminal carbon atoms. The total

spin density in H_2CN on the nitrogen and hydrogen atoms of 111%

can be interpreted in terms of about 10% negative spin density on

the central carbon atom.

An m.o. study of the H_2CN radical by Corvaja et al[113], using the

hyperconjugative model, obtained good agreement with the

experimental proton splitting. Adrian and Karplus have considered

the β-proton hyperfine coupling in the related vinyl radical[114],

and have calculated the effect of changing the angle between

the α-proton-carbon bond and the double bond. When this bond angle

is 180° the unpaired electron is in a p-orbital similar to the

situation in the H_2CN radical. It is interesting to note that the

trans proton has a larger hyperfine interaction than the cis proton,

which, it was suggested[114], is due to the relative weakness of the σ

bond between the carbon atoms at the short double C-C bond distance,

when the bonding is pure p. There is, however, no experimental

evidence for the assignment of the largest coupling to the trans

proton. Dixon[115] has also calculated the coupling to the β-protons

and obtained the high trans coupling. This he attributes to a

negative resonance integral of the π-type, between an α-C-H bond and

the unpaired electron on the α-carbon atom. Such a trans effect has

also been noticed in the m.o. theory of σ-electron systems[116].

Adrian et al[114] obtained a β-proton coupling of 70 gauss when

θ = 180°. This in good agreement with the value of about 90 gauss

in H_2CN when the shorter C-N bond is taken into account.

Further discussion of the electronic structure of H_2CN is

postponed until the next section where it is compared with the

related HCN^- radical.

C. The Hydrogen Cyanide Negative Ion

I. Related Radicals

Before discussing the hydrogen cyanide negative ion it is

instructive to consider the related formyl (HCO), vinyl (CH=CH$_2$)

and HPO$_2$ radicals.

i. The Formyl Radical

a. The Electronic and Vibrational Spectra

The electronic ground state of this radical[117-9] showed that

the radical is bent with a bond angle of 120°, and that the ground

state was $^2A'$, which had been predicted by Walsh[71](Fig 4;3).

The i.r. spectrum[120, 121] showed that the C-H bond is weak, the

C-H stretching frequency being several hundred wavenumbers below that

in formaldehyde (H$_2$CO). The results for HCO[120] are compared with

other molecules in table 4;2. All C-H stretching vibrations of

protons adjacent to a carbonyl group are of lower energy than those

of C-H bonds in the hydrocarbons, both saturated and unsaturated.

This is would indicate delocalization of the C-H bonding electrons

over the carbonyl group. The weakening of the C-H bond

is very pronounced in HCO.

The C=O stretch in HCO is of higher energy than in H$_2$CO or

CH$_3$CHO, but 200 cm^{-1} lower than in carbon monoxide (CO), which

suggests some triple bonding character in the C-O bond.

These i.r. results indicate that in HCO both the non-bonding

electrons on oxygen and the C-H bonding orbitals are delocalized and

Table 4:2

I.R. Parameters for a Number of Carbonyl Compounds

Species	C-H str.	C-D str.	C=O str.	CHO bend	Ref
HCO	2488	1937	1821	1084	120
H_2CO	2780 g 2834 s		1744 g 1712 s		122 123
CH_3CHO	2840 g 2876 s	2070 2103	1743		124
$-CH_3$	2962, 2972				125
$=CH_2$	2922, 2853				125
$\equiv CH$	2890				125
CO			2143		126

All value in cm^{-1} . g= gaseous value, s = solid state value.

— — — — — — — — — — — —

one would not expect the unpaired electron, formally on the carbon

atom to be fully localized in a non-bonding orbital.

b. The Electron Spin Resonance Spectra of HCO

The e.s.r. data for HCO[127-9] is tabulated below together with

the calculated spin densities.

Table 4:3

E.S.R. Data and Spin Densities in the HCO Radical[127-9]

Axis	g-values	$A(^{13}C)$	$A(^1H)$
x	2.0041	-4.21	-4.9
y	2.0027	17.98	-0.6
z	1.9960	-13.77	5.5
isotropic	2.0010	134.7	135.8

$$c_H^2 = 0.27 \; ; \; c_{C(s)}^2 = 0.12 \; ; \; c_{C(p_y)}^2 = 0.33 \; ; \; c_{C(p_x)}^2 = 0.10$$

The ^{13}C asymmetric tensor was split into two tensors of the form:

$$\begin{vmatrix} -4.21 \\ 17.98 \\ -13.77 \end{vmatrix} = \begin{vmatrix} 6.35 \\ -3.18 \\ -3.18 \end{vmatrix} + \begin{vmatrix} -10.56 \\ 21.16 \\ -10.56 \end{vmatrix}$$

From consideration of both the g-tensor and the ^{13}C hyperfine coupling tensor the three principal directions were assigned as follows. The y-direction along the carbon orbital occupied formally by the unpaired electron, the z-direction the other in-plane axis, and the x-direction perpendicular to the molecular plane.

The spin density in the p_x-orbital is thus in a π-orbital of the C-O bond, and the value is rather high for pure spin polarisation. This, however, is characteristic of radicals of this type (see below). The ^{13}C-tensor was obtained from an envelope spectrum and hence it is possible that the values are not as accurate as originally quoted[129]. The P_y/s ratio from the above data is 2.69 which is rather high for the known bond angle of 120°. This should produce, assuming all the in-plane σ-orbitals are identical, a p/s ratio of 2 and a tensor of the form:
$$\begin{vmatrix} -7.86 \\ 15.72 \\ -7.86 \end{vmatrix}$$

This cannot be easily accounted for in the experimental tensor by a systematic error. The delocalisation of the electron onto the proton may reduce the isotropic splitting from the carbon. Adrian and co-workers[129] calculated a bond angle of 125° using the ^{13}C hyperfine coupling tensor.

The large proton coupling in this radical (136 gauss) is typical for α-protons in radicals where the unpaired electron is in an

orbital having considerable s-character. The hyperfine coupling is so large that any mechanism used to place this spin density on the proton will significantly affect the electronic structure, unlike the mechanism for α-proton coupling in the methyl radical.

c. Spin Polarisation of the π-orbitals in σ Radicals

The relatively high spin polarisation of the π-orbitals is also found in other radicals where the unpaired electron density is in an in-plane orbital. For example in CO_2^- [83, 130] the anisotropic tensor is made up of two terms:

$$\begin{vmatrix} -5.28 \\ -7.95 \\ 13.23 \end{vmatrix} = \begin{vmatrix} -7.06 \\ -7.06 \\ 14.12 \end{vmatrix} + \begin{vmatrix} 1.78 \\ -0.89 \\ -0.89 \end{vmatrix}$$

Here the ratio of the two 2B terms is 7.9 compared with 3.3 in HCO. The spin polarisation requires a mixing in of a suitable excited state analogous to the configurational interaction in the C-H fragment described earlier. In this case, however, the polarisation is of a π- by a σ-orbital. The spin densities in the p_x and p_y orbitals in NO_2, CO_2^- and HCO are given in table 4;4, together with the p/s ratio of the localized orbital formally containing the unpaired electron. A plot of p_x/p_y (Fig 4;10) against the p/s ratio shows that the larger the s-character of the unpaired electron the higher the spin polarisation of the out-of-plane orbital.

d. The Electronic Structure of HCO

From the Walsh diagram (Fig 4;3) the electronic structure of the ground state of HCO can be represented by the m.o. scheme:

Fig 4.10

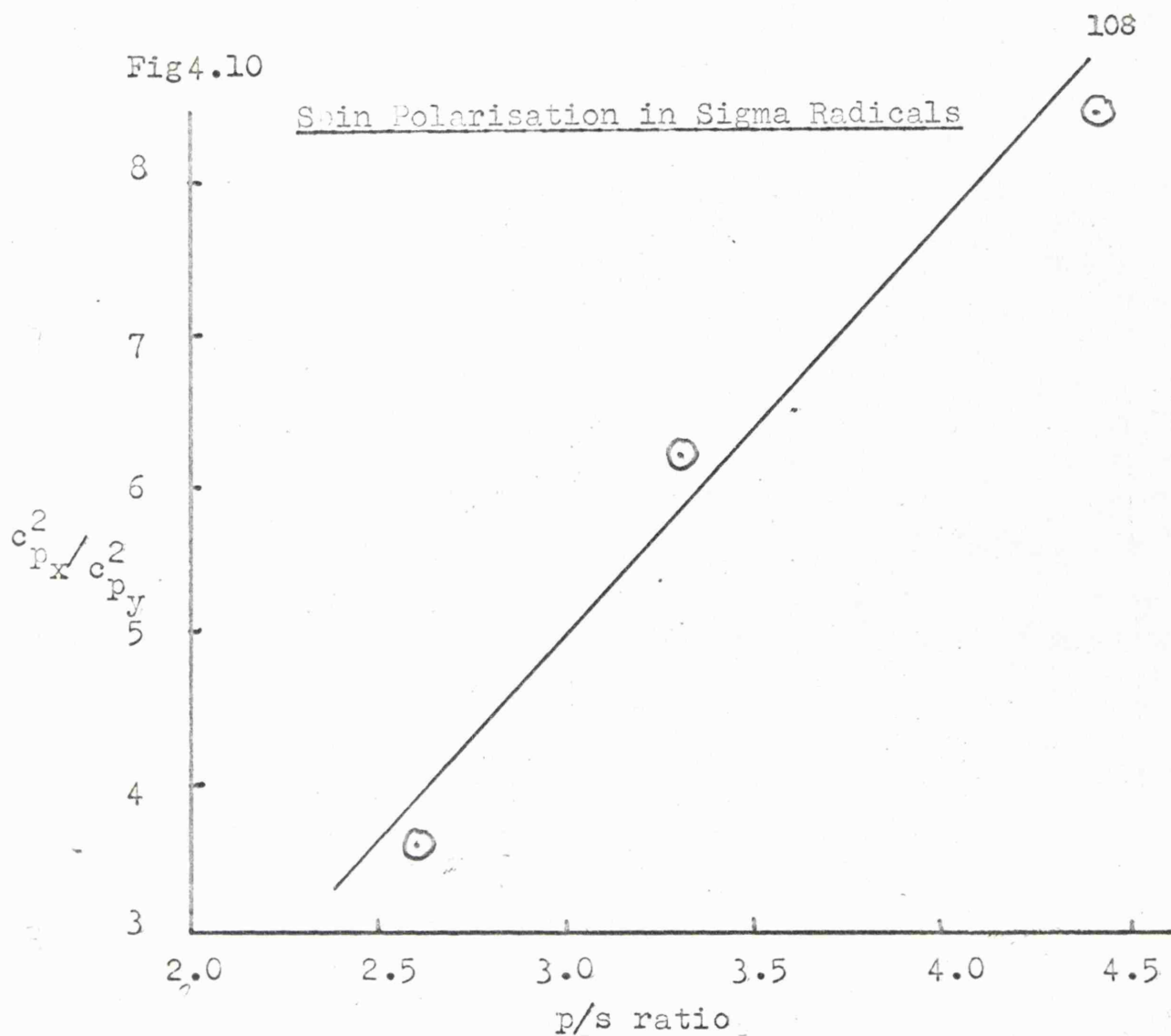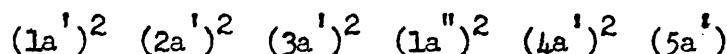Spin Polarisation in Sigma Radicals

Table 4;4

Spin polarisation in NO_2, CO_2^- and HCO radicals

Radical	$c_{p_x}^2$	$c_{p_y}^2$	$c_{p_x}^2/c_{p_y}^2$	p/s ratio	Ref
NO_2	0.44	0.05	8.5	4.4	130
CO_2^-	0.50	0.08	6.3	3.3	85, 130
HCO	0.32	0.09	3.6	2.6	129

$$(1a')^2 \quad (2a')^2 \quad (3a')^2 \quad (1a'')^2 \quad (4a')^2 \quad (5a')$$

where $1a'$ is the 2s orbital on carbon

$2a'$ and $3a'$ are the C–H and C–O σ bonds

$1a''$ the C=O π –bond

$4a'$ the lone pair on oxygen

$5a'$ the orbital on carbon which formally contains the unpaired electron

These m.o's can be considered localized, but orbitals of the same symmetry can 'mix' to form further combinations of orbitals. Thus the two highest occupied orbitals, the $4a'$ and $5a'$ can combine to form two further orbitals, both of which contain contributions from the carbon and the oxygen atomic orbitals.

The large hyperfine coupling on the proton (136 gauss) is explained on a valence bond model[127, 129] by the mixing of excited states, such as II , with the ground state (I).

$$\overset{\cdot}{C} = O \qquad \quad \overset{\cdot\cdot}{:}C \equiv O$$
$$\underset{H}{\diagup} \qquad \qquad \quad H$$
$$\quad I \qquad \qquad \qquad II$$
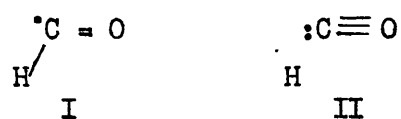
The C–H bond is weak[120] having an upper limit to the bond strength of 1.7 e.v. The energies of the two states are thus very close. Factors which stabilise the excited state are the high resonance energy of the C≡O molecule, and also that in the excited state the C–O π–bonds can be formed without promotion of the carbon atom to the tetrahedral valence state.

If a three electron approximation is used the ground state is described by:

$$\Psi_g = \frac{1}{\sqrt{12}} \left\| \mathfrak{S}_1(1) \quad h(2) \quad \mathfrak{S}_2(3) \right\| \quad (\beta\alpha\alpha - \alpha\beta\alpha)$$

where σ_1 is a carbon sp^2 orbital along the C-H bond.

σ_2 is a carbon sp^2 orbital occupied by the unpaired electron

h is the hydrogen 1s-orbital.

The excited state can be formed from an unpromoted $(2s)^2(2p)^2$ carbon

atom:
$$\psi_e = \frac{1}{\sqrt{6}} \left\| s(1) \quad h(2) \quad s(3) \right\| \beta\alpha\alpha$$

where s is the carbon 2s orbital.

The approximation neglects the effect in change in valence state of

the carbon atom on the C-O bond. By taking the energy of the excited

state to be 1.7 e.v. and a number of other approximations Adrian et

al[127] obtained a value for the hyperfine splitting of +170 gauss.

They also extended the theory[131] to calculate the α-proton coupling

in the related vinyl radical.

ii. The Vinyl Radical

The vinyl radical has the structure $\overset{\bullet}{\text{C}} = \text{C}\underset{\text{H}}{\overset{\text{H}}{\diagup}}$ and thus has

both α- and β-protons. The α-proton is similar to the proton in

the formyl radical, but the α-proton coupling in vinyl is only 16

gauss[131]. This is less than would be expected from pure spin

polarisation of the C-H bond by an electron in a p-orbital[98, 110].

This indicates that there are two mechanisms which place spin density

on the protons leading to spin density contributions of opposite sign.

Cochran et al[131] obtained valence bond expressions for three

formal structures ϕ_0, ϕ_1 and ϕ_2 in terms of the bond angle θ.

ϕ_0 is the ground state, ϕ_1 the structure which accounts for the

α-proton coupling in π-electron radicals and ϕ_3 a structure where

the α-C-H bond is broken, and the remaining bonds are formed by the

orbitals of a divalent $(2s)^2(2p)^2$ carbon atom. ϕ_1 is the structure that places negative spin density on the protons in the π-radicals, and ϕ_2 is the structure that places positive spin density on the proton in HCO. Assuming that the ground state wave function was of the form:

$$\phi = c_0\phi_0 + c_1\phi_1 + c_2\phi_2$$

and assuming likely energies for the ϕ_1 and ϕ_2 structures they calculated the coefficients c_0, c_1 and c_2 for bond angles between $120°$ and $180°$. A plot of c_0, c_1 and c_2 against bond angle is shown in fig 4;11 for both the vinyl and the formyl radicals. In the formyl radical the energy of the ϕ_2 structure is decreased because of the high resonance energy of the carbon monoxide molecule, and hence the ϕ_2 structure has a larger contribution in the formyl radical. As the molecule bends the contribution of the ϕ_2 orbital increases relative to ϕ_1 (Fig 4;11). A plot of hyperfine coupling against bond angle thus shows that as the molecule bends the hyperfine splitting becomes less negative, passes through zero, and rises to large positive values (Fig 4;12). When the bond angle is $120°$ the formyl radical has the calculated proton coupling of 139 gauss, which is in good agreement with the experimental value (136 gauss). The stability of the C–O fragment compared with that of the $C=CH_2$ fragment is the reason why at $120°$ the vinyl radical would only have a proton coupling of +45 gauss. The actual value of the α-proton coupling in vinyl can be accounted for by a bond angle between $145-165°$. The sign of the α-coupling in vinyl is not known experimentally, and it is difficult to say which of the two possibilities is the most likely. Calculations

Fig 4:11

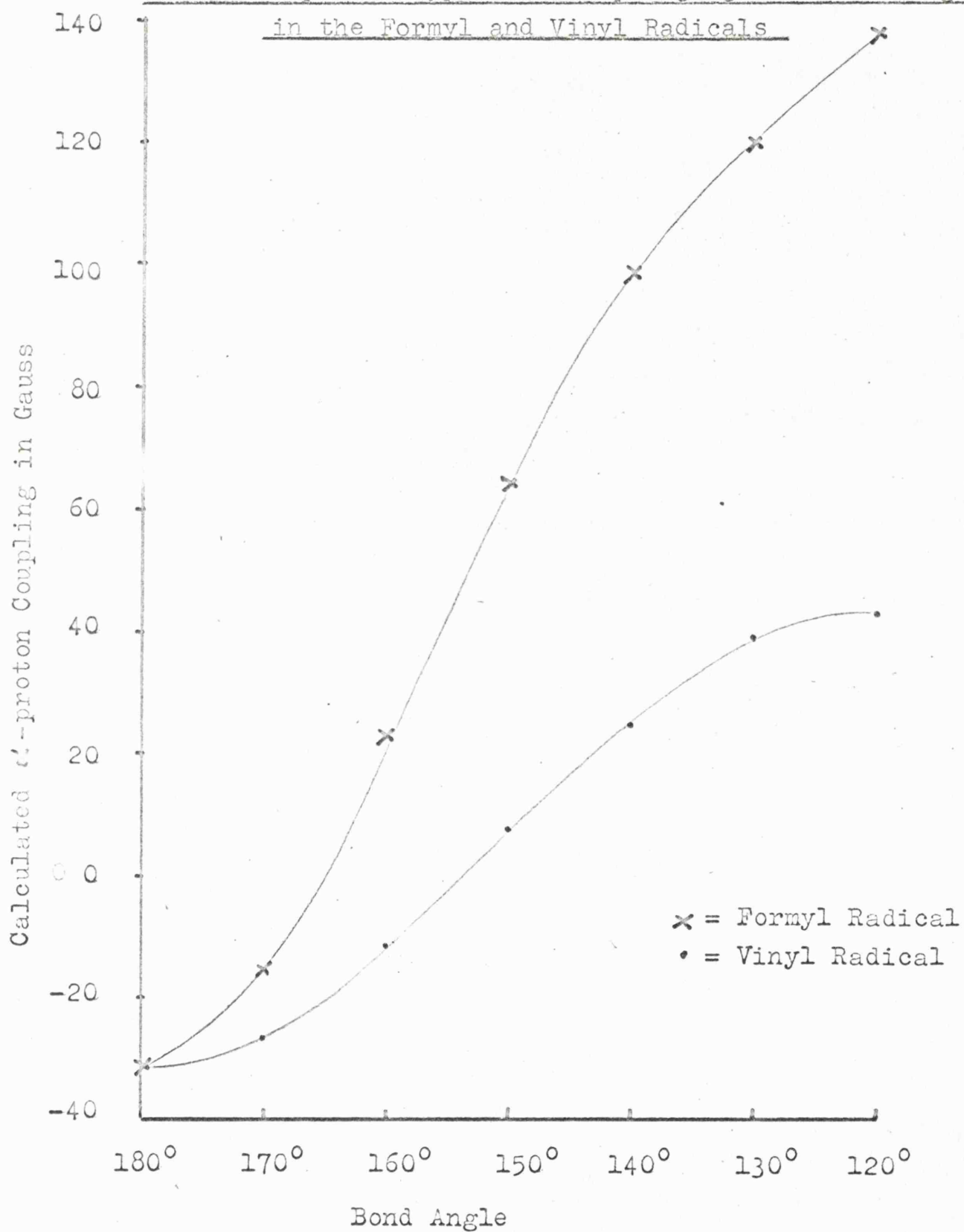Plot of Valence Bond Structure Coefficients against

Bond Angle in the Formyl and Vinyl Radicals
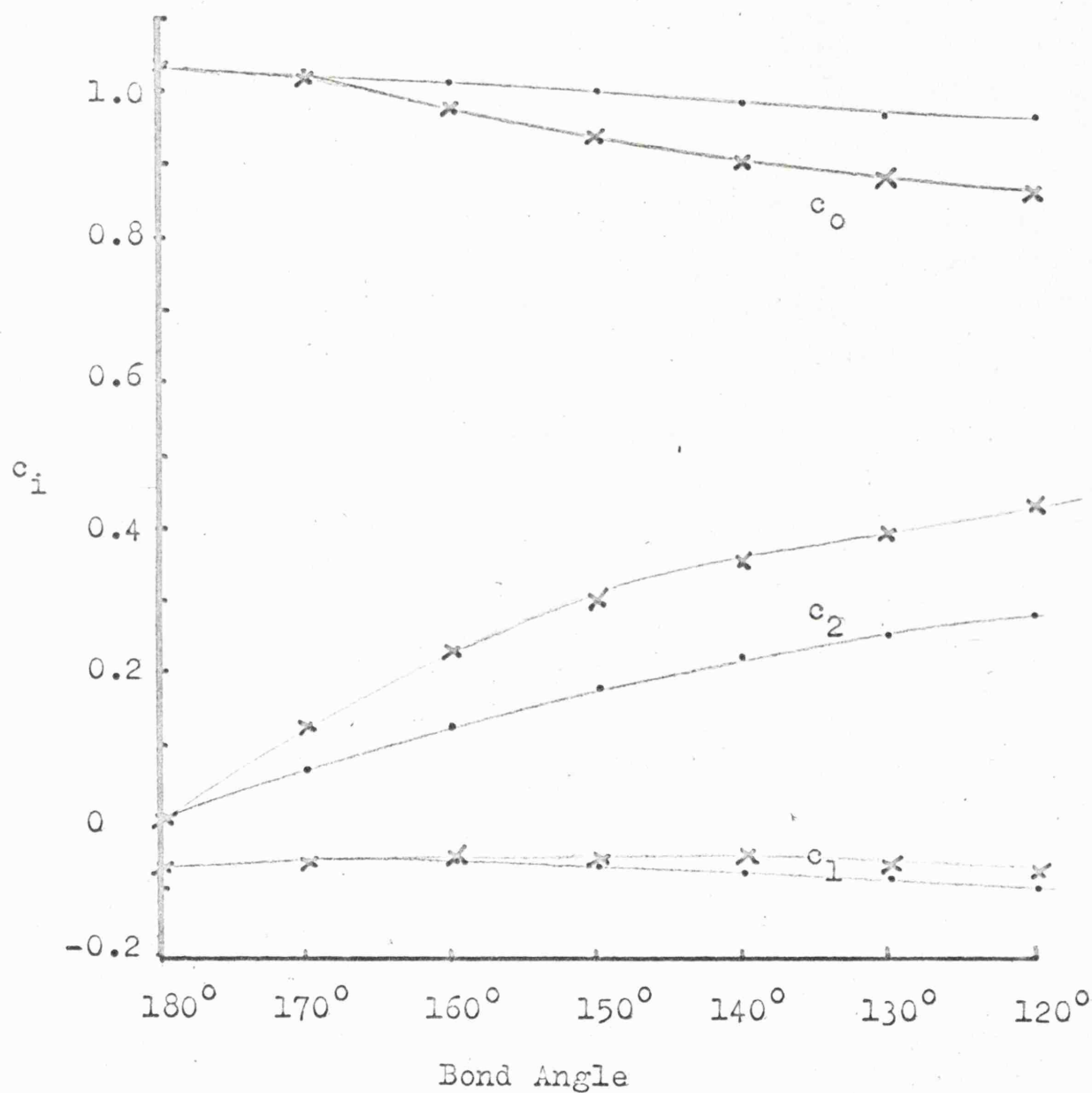
$\times$ = Formyl Radical

$\cdot$ = Vinyl Radical

Plot of α-proton Hyperfine Coupling against Bond Angle in the Formyl and Vinyl Radicals

of the β -proton coupling indicates that the bond angle is between 130-150° [114] which would indicate a positive coupling and a bond angle of about 145° (Fig 4;12)

iii. The HPO_2 Radical

In this radical there is a proton coupling of about 90 gauss. This high value suggests that the hyperfine coupling mechanism to the proton is similar to that in the formyl and vinyl radicals. In this case, however, the radical is not planar and the problem of the proton coupling has been discussed from a different point of view by Atkins et al, the mechanism is perfectly general, however, and can be invoked to explain the coupling in other radicals with α-protons[132]. These authors considered the effect of bending on a methyl radical, where the spin density at the proton is negative[97], and results in a coupling of about 23 gauss. On bending the molecule, the orbital containing the unpaired electron changes from being almost pure p, to an orbital comprising increasing amounts of s-character. Thus, as the molecule bends, mixing of the σ-bonding orbitals becomes more and more allowed. Since the orbital containing the unpaired electron is half filled it can only mix with a state with opposite spin. Hence if there is mixing with the C-H bonding orbitals, the unpaired electron will tend to pair with the electron nearest the carbon atom leaving the electron of the same spin nearest the hydrogen atom. Hence the coupling will be positive. The greater the s-character of the orbital containing the unpaired electron, the greater the interaction from both energy

and symmetry considerations. This effect will tend to weaken the C-H bond. The weak C-H bond can thus be considered a consequence of the mixing of the orbitals[132], and not the mixing a consequence of the weak bond.

Both the valence bond[129] and the molecular orbital[132] descriptions partially describe the α-proton coupling in these systems. The effect of the other groups must however be taken into account. For example the carbonyl group in acetaldehyde affects the α -C-H bond even in this singlet molecule, though, as usual, the effects of delocalization are smaller in species not containing an unpaired electron.

II. The Hydrogen Cyanide Negative Ion

i. Experimental Results

If the doped potassium chloride crystals prepared from aqueous solution and used to prepare the H_2CN radical are irradiated for only about twenty minutes, two further doublets of triplets can be observed in the e.s.r. spectrum (Fig 4;13). One of these has a doublet splitting of 137 gauss and the other 57 gauss.

The species causing the doublet splitting of 137 gauss can be obtained alone if sodium cyanide is used as the source of cyanide ions. Infra-red spectra show that such samples contain a higher concentration of cyanide ions than the potassium cyanide doped samples. On cooling to $77^{\circ}K$ the larger doublet remains isotropic (Fig 4;15), and we have thus not been able to obtain any anisotropic

E.S.R. Spectrum of KCl Doped with KCN and γ-irradiated for 10 minutes
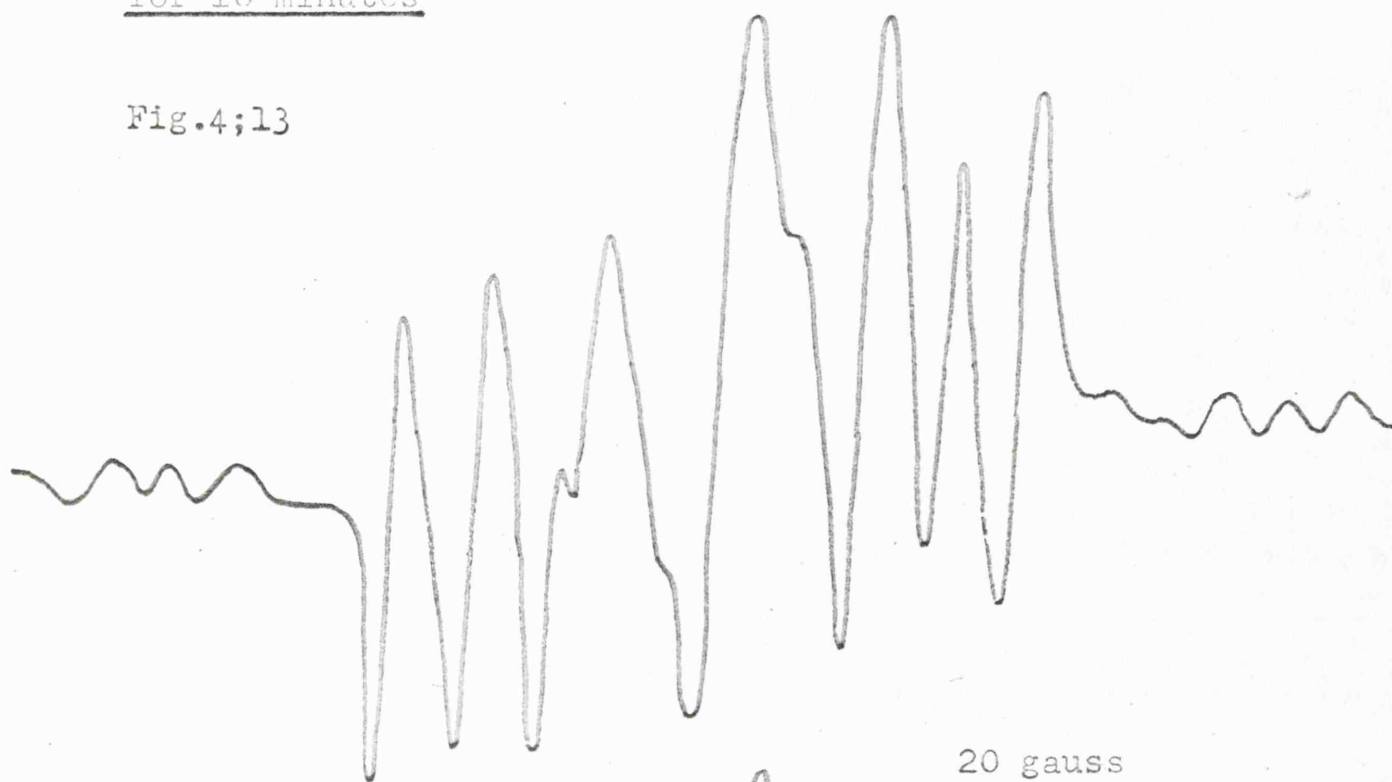
Fig.4;13

20 gauss

Fig. 4;14

The Same Sample after

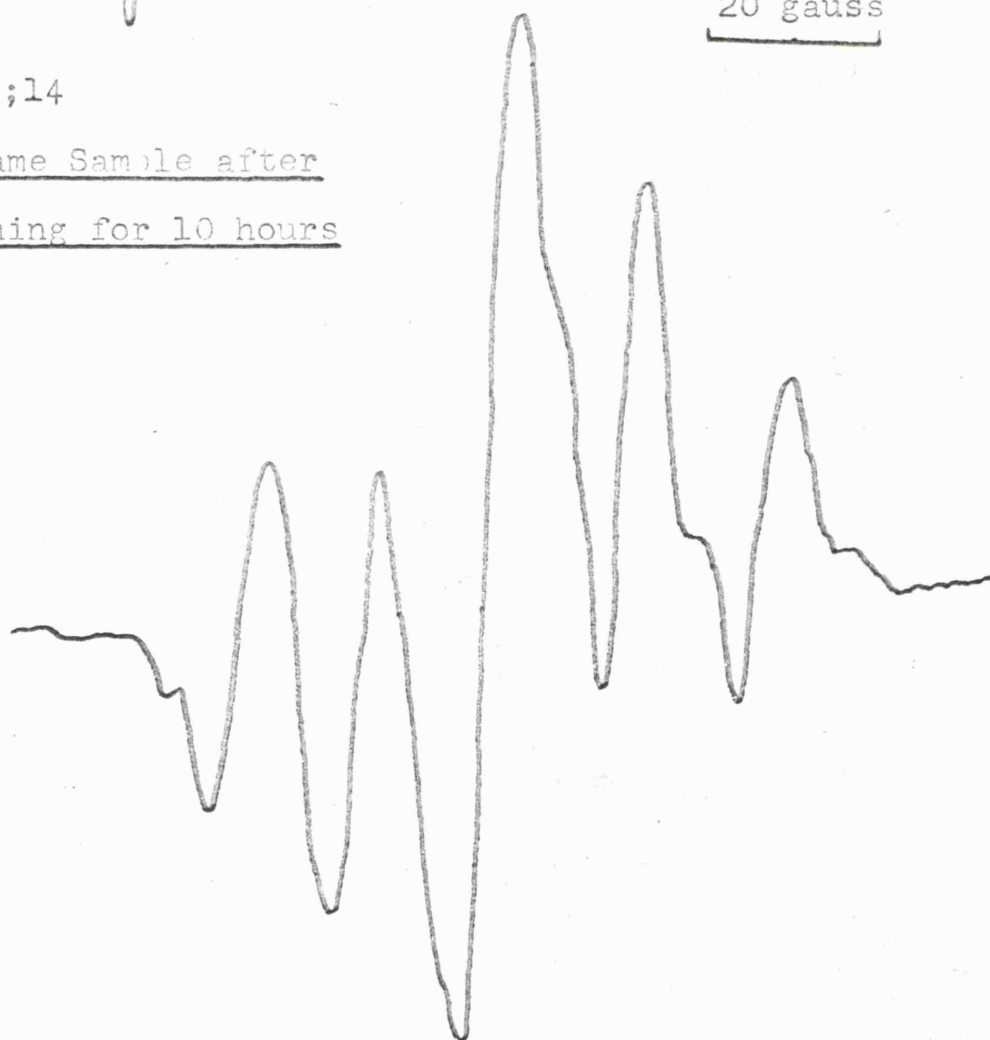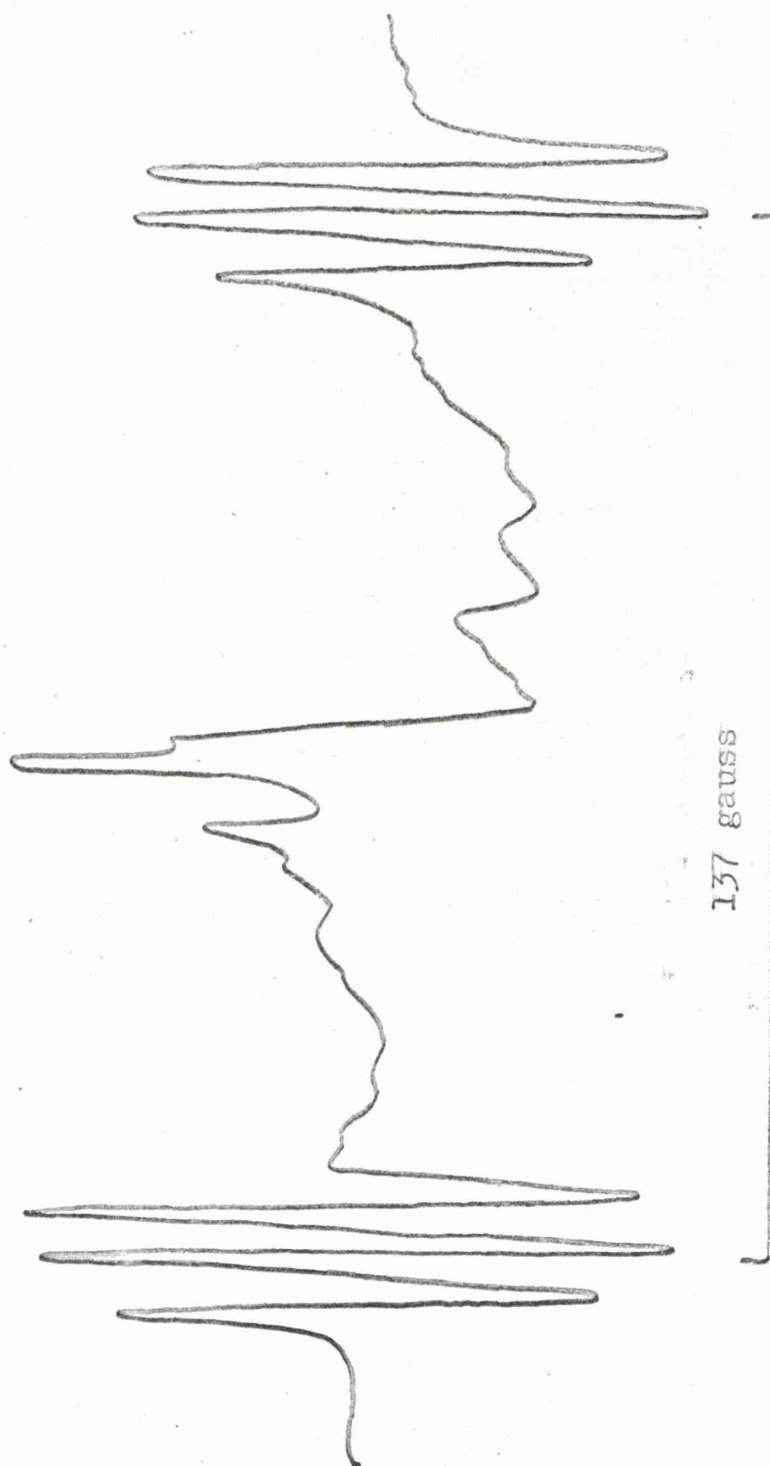Bleaching for 10 hours

Fig.4;15

E.S.R. Spectrum of KCl Doped with CN⁻ and γ-irradiated for 1 hour

Recorded at 77°K

137 gauss

parameters experimentally. By suitable isotopic substitution with $^{13}CN^-$ the presence of carbon in the radical has been confirmed, and the isotropic coupling obtained. Substitution with ^{2}H and ^{15}N has enabled the other hyperfine coupling constants to be assigned unambiguously. The full isotropic parameters are given in table 4;5. This spectrum is assigned to the HCN^- radical.

The smaller doublet (57 gauss) we have assigned to an α-protonated radical (Species A). This species can be observed in the absence of HCN^- if the potassium cyanide doped samples are recrystallised several times. This treatment reduces the amount of cyanide ion incorporated into the lattice. Species A is unstable and decomposes rapidly at room temperature. A further species can then be observed in the e.s.r. spectrum – species B (Fig 4;14). Both species have been shown to contain hydrogen and nitrogen atoms, but attempts to observe coupling to ^{13}C in enriched samples have failed. The e.s.r. data for A and B is given in Table 4;6. At $77^{\circ}K$ neither of the species A and B can be observed in the e.s.r. spectrum.

Addition of hydroxide ion impurity into the crystal lattice increases the yield of both HCN^- and the species A. Since these species are obtained wholly or in part from impurities in the halide lattice it is not surprising that the relative concentrations of the species are highly sample dependent.

Table 4;5

Isotropic E.S.R. Data for HCN^- in KCl Lattice

A (H)	$A(^{14}N)$	$A(^{13}C)$	g-value
137.5	6.5	74.3	2.0020

Table 4:6

Isotropic E.S.R. Data for Species A and B in KCl

Species	A(H)	A(^{14}N)	g-value
A	57	9.5	2.0030
B	34	17.0	2.0030

— — — — — — — — — — — — — —

ii. Identification of HCN⁻ and Derivation of Spin Densities

The large proton coupling in this species (137 gauss) could only arise from an α-proton radical similar to the formyl radical. The HCN⁻ radical is isoelectronic with the formyl radical and explains all the hyperfine coupling data. Species A forms even when the concentration of cyanide ion is low, and does not show any coupling to ^{13}C. These observations make the assignment of A to the HCN⁻ radical unlikely.

Since the spectrum of the HCN⁻ radical appeared isotropic even at 77°K and was not observed at 4°K we were not able to obtain any anisotropic parameters for this radical, and hence obtain the total spin densities on carbon and nitrogen directly. We have, however, been able to estimate indirectly the spin densities on these atoms assuming a structure similar to formyl.

The bond angles of isoelectronic radicals tend to be similar even if the central atom is different. For example the isoelectronic radicals CO_2^- and NO_2 both have a bond angle of about 134° 130. Thus if we assume that the bond angle for HCN⁻ is the same as in HCO, i.e. 120°, this will mean an sp^2 hybridisation of the orbital, and hence

the ratio of spin densities in these orbitals will be one to two.
With a spin density of 6.7% in the s-orbital this would mean a spin
density of 13.4% in the p-orbital.

It is more difficult to obtain the spin density in the p-orbitals
on nitrogen. Since, however, the isotropic coupling must be due to
spin density on the nitrogen (ρ_N) and spin density on carbon (ρ_C)
we can set a_N the anisotropic nitrogen hyperfine coupling equal
to[133]:-

$$a_N = \rho_N Q_{NC}^{N} + \rho_C Q_{CN}^{N}$$

where Q_{NC}^{N} and Q_{CN}^{N} are the appropriate spin polarisation parameters.
We would expect Q_{NC}^{N} to be very close to that for the conjugate acid
H_2CN. Using this value and neglecting the term from Q_{CN}^{N} we obtain
the value of about 50% for ρ_N. The total spin density on the HCN⁻
radical is 97% which is extremely satisfactory considering the
assumptions involved.

iii. The Species A

This species also had a high proton coupling (57 gauss) and
we have thus assigned this spectrum to HON⁺. This is isoelectronic
with HCN⁻. The species HNCO⁻, HOCN⁻ and NCH.O⁻ were eliminated
because of the total absence of coupling to ^{13}C. The alternative
tautomer to HON⁺, HNO⁺, was also unlikely because of the small
isotropic nitrogen coupling. The identity of this radical is
uncertain and so the structure will not be considered here.

iv. The Electronic Structure of HCN⁻

The m.o. structure is the same as for HCO:

$$(1a')^2 \ (2a')^2 \ (3a')^2 \ (1a'')^2 \ (4a')^2 \ (5a')$$
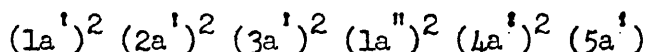
The spin densities in the various orbitals in HCO and HCN⁻ are

compared in table 4;7.

Table 4:7

Comparison of the Spin Densities in HCO and HCN⁻

Radical	c^2_H	$c^2_{C(s)}$	$c^2_{C(p_y)}$	$c^2_{X(p)}$
HCO	0.27	0.121	0.327	(0.28)
HCN⁻	0.27	0.067	0.134	(0.50)

The quantities in brackets are calculated (see text).

— — — — — — — — — — — — — —

The most surprising feature in the above comparison is the

similarity in the proton spin densities, despite the fact that the

spin density on the carbon in HCN⁻ is only about half that on the

carbon in HCO.   If the coupling mechanism described above depends

linearly on the spin density on carbon, one would expect a reduction

in the proton coupling of about one half.   Even if this is not exactly

correct one would still expect a substantial reduction in the proton

coupling.   There is, however, a further method of introducing positive

spin density onto the protons.   This is the mechanism of hyper-

conjugation from the unpaired electron density in the p_z-orbital on

the nitrogen or oxygen atom.   This will tend to even out the effect

of transferring spin density from the carbon to the oxygen or nitrogen

atom, and this will be discussed further when these radicals are

compared with H_2CN.

The high spin density on the nitrogen atom in HCN^- requires the inclusion of a further valence bond structure (III):

$$\overset{\cdot}{C} = X \qquad :C \equiv X \qquad C = X \cdot$$
$$H^{/} \qquad \cdot H \qquad H^{/}$$
$$I \qquad\qquad II \qquad\qquad III$$
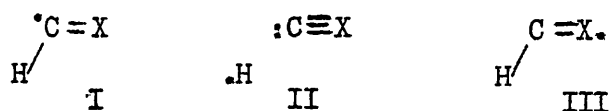
In the simple m.o. description the higher spin density on the nitrogen in HCN^- can be discussed in terms of a mixing of the localized $4a'$ m.o. with the $5a'$ m.o. to form a delocalized orbital which incorporates atomic orbitals on both the carbon and nitrogen atoms. Actually all the a' m.o's evolve from linear combinations of all atomic orbitals of the correct symmetry with expansion coefficients describing the contribution from each orbital. Thus the description of the m.o's given for HCO above in terms of the localized orbitals needs to be modified for HCN^- and probably to a lesser extent for HCO.

The fact that the nitrogen atom has the larger spin density compared with the more electronegative oxygen is typical of radicals where the unpaired electron is in an orbital which is non- or anti-bonding. For example in NO_2 and CO_2^- [130] the carbon atom has a larger share of the unpaired electron than the nitrogen

v.   The Formation of HCN^- from HCN and H_2CN

It is constructive to consider the formation of HCN^- by both the addition of an electron to hydrogen cyanide and the loss of a proton from the H_2CN radical.

a. The Addition of an Electron to Hydrogen Cyanide

From the Walsh diagram for HAB molecules (Fig 4;3) the ten

valence electrons in hydrogen cyanide completely fill the two centre

m.o's: $(1\sigma_N)^2 (2\sigma_{H-C})^2 (3\sigma_{N-C})^2 (1\pi_{N-C})^4$. The diagram also

suggests that the linear molecule is the one of lowest energy.

However, an additional electron will go into the degenerate π-anti-

bonding orbital and from fig 4;3 there will now be some advantage if

the molecule were to bend. The orbital degeneracy would be lifted,

and the π-antibonding orbital which the electron would occupy, and

which is formally centred on the carbon atom, will decrease in energy

by the incorporation of s-character. The p-character of the bonding

orbitals will of course increase and raise the energy of these

orbitals, but initially the gain in stability of the π-antibonding

orbital will be greater than the loss by the σ-orbitals. The

situation is completely analogous to the effect of adding an electron

to the linear carbon dioxide molecule to form the bent CO_2^- radical[130].

In HCN^- the two highest m.o's (the $4a'$ and $5a'$ orbitals) are

thus composed of one of the π-bonding and one of the π-antibonding

orbitals. If the unpaired electron is considered localized on the

carbon atom the $4a'$ orbital is a pure p-atomic orbital on the nitrogen.

Our results show that this localized description is a poor one and

that there is considerable spin density on the nitrogen.

b. The Removal of a Proton from the Methylene Imino Radical

The effect on the m.o's of removing a proton from H_2CN is shown

diagramatically in fig 4;16. Only the relative order of the

orbitals is indicated and no importance should be attached to the relative slopes of the correlation lines. The removal of a proton from H_2CN reduces the symmetry from C_{2v} to C_s, and this is shown in the different 'labels' of some of the orbitals in the two radicals.

In H_2CN about 70% of the unpaired electron is in the nitrogen p-orbital, while in HCN^- there is only about 50%. Further the spin density on the protons in H_2CN is about 35%, or 18% on each, while in HCN^- there is 25% on the single proton. The spin density on the carbon, on the other hand, has increased from a possible small negative value in H_2CN to a positive 20% in HCN^-. If one considers the 20% on the carbon to be equivalent to the 18% wich was on the proton the net effect of removing the proton appears to be the transfer of spin density from nitrogen to the proton.

The proton splitting in H_2CN can only be explained by actual delocalization of the unpaired electron by a hyperconjugative mechanism. The fact that the proton coupling increases on removing one of the protons from H_2CN, despite the decrease of density on the nitrogen atom, indicates that the α-proton coupling mechanism described for the formyl and the vinyl radicals places spin density more efficiently on the protons. than the hyperconjugative mechanism.

Care has to be taken in comparing H_2CN with HCN^- for the H-C-N bond angles may not be similar, and hyperconjugative effects are highly dependent on the distance of the proton from the p-orbital containing the unpaired electron. If they can be considered similar then using 'Q_B' values from H_2CN of $91.4/73.3 = 1.25$ gauss/%, the 50%

of spin density in HCN⁻ will produce a proton splitting of 62 gauss.

The remaining 75 gauss must come from the α-coupling mechanism

described earlier. If the same Q value is used, for HCO only 35

gauss would come from the 28% on the oxygen atom, leaving 102 gauss

to be explained by the α-coupling mechanism. Although this

calculation is very approximate it does show that the almost

identical splittings in HCO and HCN⁻ are not unreasonable, despite

the fact that there is almost twice as much spin density on the

carbon in HCO compared with HCN⁻.

<u>Fig 4:16</u>

<u>Molecular Orbital Correlation Diagram for the Removal of a Proton</u>

<u>from H₂CN to form HCN⁻</u>

<u>H₂CN (C₂ᵥ)</u>   <u>HCN⁻ (Cₛ)</u>

H₂CN (C₂ᵥ)		HCN⁻ (Cₛ)
Lone pair on N	2b₂ ⟍ ⟋5a'	Carbon orbital
C—N π-bond	1b₁ ⟍ ⟋ 4a'	Lone pair on N
C—H π-bond	1b₂ ⟋ 1a''	C—N π-bond
C—H σ-bond	3a₁ ⟍ 3a'	C—H σ-bond
C—N σ-bond	2a₁ ——— 2a'	C—N σ-bond
s-orbital on N	1a₁ ——— 1a'	s-orbital on N
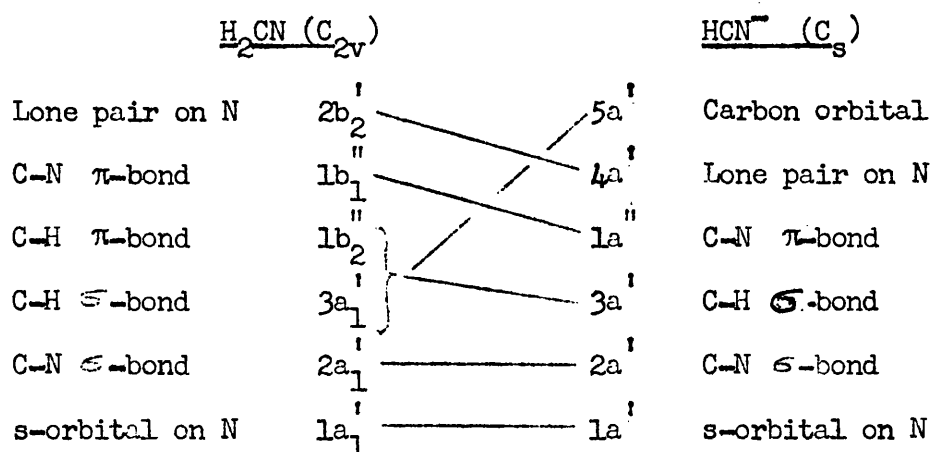
This diagram is not to scale, and no weight should be placed

on the slopes of the correlation lines, except for the C—H bonds in

H₂CN to 5a' in HCN⁻.

Note that all orbitals of the same symmetry can 'mix' and that

the formal description of each m.o. is only an approximation.

D. The Cyanogen Negative Ion

I. Experimental Results

i. Powder Spectra

One set of absorption bands in the e.s.r. spectrum of γ-irradiated powders of sodium and potassium cyanide and of potassium chloride doped with cyanide ions, when recorded at 77°K, were identical except for minor differences in resolution and g-values. These differences can be understood, at least partly, in terms of the phase changes which occur in sodium and potassium cyanide on cooling, reducing the symmetry from cubic to orthorhombic[62]. The e.s.r. spectra at X and Q band frequencies are shown in figs 4;17 and 4;18. The interpretation beneath the spectra is based on comparison with results from single crystal spectra. These powder spectra are complicated by the fact that the g-tensor is not axially symmetric, in contrast with the hyperfine $A(^{14}N)$ tensor. This has resulted in non-principal lines being displaced to higher field relative to the principal lines and hence the extra lines and bad resolution to high field. This spectrum has been assigned to the $(CN)_2^-$ radical.

Attempts to resolve this radical in other alkali halides have failed, despite the fact that i.r. spectra revealed that cyanide ions had been incorporated. A similar effect is also found with the hydrogen cyanide negative ion, which is only well resolved in a potassium chloride host lattice.

Irradiation of cyanide doped potassium chloride crystals at 77°K followed by measurement without warming gave a spectrum characteristic
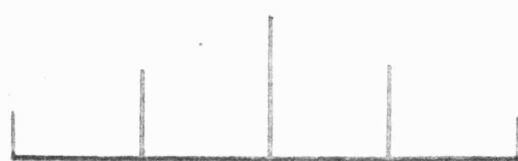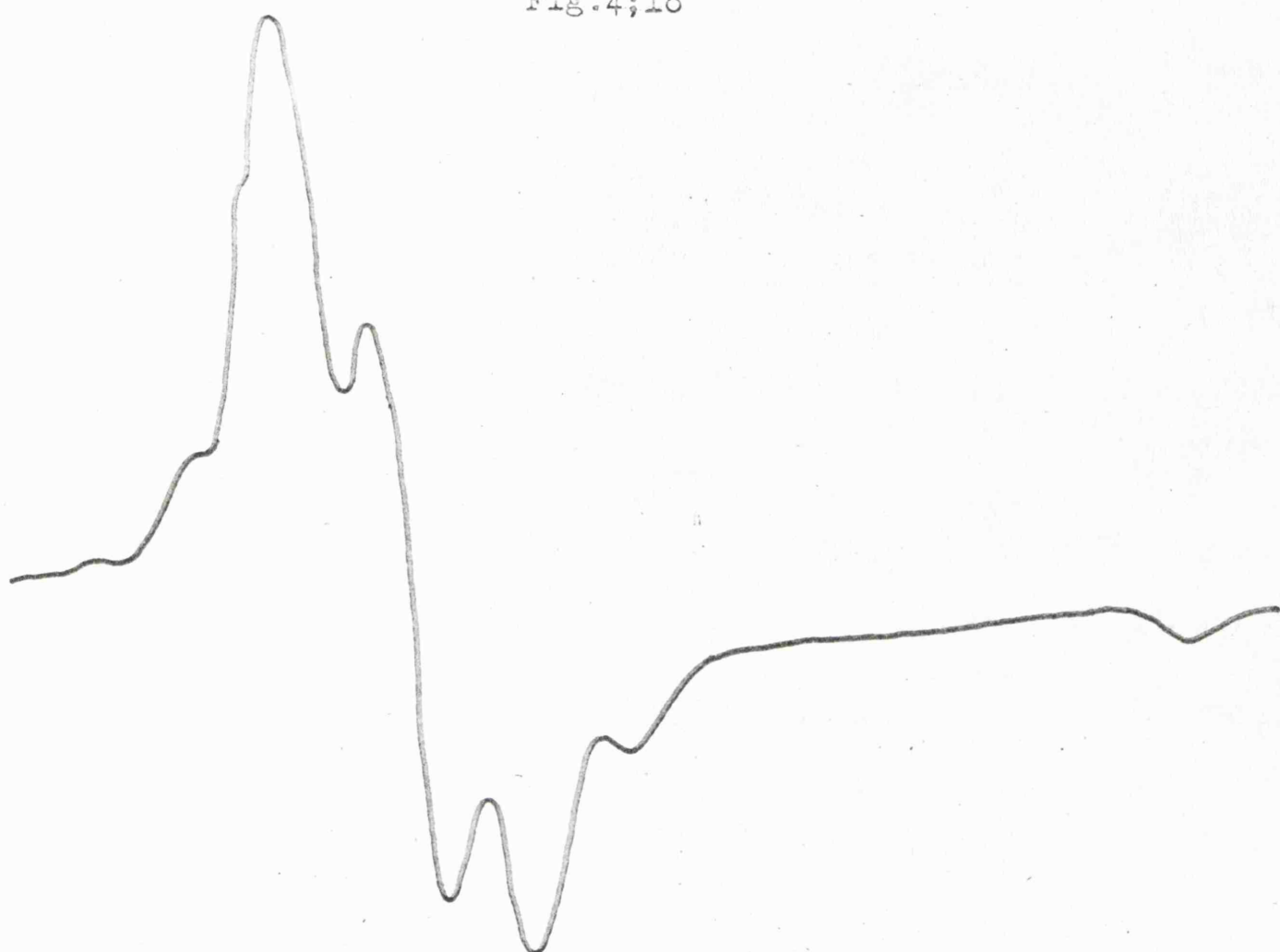
Fig.4;17
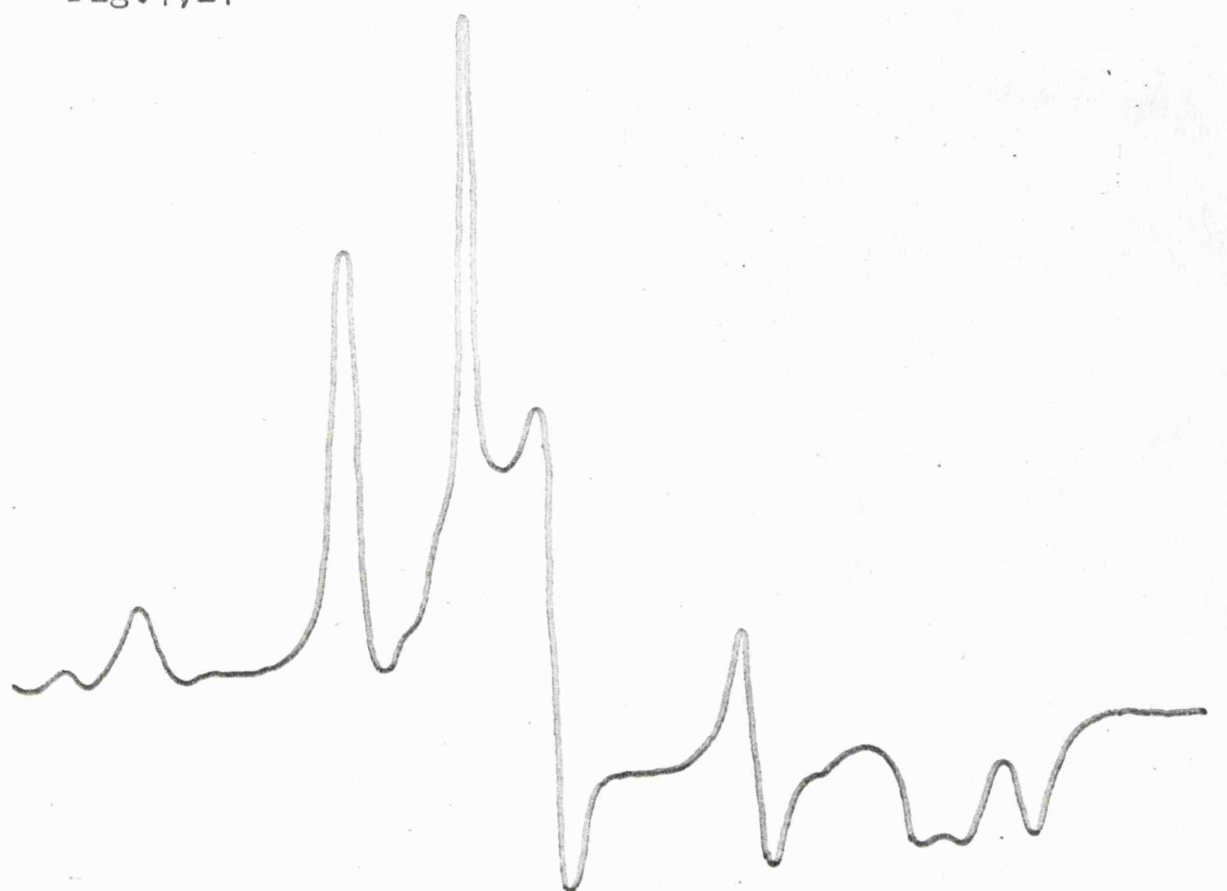
g = 1.9806

$g_x = 2.0013$

$g_y = 2.0058$

$g_z = 1.9851$

E.S.R. Spectrum of γ-irradiated Polycrystalline KCl
Doped with CN⁻, Recorded at 77°K (X-band)

Fig.4;18

$g_x = 2.0012$

$g_y = 2.0060$

$g_z = 1.9860$

E.S.R. Spectrum of γ-irradiated Polycrystalline KCl
Doped with CN⁻, recorded at 77°K (Q-band)

of the Cl_2^- radical (Fig 4;19a). The spectrum attributed to $(CN)_2^-$ is very weak by comparison, but when the sample was warmed and re-cooled to $77^\circ K$ the Cl_2^- radical was not detected and the signal due to the $(CN)_2^-$ radical was increased several fold (Fig 4;19b). The signal attributed to the H_2CN radical appears to remain at constant intensity, before and after warming (Fig 4;19a and b). Irradiation of pure alkali metal cyanides at $77^\circ K$ yields the spectrum assigned to $(CN)_2^-$ directly and warming the samples has no noticeable effect on the spectrum.

ii. Single Crystal Spectra

Since the powder spectra of the $(CN)_2^-$ radical in the pure cyanides and in the cyanide doped potassium chloride lattice are so similar, only single crystal spectra of the irradiated potassium chloride crystals were used, as these were easier to grow and handle. Further these crystals suffer no change of phase on cooling, which nevertheless resulted in a marked narrowing of the lines. With the pure cyanides the spectra at room temperature were complicated by other species, such as the F-centre. The crystals used in this study were grown in a Stockbarger crucible under vacuum, but crystals grown from aqueous solution gave the same spectra.

On rotation about an axis perpendicular to a 100 plane, at most orientations, two distinct sets of quintets are observed. Figs 4;20 and 4;21 show the position of the lines of each of these quintets as the crystal was rotated. Each of these quintets is repeated every 90° and the two sets are out of phase by 45°. In

Fig.4;19

E.S.R. Spectra of γ-irradiated Polycrystalline KCl Doped with

CN⁻. Recorded at 77°K.

a. X-band spectrum after irradiation at 77°K
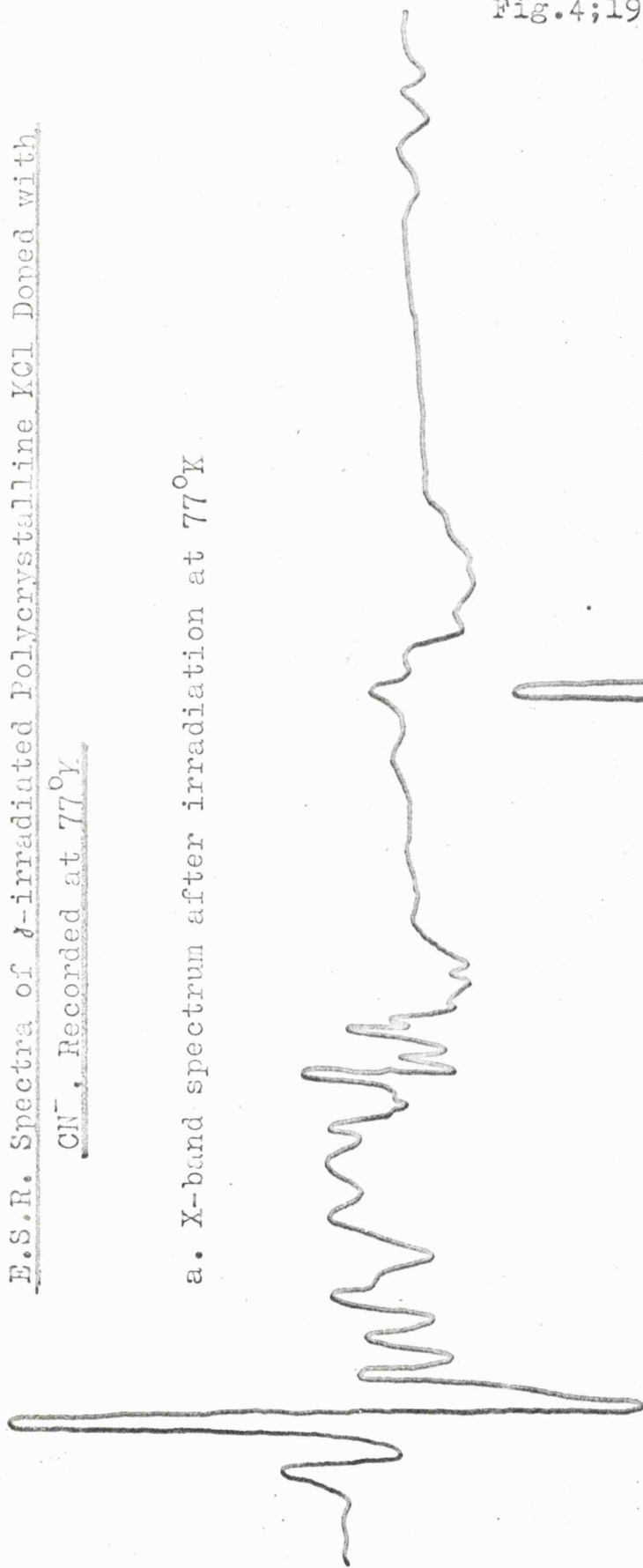
b. X-band spectrum of same sample
after warming to 300°K.
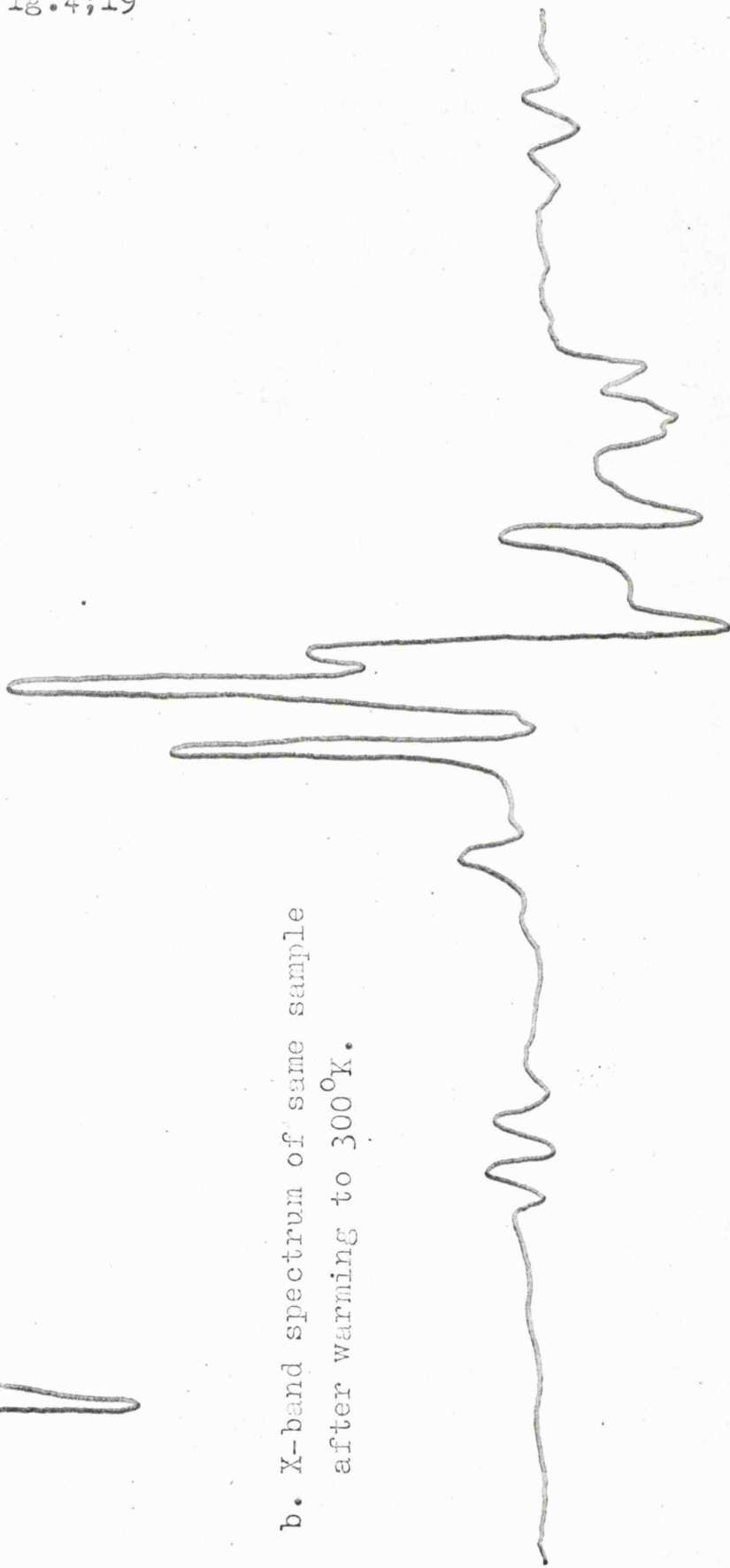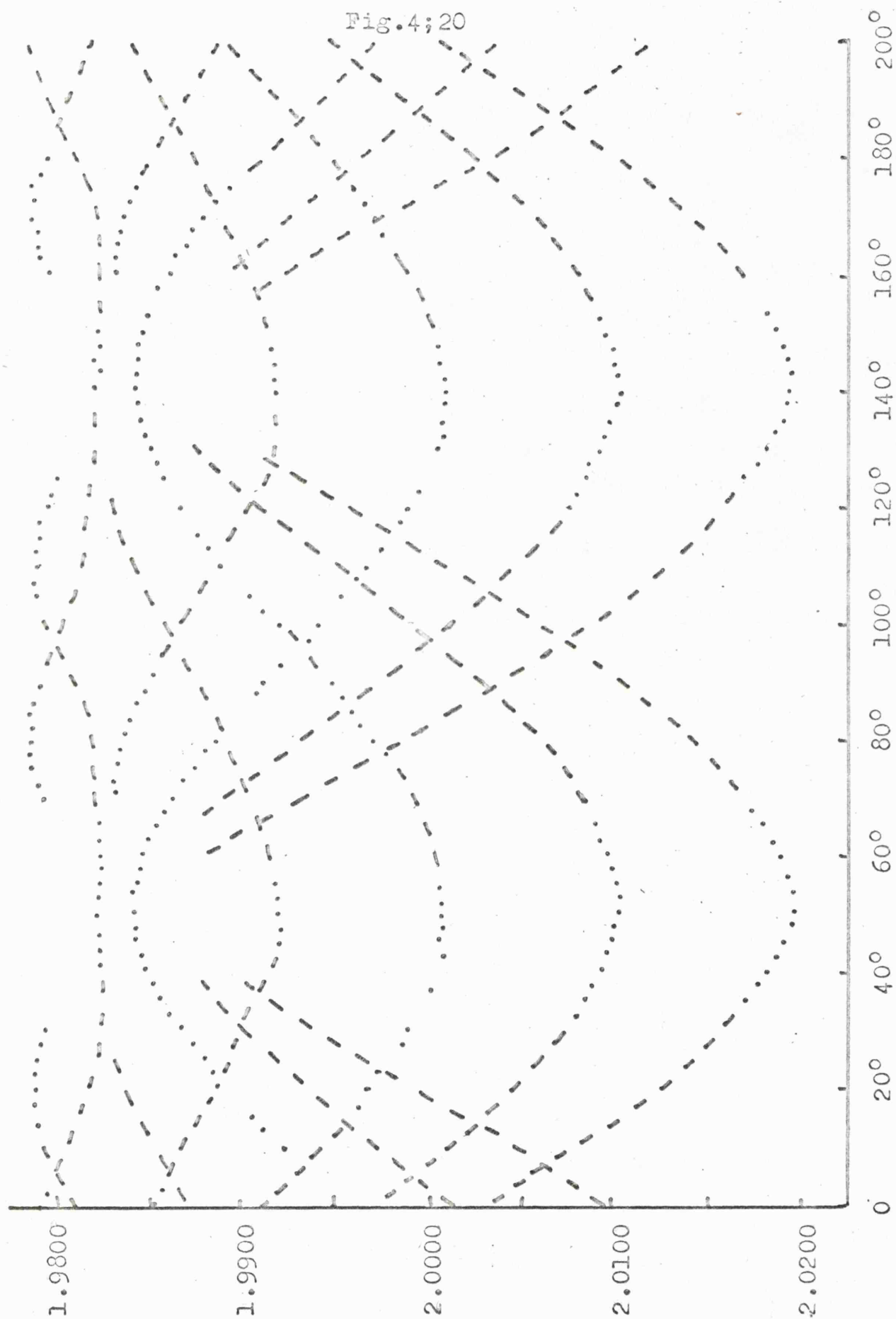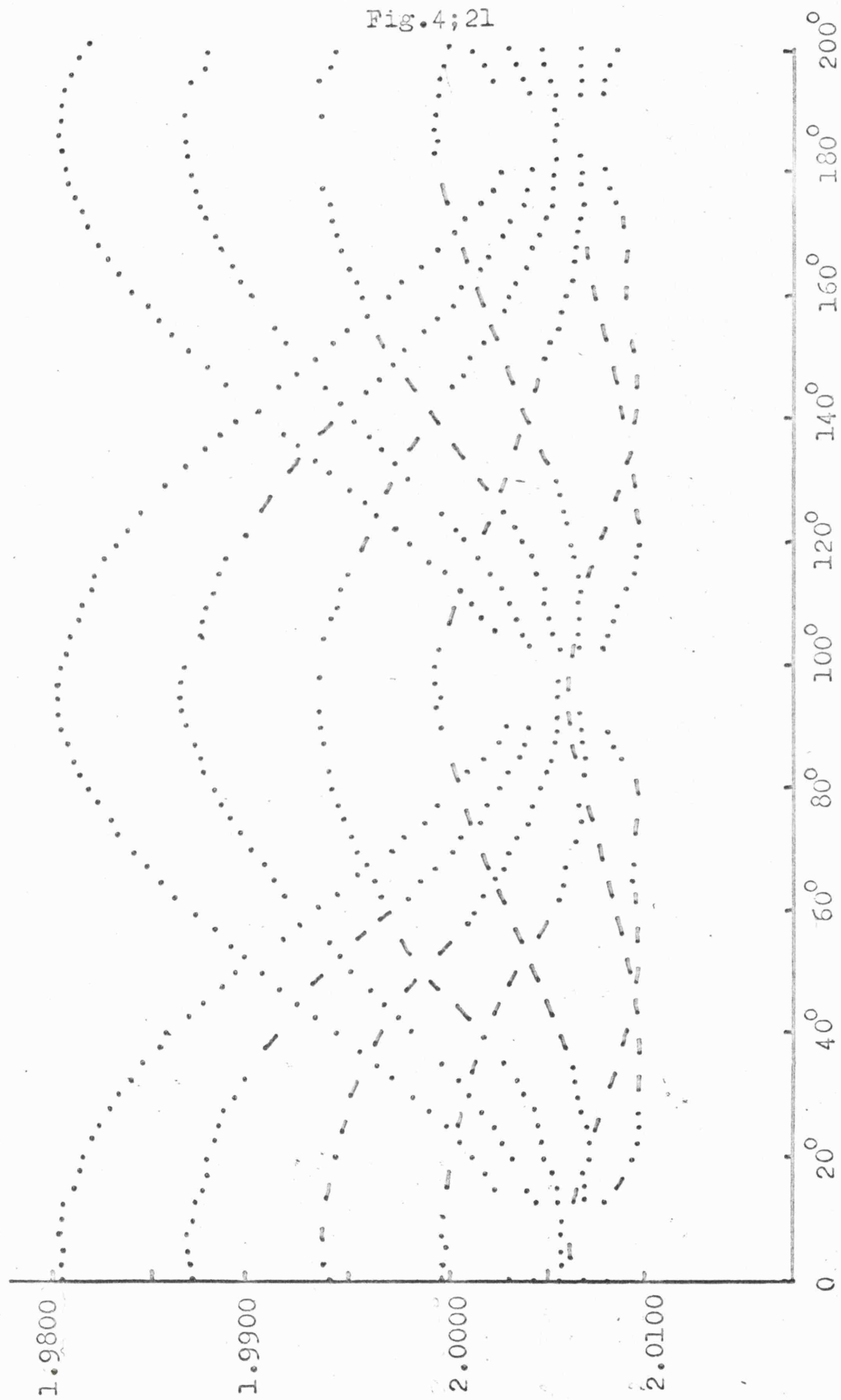
Fig.4;20

Variation of $A(^{14}N)$ and g with angle of rotation, rotating the crystal about an axis perpendicular to the 100 plane

Fig.4;21

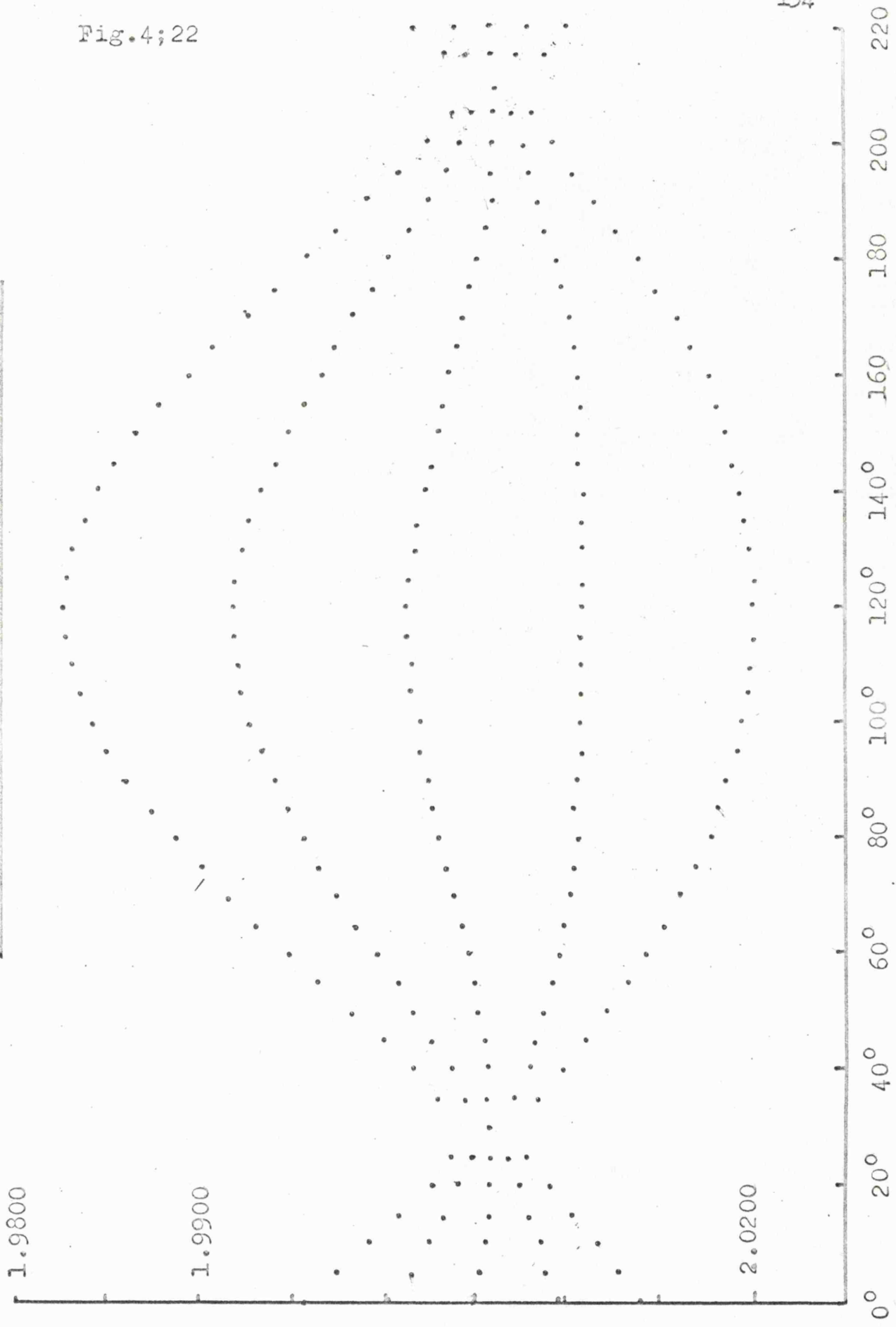Variation of A(14N) and g- with Angle of Rotation, Rotating the Crystal about
an Axis Perpendicular to the 100 Plane

1.9800
1.9900
2.0000
2.0100

0   20°   40°   60°   80°   100°   120°   140°   160°   180°   200°

132

figs 4;20 and 4;21 and all subsequent figures of this type dotted

points indicate actual experimental observations, and broken lines

join extrapolated points where the lines were obscured by other over-

lapping lines. To facilitate the following of the many lines the

spectra were recorded and calibrated every $2\frac{1}{2}^{\circ}$. Identical results are

obtained on rotation about axes perpendicular to the other faces of

the crystal.

These results can be attributed to a radical which is oriented

parallel to a face diagonal of the unit cell of the halide. If this

is correct a less complicated spectrum will be obtained by rotation of

the crystal about an axis perpendicular to the 110 plane (Fig 4;26).

There will be then two sets of lines due to rotation of the radical

about two of its principal axes (only two of each) and these two sets

should be in phase. There should also be some other lines due to the

radical being rotated such that at no time will it be oriented along

one of its principal directions. The sets of lines observed are

shown in figs 4;22, 4;23 and 4;24. One of the sets of quintets is

not resolved (Fig 4;23). Fig 4;24 shows the quintet due to the

rotation about non-principal axes; there were in fact two sets of

quintets which appear as mirror images, but for simplicity only one

set is shown. From fig 4;24 it can be seen that the non-principal

lines have been displaced to high field relative to the principal ones

(Figs 4;22 and 4;23), and hence will give rise to extra features in the

powder spectrum. For example, line A in fig 4;17 has a g-value of

1.9806, and the point A in fig 4;24 has a g-value of 1.9805. Fig

4;25 shows the spectrum of the single crystal at 30° and 120° (scale

Variation of A(^{14}N) and g with Angle of Rotation, Rotating the Crystal
about an Axis Perpendicular to the 110 plane.

Fig.4;22

134

Fig.4; 23

Variation of A (^{14}N) and g with angle of Rotation, Rotating the Crystal about an Axis Perpendicular to the 110 plane

135

Variation of A(^{14}N) and g with Angle of Rotation, Rotating the Crystal about an Axis Perpendicular to the 110 plane
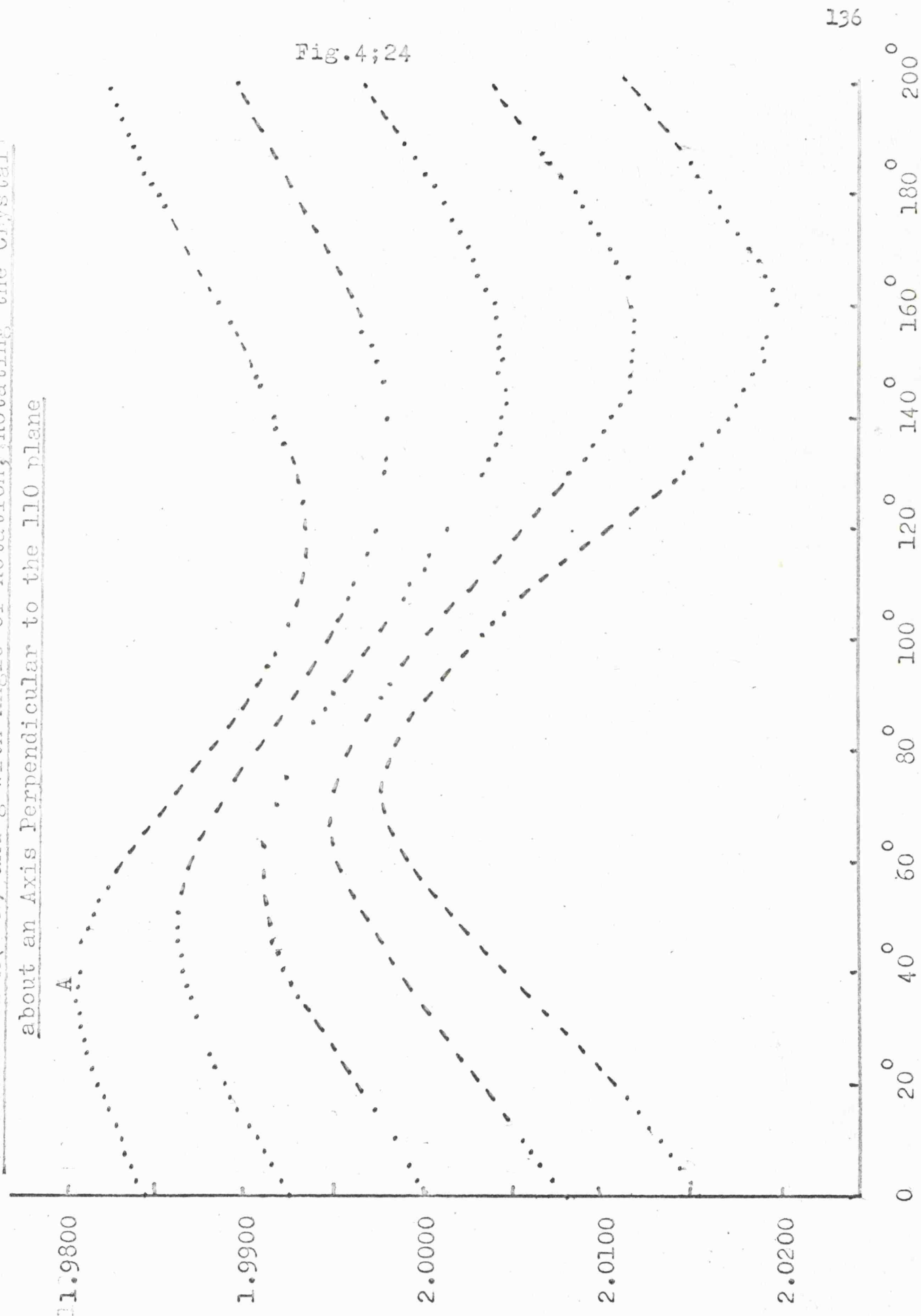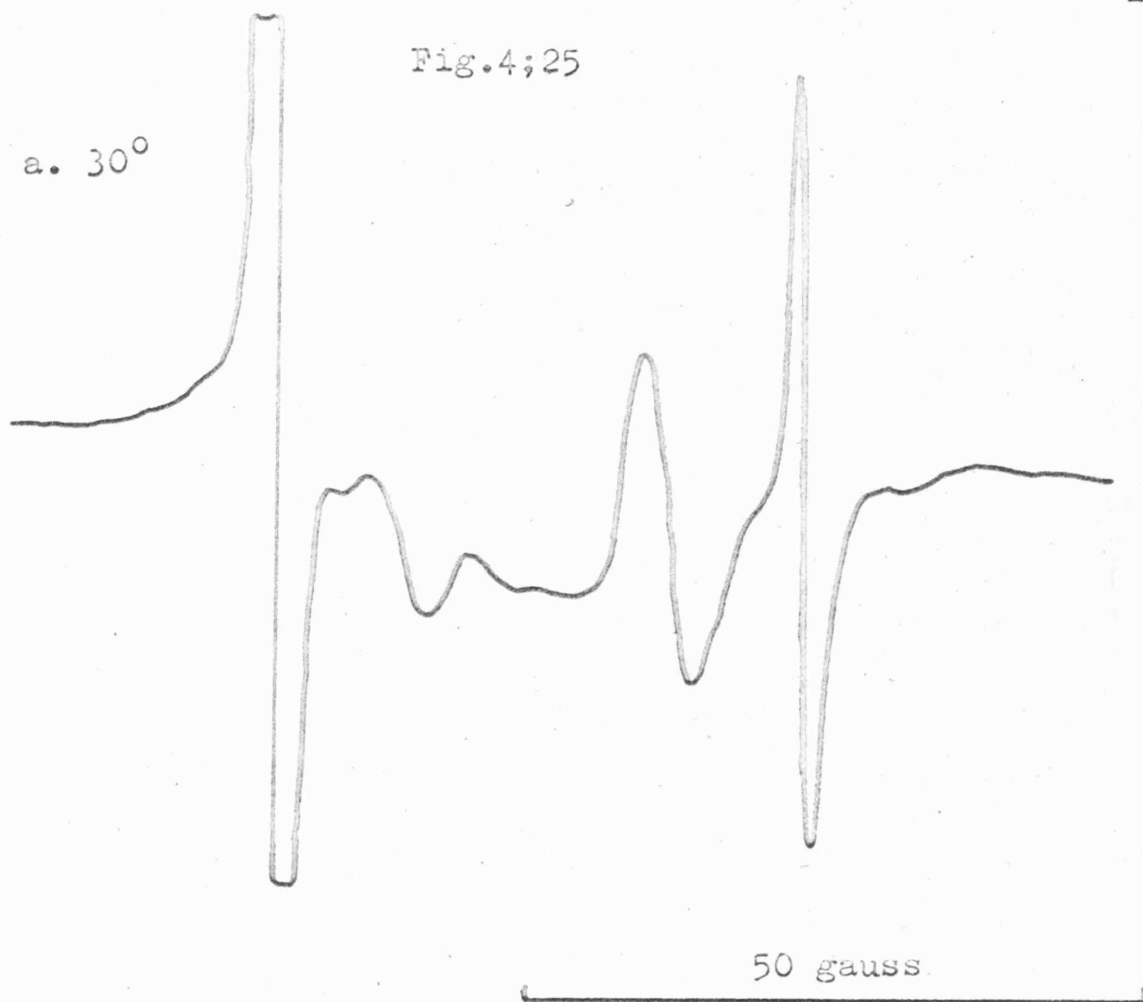
Fig.4;24

136

Fig.4;25

a. 30°

50 gauss
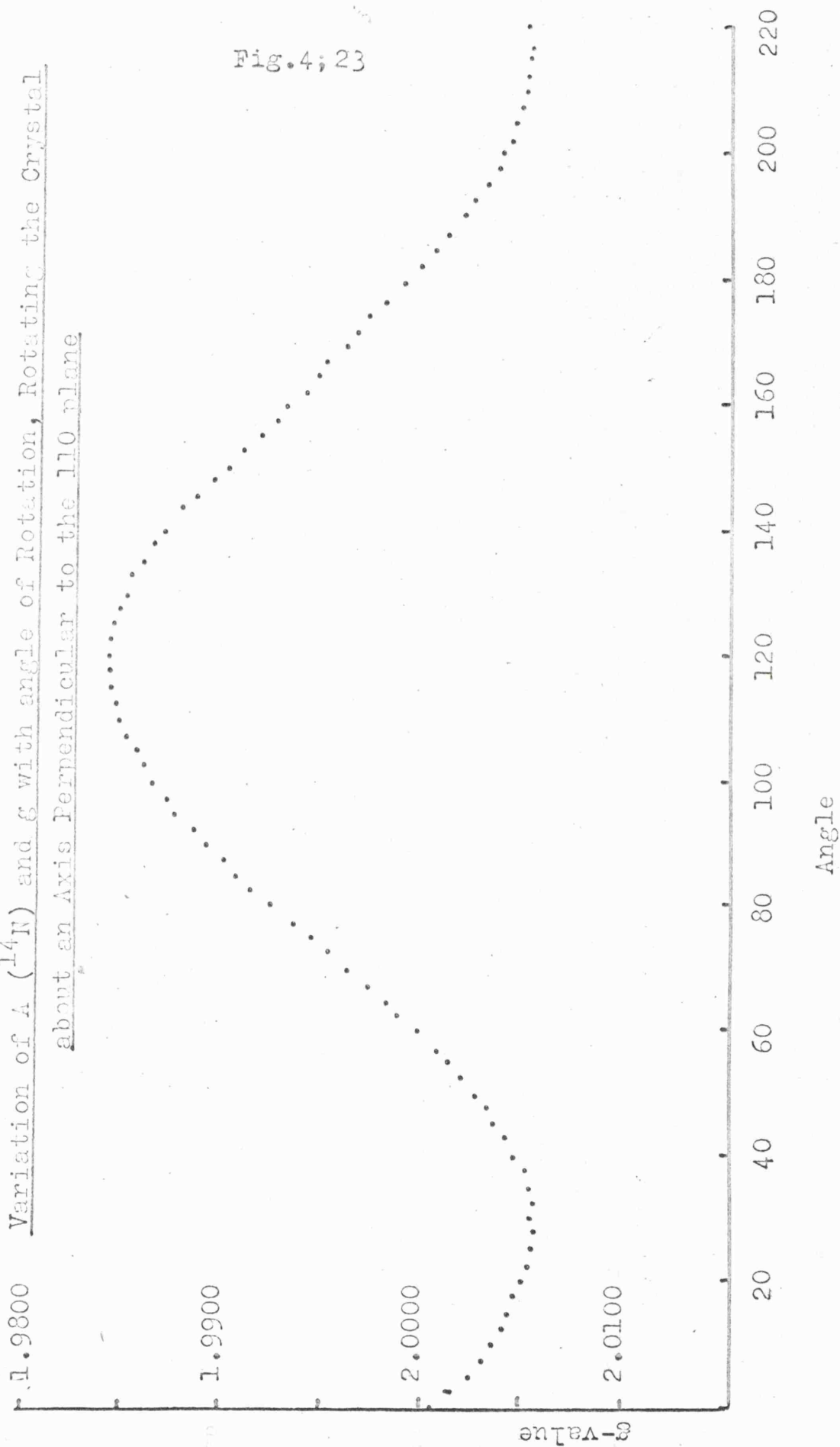
b. 120°
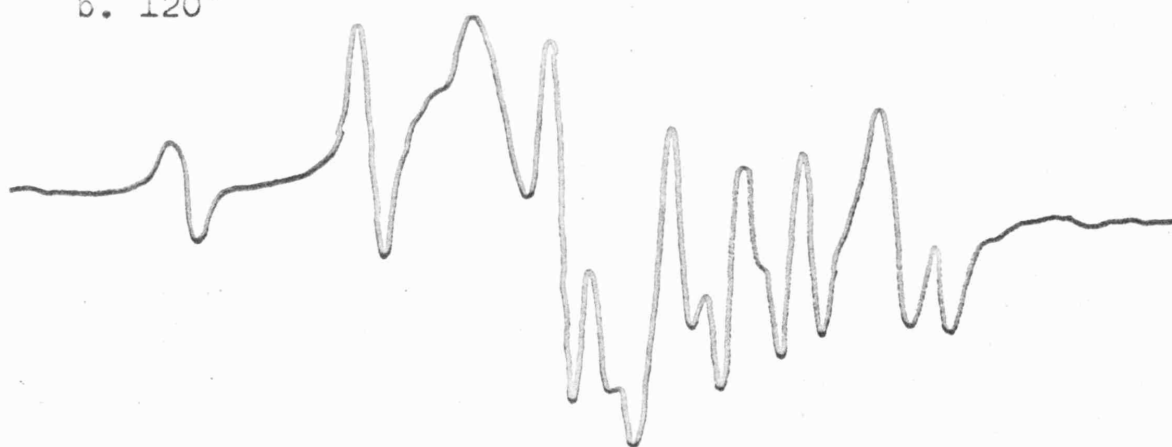
Single Crystal X-band Spectra of irradiated KCl Doped
with CN⁻, Rotating the Crystal about the 110 plane

Fig.4;26
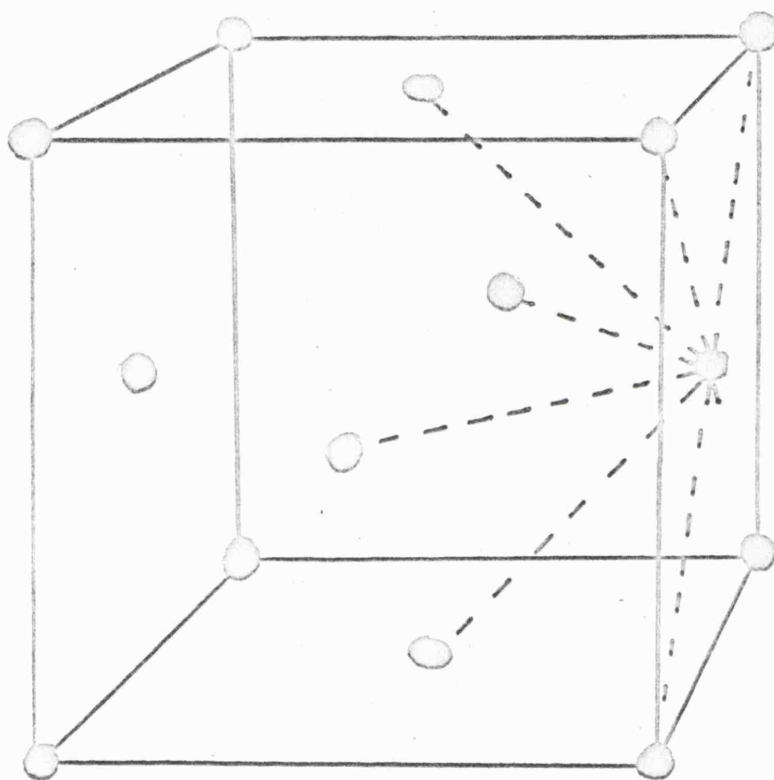
The Anion Sub-lattice of a KCl Crystal, Showing the
Possible Orientations of the Radical Relative to the
Axes of the Crystal

same as in figs 4;22-4;25).

Weak lines, which are assigned to coupling with ^{13}C nuclei, were detected for the centre lines of the quintet. Although for some orientations they were obscured by the much more intense nitrogen hyperfine lines, they were easily observable in the region of two of the $A(^{14}N)$ principal directions. The splitting between these weak lines corresponds exactly with the nitrogen hyperfine coupling and hence two of the principal ^{13}C tensor values could be measured unambiguously. Enough of the ^{13}C tensor could be observed to confirm that its principal axes are within 15° of the $A(^{14}N)$ and g-tensor axes directions. The large uncertainty is mainly due to the small anisotropic component, which makes it difficult to state at which angle the largest ^{13}C coupling occurs.

The A- and g-tensors are given in table 4;8. Comparison of the single crystal results with the powder spectra makes the interpretation of the spectra relatively easy. The spectra from fig 4;22 and 4;23 are of a radical rotated about an axis along the σ-bonding system (A_1 in fig 4;27) and along the π-orbital containing the unpaired electron (A_2 in fig 4;27) respectively. In fig 4;20 the spectra are of the radical rotated about an axis perpendicular to A_1 and A_2 in fig 4;27 (A_3).

In table 4;9 the ^{13}C and ^{14}N tensors have been separated into their isotropic and anisotropic parts. The nitrogen tensor has a sign ambiguity and both possible values are given. It will be shown later that the second set is the most likely.

Fig.4;27
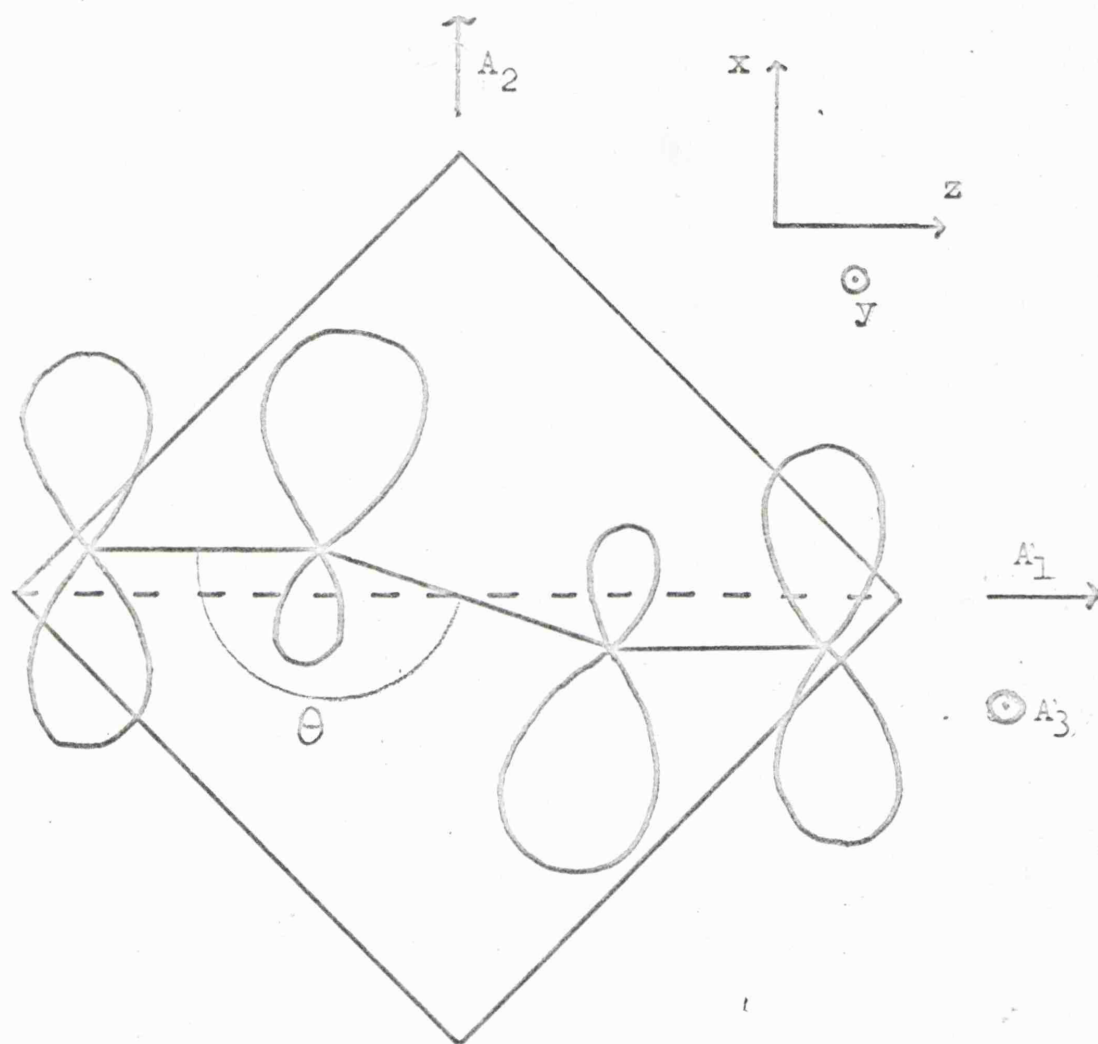
Orientation of the Radical in a 100 plane of the
Crystal, showing the Principal Directions of the g-
and the ^{14}N- tensor

Table 4:8

Experimental Hyperfine Coupling and g-tensors for $(CN)_2^-$

Axis	$A(^{14}N)$	$A(^{13}C)$	g-tensor
x	14.8	67.0 ±0.5	2.0013
y	2.5	56.0 ±0.5	2.0058
z	2.5	56.0 ^{x}	1.9851

x assumes axial symmetry for (^{13}C) A-tensor.

Table 4:9

The Isotropic and Anisotropic Terms and Spin Densities for $(CN)_2^-$

	$A(^{14}N)$	$2B(^{14}N)$	$c^2_{N(s)}$	$c^2_{N(p)}$
a.	5.9	8.9	0.011	0.261
b.	3.9	10.9	0.007	0.320

$A(^{13}C)$	$2B(^{13}C)$	$c^2_{(s)}$	$c^2_{C(p)}$
59.6	7.33	0.054	0.113

- - - - - - - - - - - - - - -

II. Identification of the $(CN)_2^-$ Radical

Identification of the spectra to the cyanogen negative ion

$N = C - C \equiv N^-$ is based on the following considerations:

1. The e.s.r. spectrum shows the presence of two equivalent nitrogen

atoms, and also ^{13}C satellite lines which are twice as intense as

would be expected for one carbon atom per molecule in natural abundance.

2. The species is observed in γ-irradiated alkali metal cyanides,

and in cyanide doped potassium chloride. Thus as both carbon and

nitrogen atoms are present the radical probably contains $C \equiv N$ units.

The low temperature irradiation experiments indicate that the

species is a secondary radiation product.

3. The low temperature irradiation experiments also indicate that the species is electron deficient and related to Cl_2^-.

4. The single crystal experiments show that the species is oriented so that it lies across the face of the unit cell (the 110 plane) of the halide lattice with the unpaired electron in an orbital in this plane. This orientation is similar to that of the V_k-centres in irradiated alkali halides[54].

5. Crystals doped with cyanate or nitrite did not contain this radical after irradiation.

The simplest species consistent with these considerations is the $N \equiv C - C \equiv N^-$ radical. This radical is also consistent with the detailed quantitative examination of the e.s.r. results which are discussed below.

III. Structure of the $(CN)_2^-$ Radical

i. Orientation in the Potassium Chloride Lattice.

The single crystal spectra show that the principal g-, the nitrogen, - and possibly the carbon anisotropic tensors are oriented normal to the 100 plane and along two of the diagonals of the side of the unit cell in the 100 plane (Fig 4;27) The unpaired electron is in an orbital in the 100 plane, and the parallel direction of the nitrogen tensor is thus diagonally across this plane normal to the N-C bond, and this is taken as the direction of the nitrogen 2p-orbital containing the unpaired electron.

Each cyanide ion has twelve nearest neighbour anions (Fig 4;26)

and it is thus possible for the radical to form even when the

concentration of the cyanide ion is quite low.   It can also be seen

from fig 4;26 that if two cyanide ions dimerise they will be oriented

as described above.

ii. The Geometry of the Radical

The orientation of the ^{13}C anisotropic hyperfine tensor cannot

be found accurately enough for this to be a definitive test of whether

the radical is linear or bent.   There is however good evidence for

the bent structure.

The unpaired electron will be in a π-antibonding orbital and

if the radical is linear this orbital will be doubly degenerate.

However this degeneracy must be lifted so that the orbital in the

100 plane is favoured, to explain the e.s.r. results.   The degeneracy

can be lifted either by a crystal field or as the result of bending.

Examination of the environment of the radical shows that a crystal

field can yield different envirònments for the two π-orbitals, one

in the 100 plane and the other normal to it.   It is not clear

however which one will be the lower energy orbital and the energy gap

will be very small.   Thus with a crystal field lifting of the

orbital degeneracy, the energy difference will not be enough to

prevent strong mixing of the two π-orbitals.   Hence when the

magnetic field is aligned along the N-C bond the g-shift will be

large and negative.   The actual g-shift is negative, but is

comparatively small, indicating that the degeneracy has been lifted

significantly.   Further, if the degeneracy is lifted only by a

crystal field it is normally necessary to cool samples below $77^{\circ}K$

before the radical can be observed by e.s.r. In the single crystals

of halide containing $(CN)_2^-$ the signal could be observed at room

temperature.

If the molecule is linear the unpaired electron is in a pure

π-system and hence any isotropic terms must be the result of spin

polarisation, and would be small. Despite the sign ambiguity in the

nitrogen coupling tensor both sets of p/s ratios are too high to be

attributed to a pure π-system, and the high ^{13}C isotropic term can

only be explained by a bent molecule.

Fig 4;27 shows the radical in a 100 plane. The bond angle θ

cannot be too small since the ^{13}C tensor is roughly aligned with

the ^{14}N-tensor. We suggest a bond angle of about 150°. The

position shown and its mirror image are the only possible orientations

which readily explains why on rotation about an axis A_3 only one

series of lines is observed.

iii. Comparison of $(CN)_2^-$ with H_2CN to Resolve the Sign Ambiguity in A_N

In the bent form of $(CN)_2^-$ the structure is similar to HCN^- and

H_2CN. We can thus compare the p/s ratio from the two possible

nitrogen isotropic and anisotropic terms, in $(CN)_2^-$, with the p/s

ratio of 43 in H_2CN. The first and second sets for $(CN)_2^-$ have p/s

ratios of 24 and 43, and so the second set has been taken as the

correct one. The total spin density summed over the whole molecule

is then 97.3%, which is well within the limits of experimental and

theoretical accuracy. The other set gave 87%.

iv. The Electronic Structure of (CN)$_2^-$

For a linear molecule the possible π-orbitals are shown in

Fig 4;2, each π-orbital being doubly degenerate. In the cyanogen

molecule, which is linear, all the bonding orbitals are filled with

the eight π-electrons. An additional electron will go into either

a $\pi_{g(x)}$ or a $\pi_{g(y)}$-orbital. The situation is similar to the

addition of an electron to the hydrogen cyanide molecule to form

HCN$^-$. The similarities between the HCN and the NCCN molecules have

been pointed out by Burnelle[134]. If the S.C.F. wave functions of

Clementi and McLean[135] are used for these molecules, the effect of

chemical bonding on the electron density in the atomic orbitals of

these two molecules is very similar, and delocalization due to

conjugation in cyanogen is very small. It should thus be possible

to treat the two halves of the cyanogen molecule separately; and

discuss the effect of adding an extra electron.

In this case we are, in effect, adding half an electron to

each -C-N fragment. We would thus expect some bending of the

molecule, but not to such a large an extent as in HCN$^-$. In fact

the ^{13}C tensor is not consistent with a bond angle of 120°. The

lowest g-value of 1.9850 shows that there is probably more mixing

of the π-orbitals than in the HCO radical (Table 4;3), which would

also indicate a larger bond angle than 120°.

In HCN$^-$ there are three electrons distributed in two m.o's,

which in the linear molecule were the π-bonding and π-antibonding

orbitals. In HCN$^-$ there is a large amount of delocalization, about

50% of the spin density being on the nitrogen and 25% on each of the

carbon and hydrogen nuclei. This is characteristic of σ-radicals

where the unpaired electron is in the plane of the molecule. The

high spin density in the s-orbitals of the proton in HCN⁻ was

explained earlier in terms of delocalization from the spin density

on the carbon and nitrogen atoms.

The coupling from the a-atom in σ-radicals is only high in the

case of protons. In FCO, for example, there is only 2% of the total

spin density in the s-orbital of the fluorine atoms, although there

is at least 25% of the spin density on the carbon atoms[129]. This

can be explained; in part,.by both an increase in bond angle, and the

small s-character of the C-F bond, but the high electronegativity of

the fluorine atom must also be considered. This will lower the

energy of the C-F σ-bonding orbital and hence lower the amount of

interaction with the unpaired electron on carbon. This also partly

explains the small isotropic coupling to the nitrogen nucleus in

HCN⁻.

The p/s ratio of the spin density on the carbon atom in $(CN)_2^-$

is just over two. This would indicate that the bond angle is about

120°. This is too small for the reasons explained earlier. It is

in fact larger than the p/s ratio found in HCO[129]. The high s-

character we suggest is due to a similar mechanism to that of placing

the spin density on the proton in HCN⁻. The electronegativity of

carbon is similar to that of hydrogen. The effect of placing spin

density into the C-C σ-bond will also have the effect of reducing the

magnitude of the principal values of the anisotropic part of the
$A(^{14}N)$ tensor, and hence decrease the p/s ratio. This will also
yield a non-axial tensor, but the experimental error in obtaining
the third $A(^{13}C)$ value and the small anisotropic contribution is such
that we have not been able to distinguish this feature.

In a valence bond treatment of the spin density distribution
in $(CN)_2^-$ the following resonance structures are considered:

$$N \equiv C' \quad :\bar{C} \equiv N \quad \bar{N} \equiv C - C \equiv N \quad N \equiv C - C \equiv \bar{N}^- \quad N \equiv \bar{C}: \quad ^\bullet C \equiv N$$

The $.C \equiv N$ -fragment is the cyanogen radical and one expects a high
spin density in the carbon s-orbital in this species. As the radical
is not linear two other structures are possible:

$$N \equiv C^\bullet \diagdown_{C \equiv N} \qquad \bar{N} \equiv C \diagdown_{C \equiv N}$$

The molecular orbital treatment is similar to that for HCN^- with
the carbon atoms replacing the proton. In the $(CN)_2^-$ radical the
bending is less and so the coupling to the α atom will be smaller,
but it would still be enough to explain the high s-character of the
spin density on the carbon atom.

As with the HCN^- radical the mechanism of placing spin density
on the α atom reduces the strength of the σ -bond. In this
sense the orbital containing the unpaired electron can be considered as
antibonding over the whole molecule. The C-C bond will then be
weaker than in the cyanogen molecule.

IV. Comparison of $(CN)_2^-$ with the V_K-centres in the Alkali Halides

Both the Hal_2^- and the $(CN)_2^-$ radicals are prepared by γ-irradiation of a suitable alkali metal salt. The ions themselves are electron deficient, and formed by the ionisation of a neutral molecule and an ion. Both species will decompose if an extra electron is added to them, to form the respective ions. There is however the possibility of forming a species $(CN)_2^{2-}$ and even $(CN)_2^{3-}$, for the latter is isoelectronic with the $(N)_4^-$ radical, which has been observed[137] in irradiated azide crystals. $(N)_4^{2-}$ and $(CN)_2^{4-}$ are isoelectronic with the dimer of NO which has a square planar environment, and a square planar environment would explain the presence of four equivalent nitrogen atoms in $(N)_4^-$.

In the Hal_2^- species the unpaired electron is in a σ-antibonding orbital, while in the $(CN)_2^-$ radical it is in a π-antibonding orbital. This is probably why, although the Hal_2^- radicals are not stable above about $77^\circ K$, the $(CN)_2^-$ radical is stable even at room temperature, and will form merely by warming crystals containing Hal_2^- radicals and CN^- ions above $77^\circ K$. It should be possible to prepare mixed species such as $ClCN^-$, but we have not observed these species in the irradiated samples described above. The $ClCN^-$ radical may be the intermediate in the formation of $(CN)_2^-$ on warming crystals containing Cl_2^- radicals.

Chapter 5

The Effect of Radiation on Complex Cyanide Ions

Incorporated into Alkali Halide Crystals

Complex Cyanide Ions

The purpose of this chapter is to show how a combination of information from infra-red, electronic and electron spin resonance spectroscopy can be used to study the effect of electromagnetic radiation on transition metal complexes incorporated into alkali halide lattices. Cyanide complexes are ideal for this study as they have sharp i.r. bands and they form low spin complexes. Low spin complexes of Fe(I) and Ru(I) d^7 ions have a doublet ground state and hence a relatively simple e.s.r. spectrum.

I. The Bonding in Cyanide Complexes

i. The Cyanide Ion as a Ligand

The m.o's of the cyanide ion can be described as follows[126]:-

$$KK \quad (1\sigma)^2 \quad (2\sigma)^2 \quad (1\pi)^4 \quad (3\sigma)^2$$
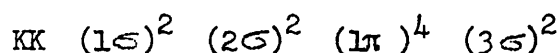
The three σ-orbitals can be regarded as a C-N σ-bond and lone pair orbitals on carbon and nitrogen. In cyanide complexes the metal is bonded to the carbon atom[138], and the lone pair on the carbon acts as as a dative bond to the metal. The ligand-metal σ-bonds can be treated by a ligand field approach shown in fig 5;1a, for an octahedral complex. The t_{2g}-orbitals take no part in this σ-bonding, but have the correct symmetry for bonding with the π-antibonding orbitals on the cyanide ion. This overlap will affect the energies of the orbitals, as shown in fig 5;1b. The e_g^x and t_{2g} orbitals can be considered as consisting mainly of the metal d-orbitals and so the effect of this π-bonding to the ligand is to increase the energy gap Δ between the two sets of d-orbitals. This is

a. Ligand Field of Cyanide σ-orbitals

t_{1u}

a_{1g}

p
s

d

e_g

Δ

t_{2g}

σ

e_g

t_{1u}
e_{1g}
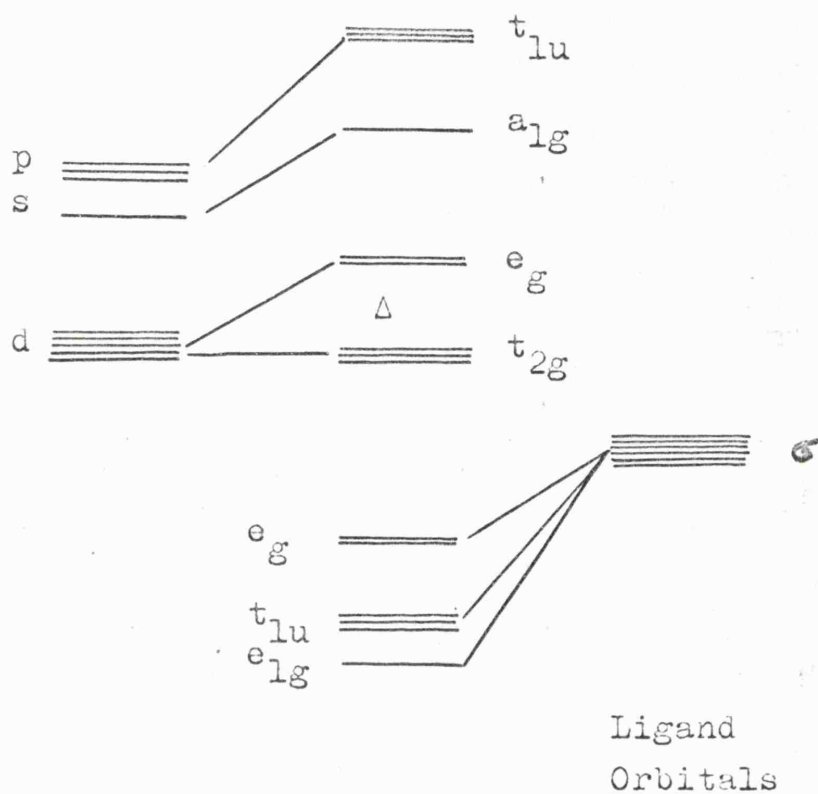
Ligand
Orbitals

b. Ligand Field of Cyanide π-orbitals

t_{2g}

e_g ———————— e_g

π^*

t_{2g}

Δ

t_{2g}

σ
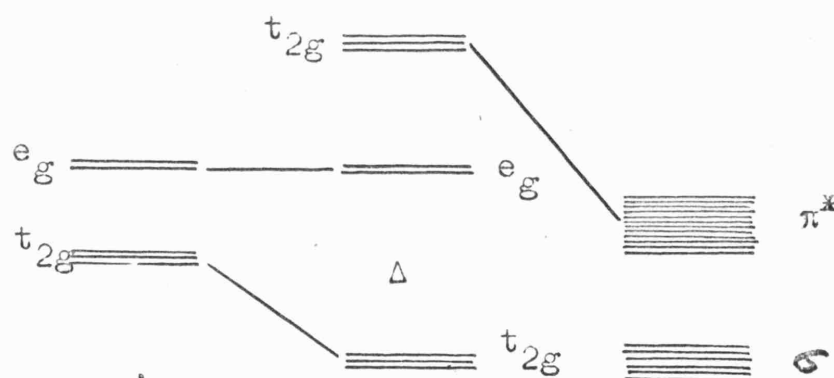
These diagrams are simplified for ease of representation

partially the reason why these complexes are low spin. This delocalization into the cyanide antibonding orbitals of the electrons from the metal enables the cyanide ion to stabilise low oxidation states of the metal, However, since the ligand is negatively charged it is not as good an electron acceptor as the neutral carbonyl molecule. This is possibly the reason why few zero oxidation state cyanide complexes are known.

ii. The Effect of the π-bonding on the Infra-red Spectrum

The effect of delocalization of the electrons into the π- antibonding m.o's of the cyanide ion is to weaken the C-N bond and to increase the strength of the metal-carbon bond. This decreases the C-N stretching frequency and increases the M-C stretching frequency. The greatest effect is expected for the lower oxidation state complexes. Table 5;1 shows the force constants for the free cyanide ion and a number of complexes. In all cases the C-N stretching force constant is reduced, the effect being greatest with the low oxidation state complexes.

<p style="text-align:center">Table 5:1</p>

<p style="text-align:center">Force Constants in Cyanide Complexes[139]</p>

Compound	Oxidation State	k_{M-C}	k_{C-N}
KCN			17.5
$K_3Fe(CN)_6$	III	1.73	17.0
$K_3Co(CN)_6$	III	2.31	16.5
$K_4Fe(CN)_6$	II	2.43	15.1
$K_4Ru(CN)_6$	II	2.79	15.3
$K_4Os(CN)_6$	II	3.34	14.9

II. Incorporation of the Complexes into Alkali Halide Crystals

i. Experimental Results

The following cyanide complexes were incorporated into potassium chloride crystals from an aqueous solution containing 1% of the complex: i. $Fe(II)(CN)_6^{4-}$, ii. $Ru(II)(CN)_6^{4-}$, iii. $Fe(III)(CN)_6^{3-}$, iv. $Co(III)(CN)_6^{3-}$. The i.r. spectra of the doped halides, in the form of pressed discs were recorded. The Fe(II) and Ru(II) complexes incorporate very easily, fig 5;2 shows the i.r. spectrum for the $Fe(II)(CN)_6^{4-}$ complex obtained from a solution containg 0.2 and 0.0002 % of the complex. The only other complex cyanide which incorporates easily is the $Ag(I)(CN)_2^{-}$ ion. The other complexes in the oxidation state (III) were only incorporated in very small amounts. In the case of $Fe(III)(CN)_6^{3-}$ the largest bands in the i.r. spectrum were due to impurity $Fe(II)(CN)_6^{4-}$.

The $Fe(II)(CN)_6^{4-}$ ion concentration increases markedly on recrystallization. Fig 5;3 shows the i.r. spectra due to the ferrous ion before and after one recrystallization.

The i.r. absorption bands for each complex in a potassium chloride lattice are given in table 5;2, also included are the bands obtained for $K_4Fe(CN)_6$ in a potassium chloride pressed disc. In the latter there are bands due both to the solid complex and also some bands of the ion incorporated into the potassium chloride lattice.

Fig 5;2

I.R. Spectrum of $Fe(II)(CN)_6^{4-}$ in KCl Lattice

1980

2000

2020

2040

2060

2080

I.R. Spectra of Fe(II)(CN)$_6^{4-}$ in KCl Lattice

2100   2000   2100   2000

Before   After

Recrystallisation
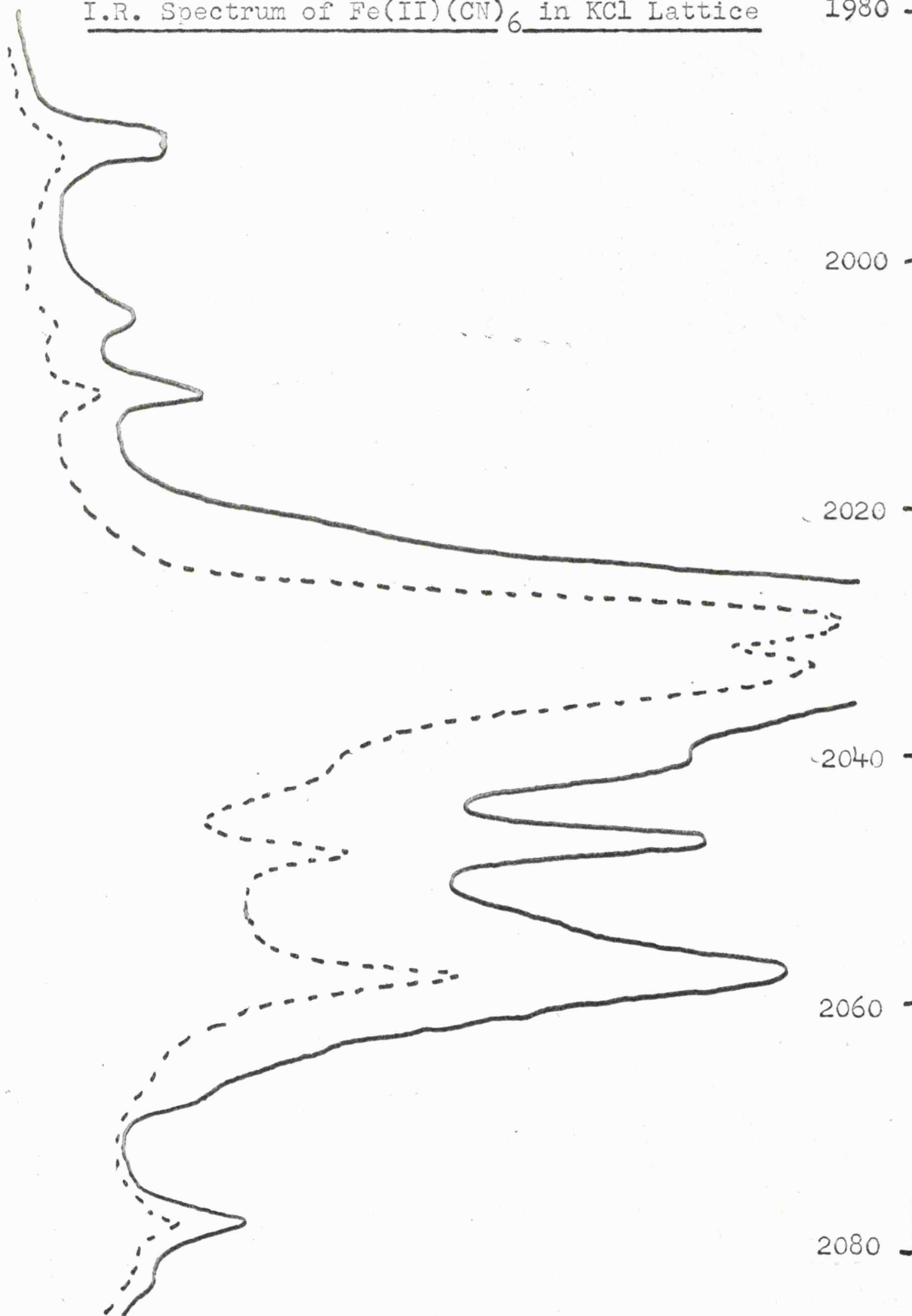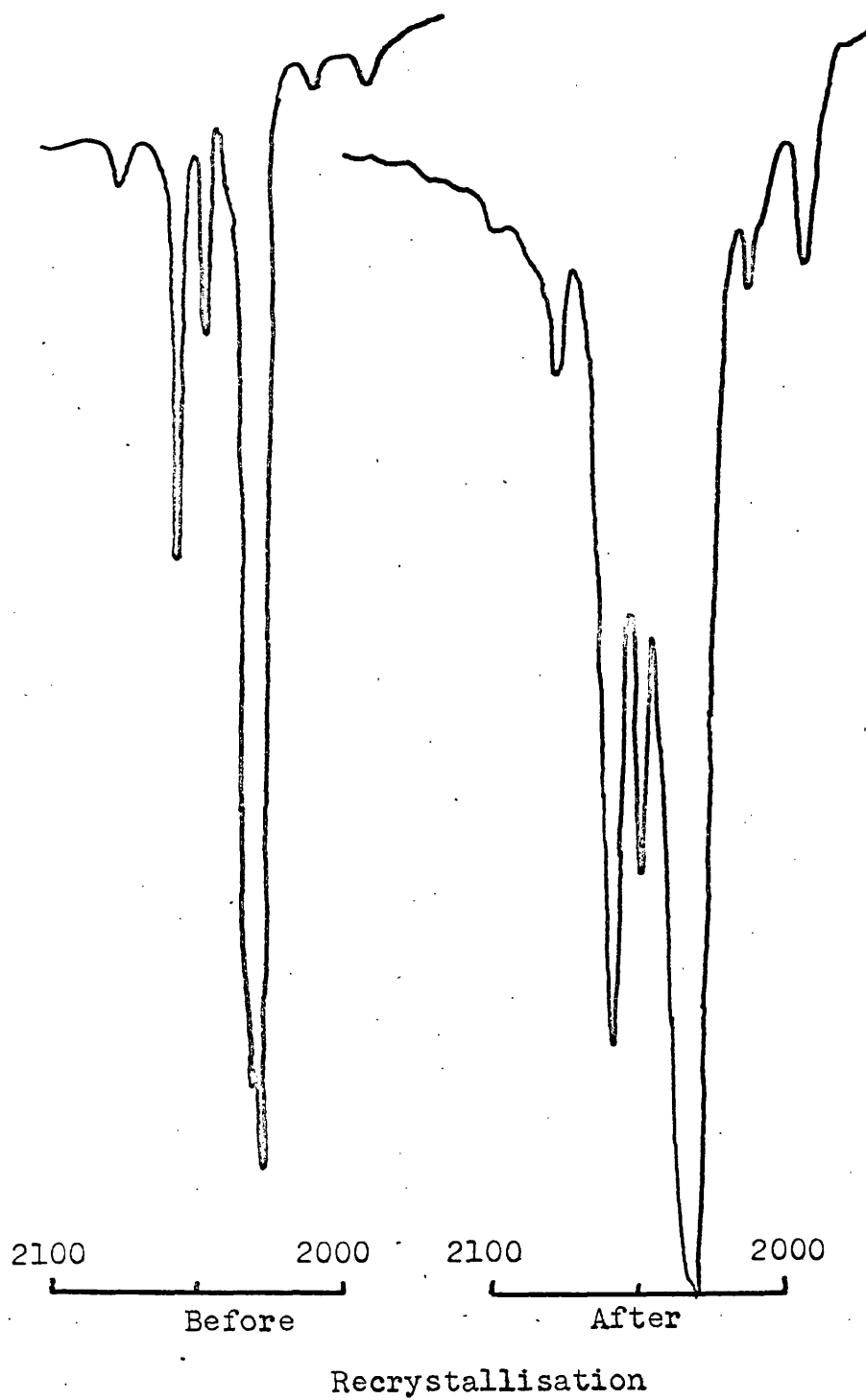
Table 5:2

Infra-red Absorptions of Complex Cyanide Ions in KCl Lattices

a. The Cyanide Stretching Region

$Fe(II)(CN)_6^{4-}$		$Ru(II)(CN)_6^{4-}$
KCl/K$_4$Fe(II)(CN)$_6$	KCl/Fe(II)(CN)$_6^{4-}$	KCl/Ru(II)(CN)$_6^{4-}$
2092 w	2088 sh	2098.5 w
	2078 w	2078 sh
2057 sh	2058 m	2072 m
2048 s	2047 m	2063 m
	2040 sh	2052 sh
2034 m	2032 s	2041.5 s
2029 m	2029 s	2045.5 s
2014 w	2011 w	2023 w
	2004 w	2018 w
	1990 w	2006 w

KCl/Ag(I)(CN)$_2^-$	KCl/Co(III)(CN)$_6^{3-}$	KCl/Fe(III)(CN)$_6^{3-}$
2140 sh	2127.5	2103
2133 w	2119.5	2110
2111 sh	2112.5	
2101 s	2109	
2092 m		
2072 w		
2058 w		

b. The Metal-Carbon Stretching Region (v_7)

	$Fe(II)(CN)_6^{6-}$	$Ru(II)(CN)_6^{4-}$
This Work	577	546
Solid State[140]	585	550

All frequencies in cm^{-1}

11. Incorporation of the Ions into the Lattice

Octahedral $M(CN)_6^{n-}$ ions can be incorporated into an alkali halide lattice either into an interstitial position or in place of one or more ions. The interstitial position and the replacement of one ion would greatly distort the lattice and so the most likely method of incorporation is the substitution of an $M(Hal)_6^{5-}$ (or $HalM_6^{5+}$) unit. If the complex has five negative (or positive) charges there will be complete charge balance and the ion should be easily incorporated into the lattice. In the case of the $Fe(II)(CN)_6^{4-}$ ion there are only four negative charges on the ion and so for complete neutrality in the crystal the charge difference has to be compensated for by either an impurity ion, or a cation vacancy. The greater the difference in charge on the ion from five the greater the difficulty of incorporation into the lattice. The difference in ease of incorporation of $Fe(II)(CN)_6^{4-}$ and $Fe(III)(CN)_6^{3-}$ ions may be due in part to differences in solubility and size, but the charge difference is the most likely explanation of the strong affinity of the ferrous ion for the lattice.

The i.r. spectrum of the doped halides shows that the ions have been incorporated substitutionally, and not in clusters, for the spectrum . of the ion is different from that in the pure complex cyanide. The solution grown samples have a different spectrum to those where the complex has been merely ground up with the potassium chloride prior to preparing the pressed discs. After the normal length of grinding only a broad peak is observed, but after prolonged

grinding other peaks can be observed, which on further grinding are well resolved, and can be recognised as the main doublet in the "solution grown" spectrum.

In these doping experiments the $Fe(II)(CN)_6^{4-}$ ion was a common impurity. This was removed from solution by adding an excess of potassium chloride and crystallizing out the halide with the impurity. If this was repeated several times samples free from the ferrous ion could be obtained.

iii. Infra-red Spectra

In chapter 1 (page 27) the i.r. spectrum of the octahedral $M(AB)_6$ ion was discussed. In a purely octahedral environment only one i.r. peak is expected in the cyanide stretching region. In the solid state, however, a number of other bands occur due to the effect of site symmetry[24, 25]. A number of i.r. investigations have been carried out on the octahedral complexes in the solid state. G. Bonio et al [141] found a large number of bands in the 2000-2200 cm^{-1} region for the anhydrous $K_4Fe(CN)_6$ complex (Fig 5;4). The large number of bands were accounted for in terms of the low site symmetry in the solid compound.

In table 5;3 the energy of the normal modes are given for both $Fe(CN)_6^{4-}$ and $Ru(CN)_6^{4-}$ in solution[144, 145]. Since $\nu_6 < \nu_3 < \nu_1$ we have assigned the bands at 2029 and 2032 cm^{-1} to ν_6 normal modes of the octahedral complex. The degeneracy of the ν_6 mode having been lifted by the site symmetry.

In chapter 1 the effect of a neighbouring charge compensating
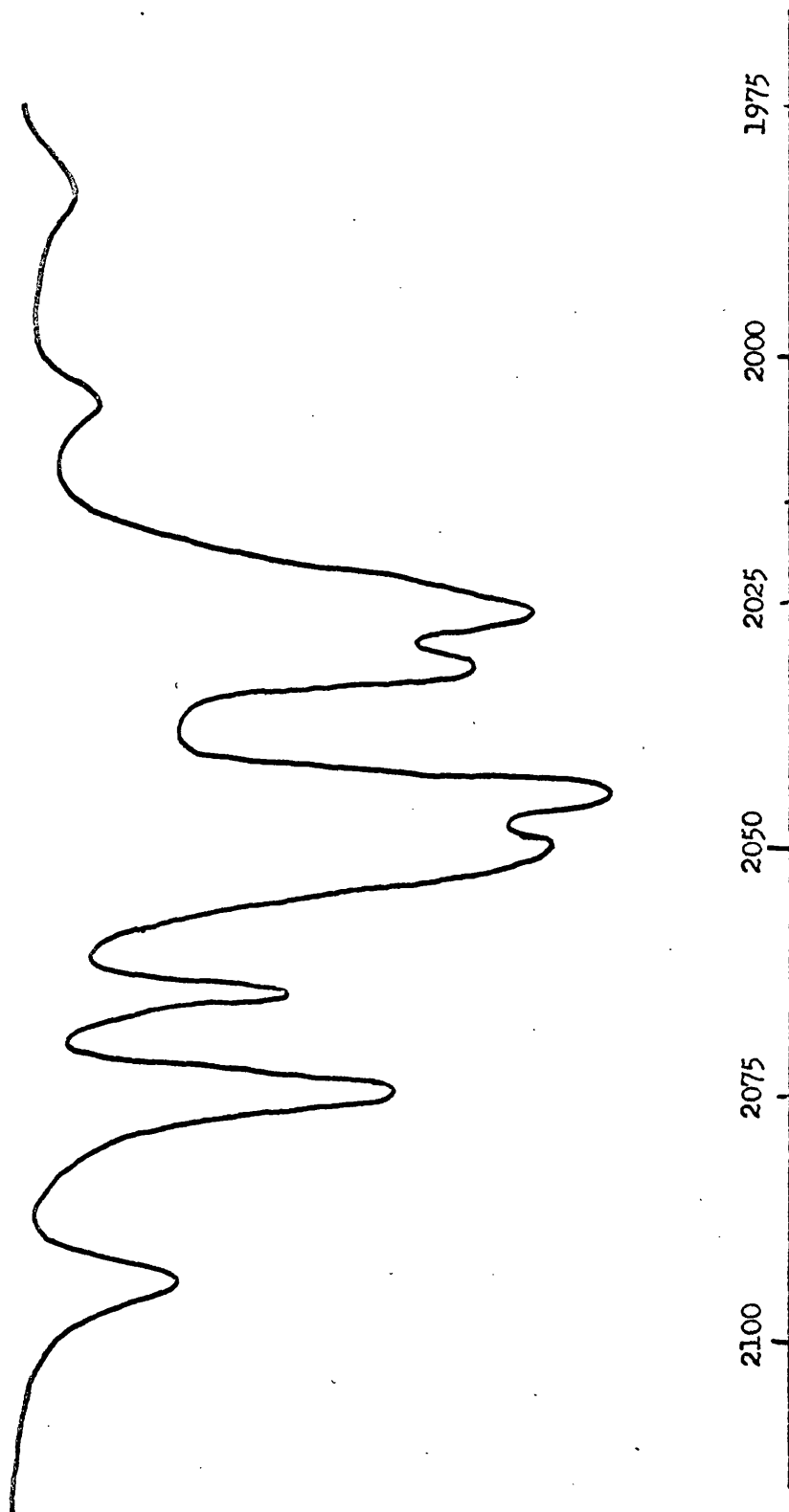
The I. R. Spectrum of $K_4Fe(CN)_6$ as the Solid [141]

vacancy was discussed. If the vacancy is along an N-C+M-C-N direction the site symmetry is C_{4v} and four C-N stretching bands can, in principle, be observed. Fig 5;2 shows that in the case of $Fe(II)(CN)_6^{4-}$ in a potassium chloride lattice there are at least four absorption bands.

Table 5;3

The Frequencies (in cm^{-1}) of some of the Normal Modes of Vibration in solution for $Fe(II)(CN)_6^{4-}$ and $Ru(II)(CN)_6^{4-}$ 144,145

	v_1	v_3	v_6	v_7	v_8
$Fe(CN)_6^{4-}$	2096	2063	2044	583	416
$Ru(CN)_6^{4-}$	2100	2067	2048		

Table 5;4

The Infra-red Bands Observed in Irradiated KCl containing Complex Ions

$Fe(II)(CN)_6^{4-}$		$Ru(II)(CN)_6^{4-}$		$Co(III)(CN)_6^{3-}$	
2011	m	2010	m	2078	w
1997	w	1998	m	2067	s
1992.5	w	1992	w		
1989	m	1985	m	1990	w
1973.5	m	1971	s	1979	w
1970	w	1938	w	1972	w
1955	m			1960	s
1950	sh				
1947	s				

After 48hrs γ-irradiation all complexes yielded peaks at 2182 and 2170 cm^{-1} (in potassium chloride lattices).

III. Irradiation of Complexes Incorporated into Alkali Halide Lattices

1. Experimental Results

a. Infra-red Spectra

1. _Ferrous_hexacyanide_: If a disc of a solution grown sample of potassium chloride doped with $Fe(CN)_6^{4-}$ is γ-irradiated for one minute a new i.r. band is observed at 1947 cm^{-1}. On further irradiation the intensity of this band increases rapidly and other bands appear in this region. Fig 5;5 shows the effect of irradiation on a weakly doped sample, and fig 5;6 is a plot of the areas under the absorption bands at 1947 cm^{-1} and the doublet at 2030 cm^{-1}, against irradiation time. The new peaks are formed at the expense of the species causing the doublet at 2030 cm^{-1} (Fig 5;5 and 5;6). A further new peak is observed at 550 cm^{-1}, near the metal-carbon stretching frequency. Fig 5;7 shows the new peaks after 7 days irradiation, and fig 5;8 the peaks when the sample is cooled.

After a few days irradiation another peak is observed at 2182 cm^{-1} (Fig 5;9). If the matrix is potassium bromide this new peak is at 2170 cm^{-1}. This shift is characteristic of an isolated cyanate ion in alkali halide lattices[147]. The position of the radiation produced i.r. bands are given in table 5;4.

Ultra-violet irradiation produces similar peaks at 1947 cm^{-1} and above. The rate of growth of the bands is only slightly less than with the γ-irradiation experiments, a band being observed after only five minutes irradiation. However, no band at 2182 cm^{-1} develops even after several weeks of irradiation.

Effect of Irradiation on the I.R. Spectra of Fe(II)(CN)$_6^{4-}$

No Irradiation

10 minutes
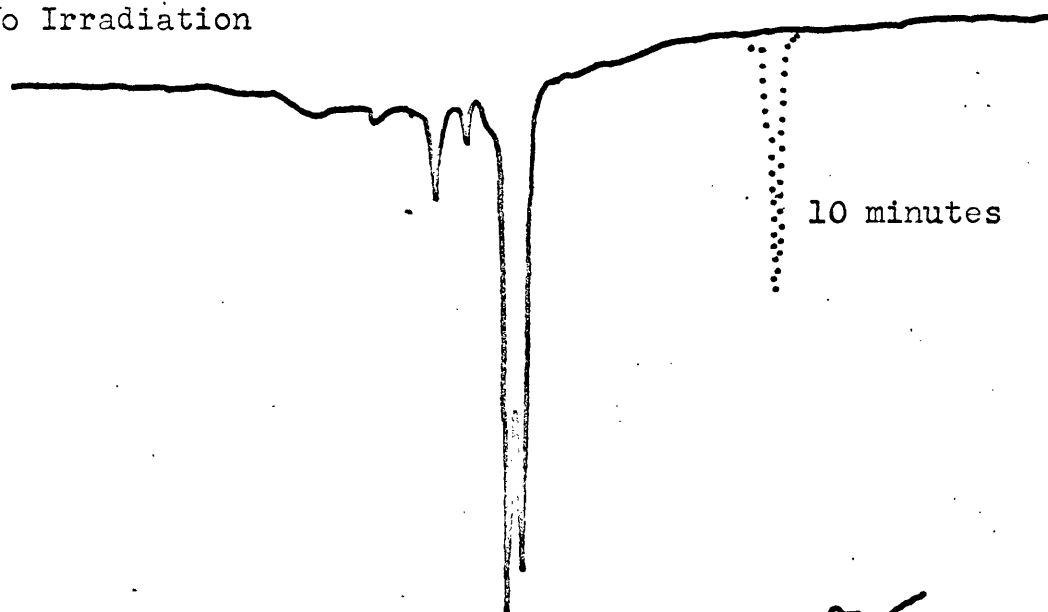
5 Hours Irradiation
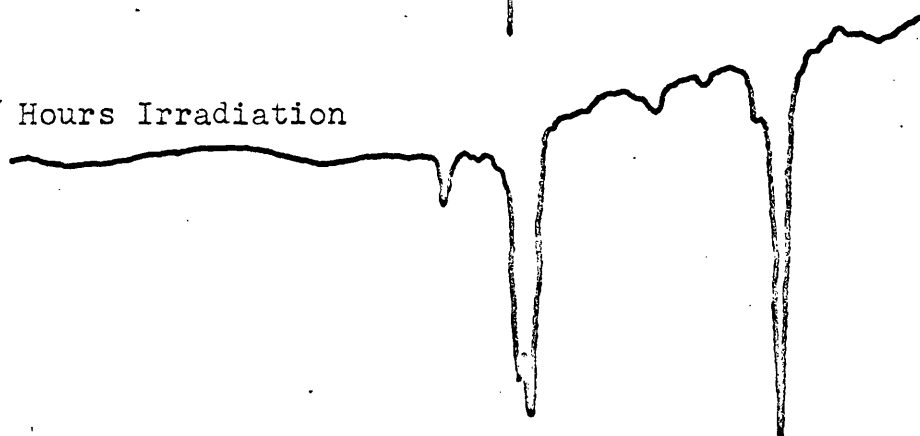
100 Hours Irradiation

2200   2100   2000   1900

Fig 5;6

162
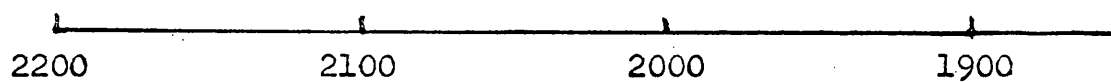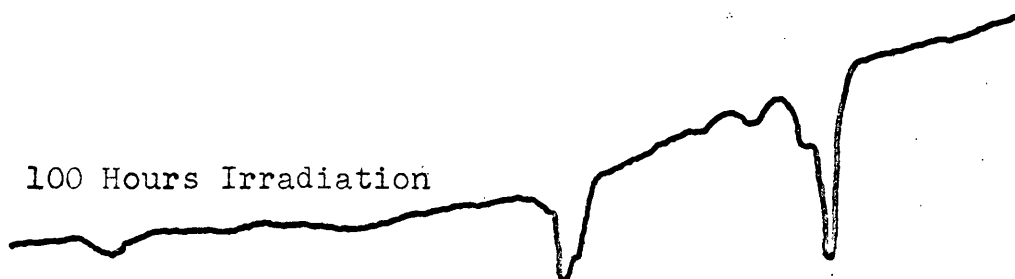
Plot of Area Under the Absorption Peaks at 2030 and 1947 cm^{-1} Against

Irradiation Time

A= doublet at 2030 cm^{-1}

B= peak at 1947 cm^{-1}

A

B

Irradiation Time (Minutes)

0   20   40   60   80   100   120   140   160   180
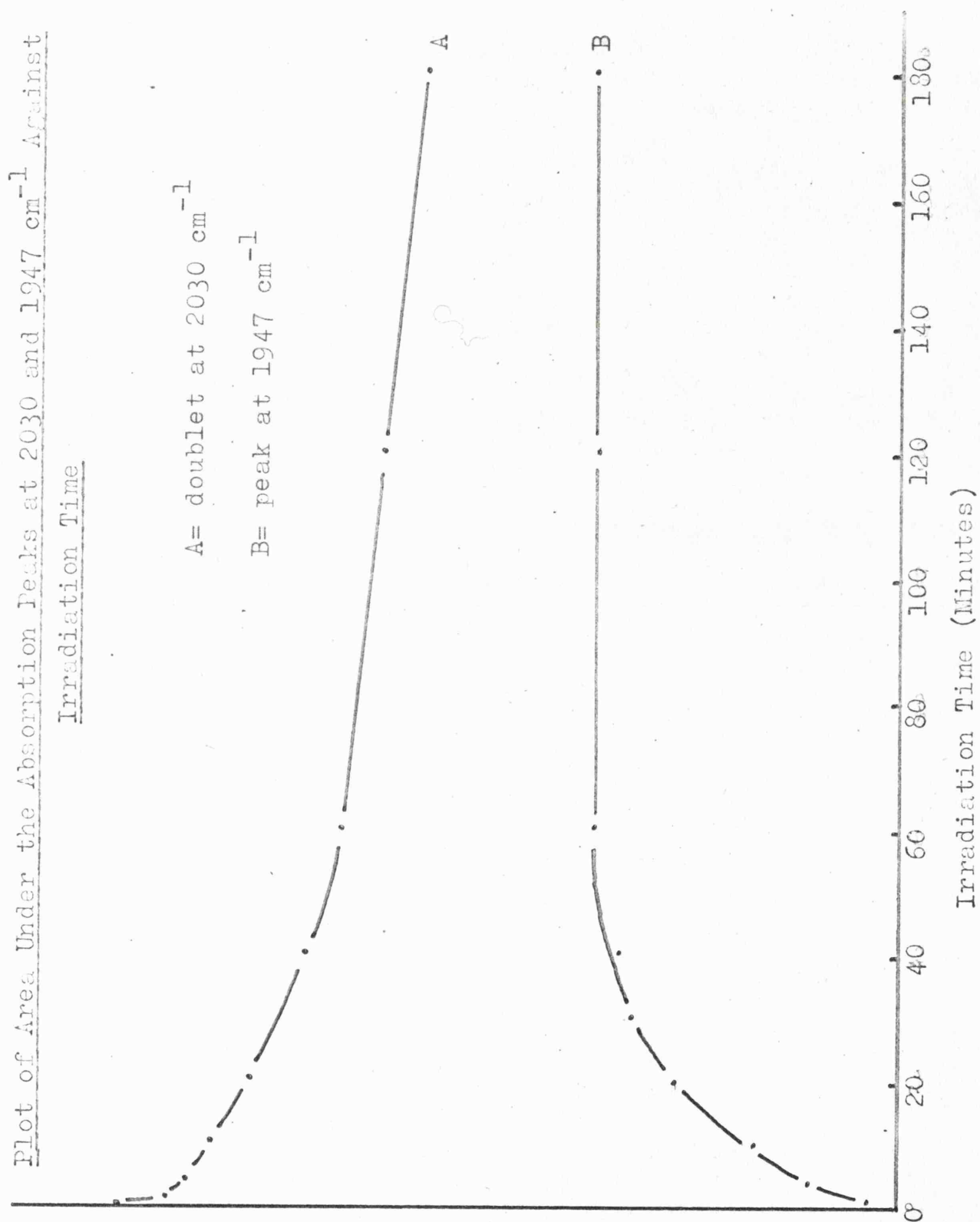
Fig. 5;7

I.R. Spectra of Fe(II)(CN)$_6^{4-}$ in KCl

After 7 days γ-irradiation

163

Fig 5;8   164

I.R. Spectrum of Irradiation Products Recorded at:
a. 300°K   b. 100°K

a. 300°K ———
b. 100°K ······

2000   1980   1960   1940   1920

Fig 5;9
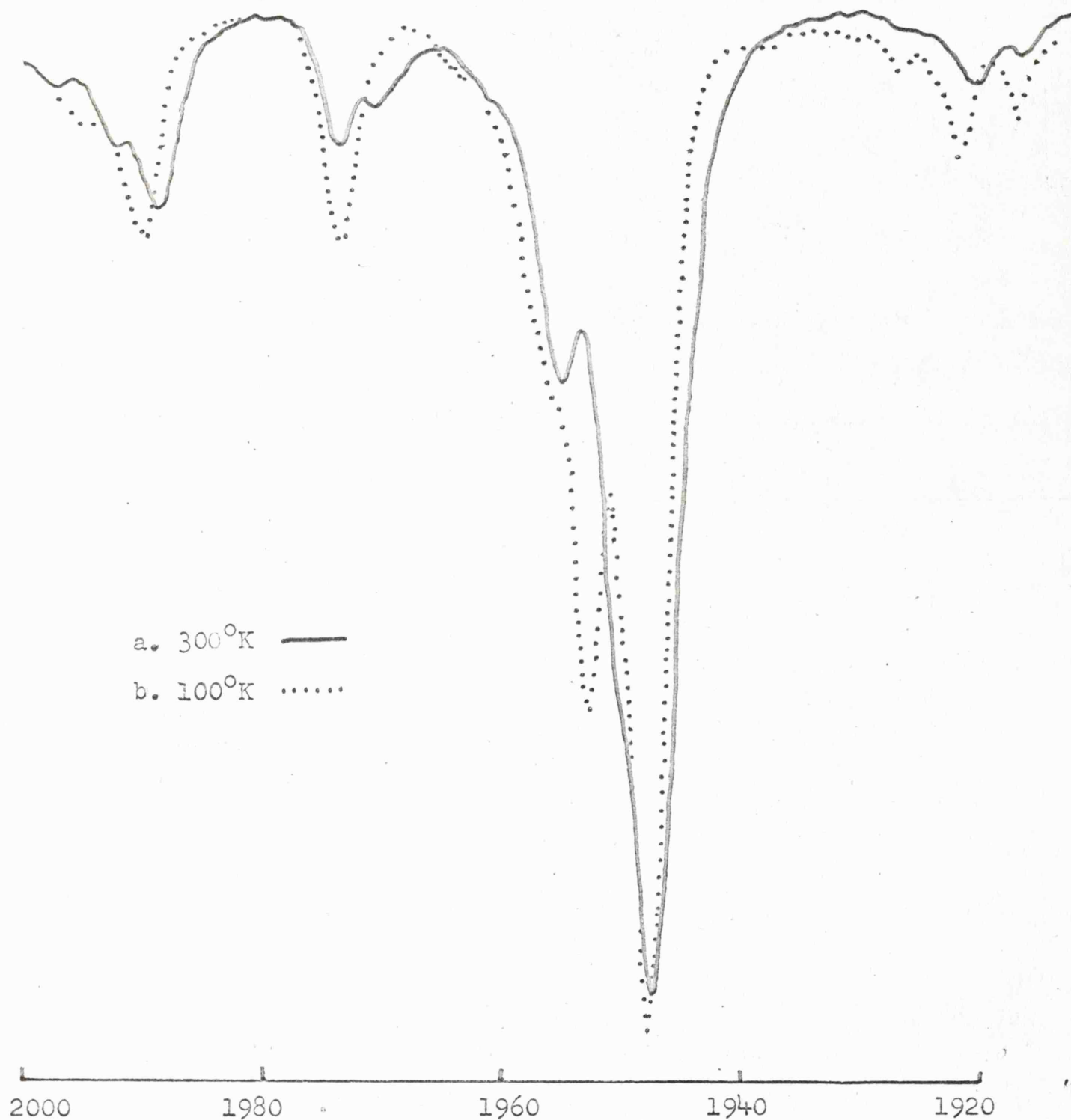
I.R. Spectrum of Fe(II)(CN)$_6^{4-}$ γ-irradiated for 8 days

CNO$^-$
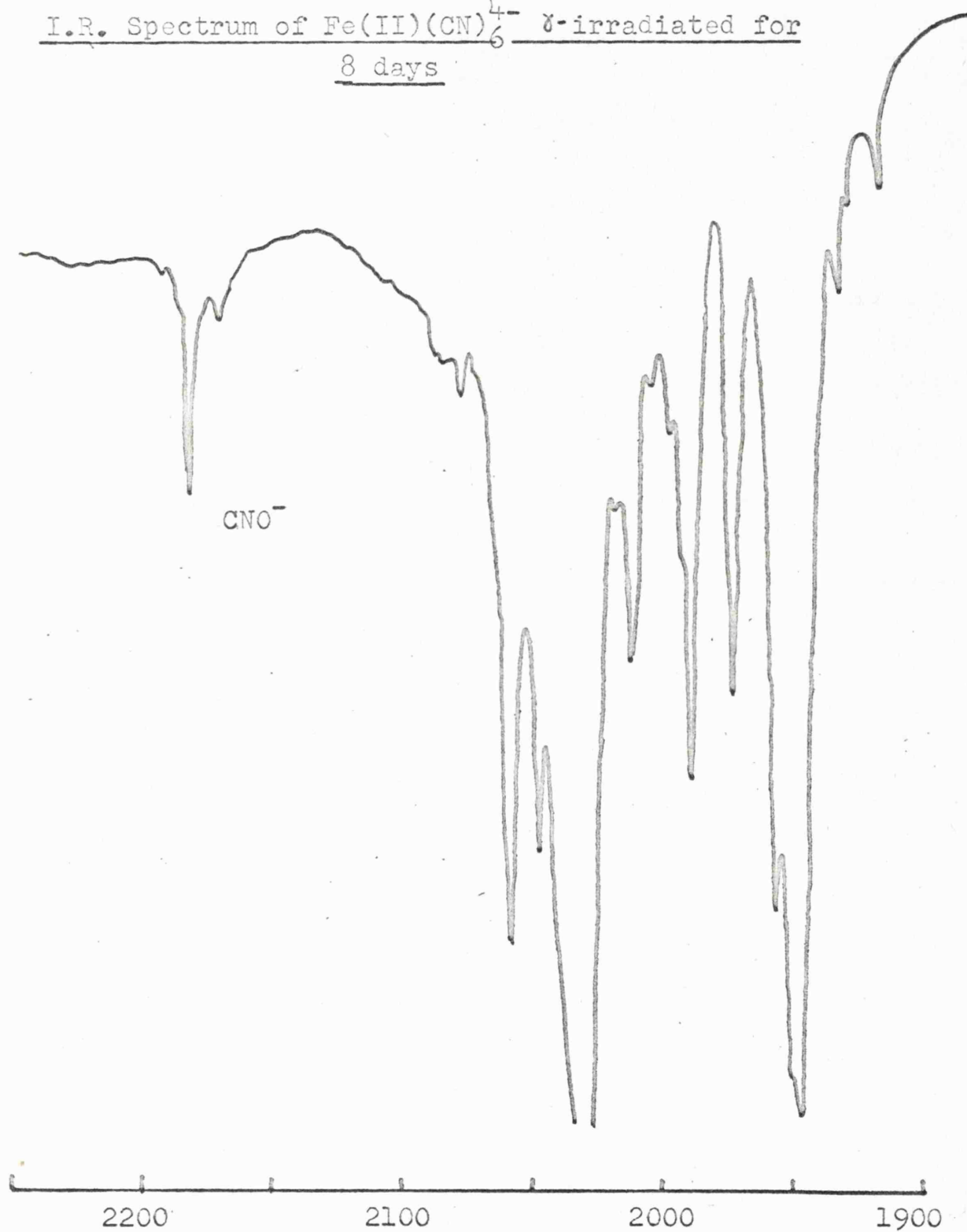
When a strongly irradiated sample which has been thermally bleached in the i.r. spectrometer is dissolved in water a small quantity of gas is given off. It has not been possible to analyse the gas, because of the small amount evolved. On evaporation at room temperature, and careful preparation of the pressed disc, there is no sign of the i.r. bands below 1980 cm^{-1}. The doublet at 2030 cm^{-1} and associated peaks increase, but the cyanate peak at 2180 cm^{-1} is much weaker and broader.

2._Ruthenium_hexacyanide_: With the ruthenium the changes in the spectrum on irradiation are similar to the changes for the ferrous ion. The new peaks are given in table 5;4.

3._Other_complexes_: The only effect of irradiation on the alkali halides doped with $Ag(I)(CN)_2^-$ is the formation of a small amount of cyanate ion after γ-irradiation for several days.

The samples containing $Co(III)(CN)_6^{3-}$ were very dilute and hence the i.r. bands were weak, but on irradiation two series of peaks are observed, one around 2067 cm^{-1} appears after a short period of irradiation and the other around 1960 cm^{-1} after about ten hours irradiation.

b. Electronic Spectra

The electronic spectra of the cyanide complexes incorporated into potassium chloride lattices are the same as the spectra of the pure solid complex cyanide. On γ-irradiation a further band due to the F-centre appears. The diffuse reflectance spectra of the $Fe(CN)_6^{4-}$ complex in potassium chloride after one hours γ-irradiation

is shown in fig 5;10. The broken line is of an identical disc of pure potassium chloride which had also been irradiated for one hour.

The silver cyanide complex darkened on γ-irradiation, probably due to the formation of silver atoms; there was also a weak F-band present.

The rate of bleaching is enhanced by the presence of the complex cyanide ions in the crystal. It is possible to bleach the discs almost completely in about five minutes at room temperature while the pure potassium chloride discs take over an hour to bleach in the same conditions.

c. Electron Spin Resonance Spectra

1._Ferrous_hexacyanide_: After 15 minutes γ-irradiation, or about one hours ultra-violet irradiation the X-band e.s.r. spectrum recorded at room temperature shows two distinct features (Fig 5lla). On cooling the sample to $77^{\circ}K$ the low field line was resolved into three.(Fig 5;llb). On further irradiation other lines appear on both sides of the low field feature (Fig 5;12). These new lines can be attributed to a different species since the relative intensities of these side lines and the main triplet are dependent on the irradiation time. Changing the lattice merely alters the g-value and the resolution of the low field triplet.

Single crystal studies of doped potassium chloride and bromide and of sodium chloride lattices were completed. A plot of angular dependence of the g-value of the lines in potassium chloride, rotating the crystal about an axis perpendicular to the 100 plane, is shown in

Fig. 5;10

168

Diffuse Reflectance Spectra of KCl and KCl Doped with Fe(II)(CN)$_6^{4-}$

After 1 hour γ-irradiation

Pure KCl

F-band

KCl doped with Fe(II)(CN)$_6^{4-}$

mµ
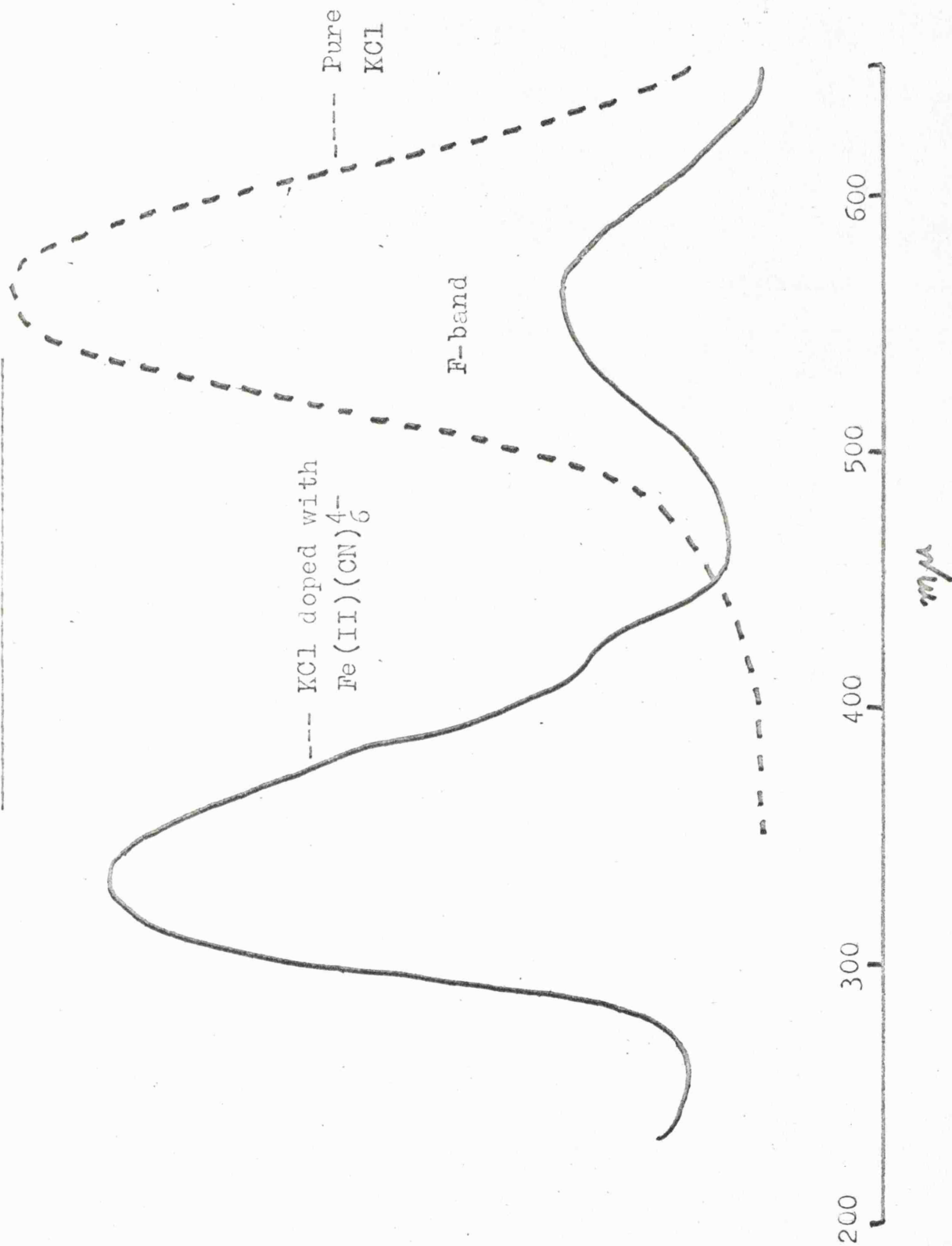
E.S.R. Spectrum of Fe(II)(CN)$_6^{4-}$ in KCl Lattice after

15 Minutes γ-irradiation

a. Spectrum Recorded at 300°K

150 gauss

$g_{\perp} = 2.095$ $g_{//} = 1.999$

b. Spectrum of Low Field Peak
   Recorded at 77°K.

10 gauss
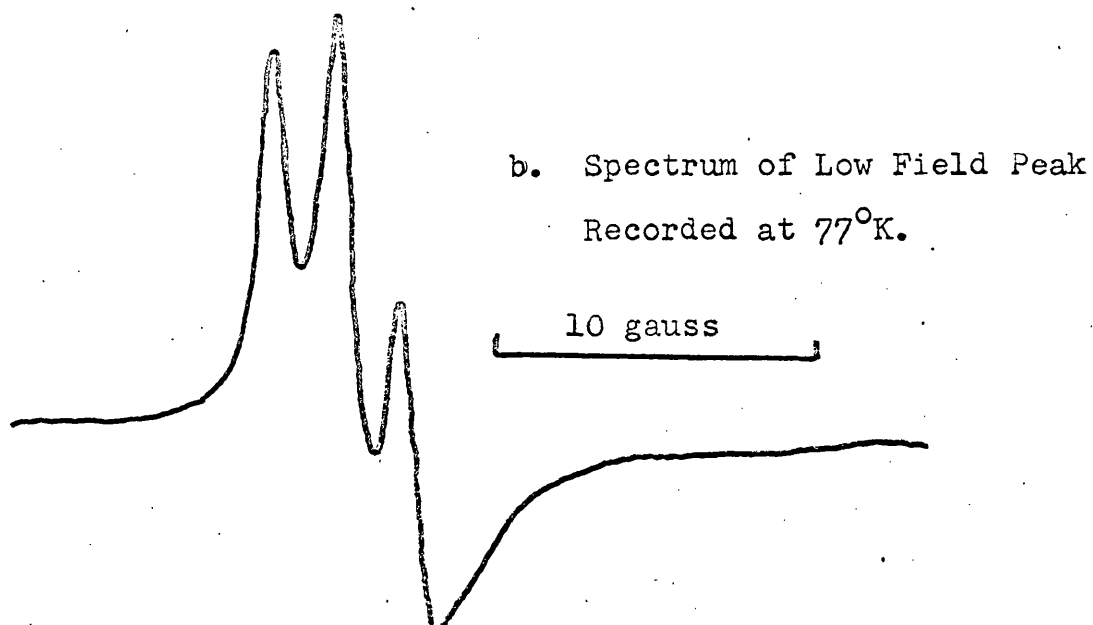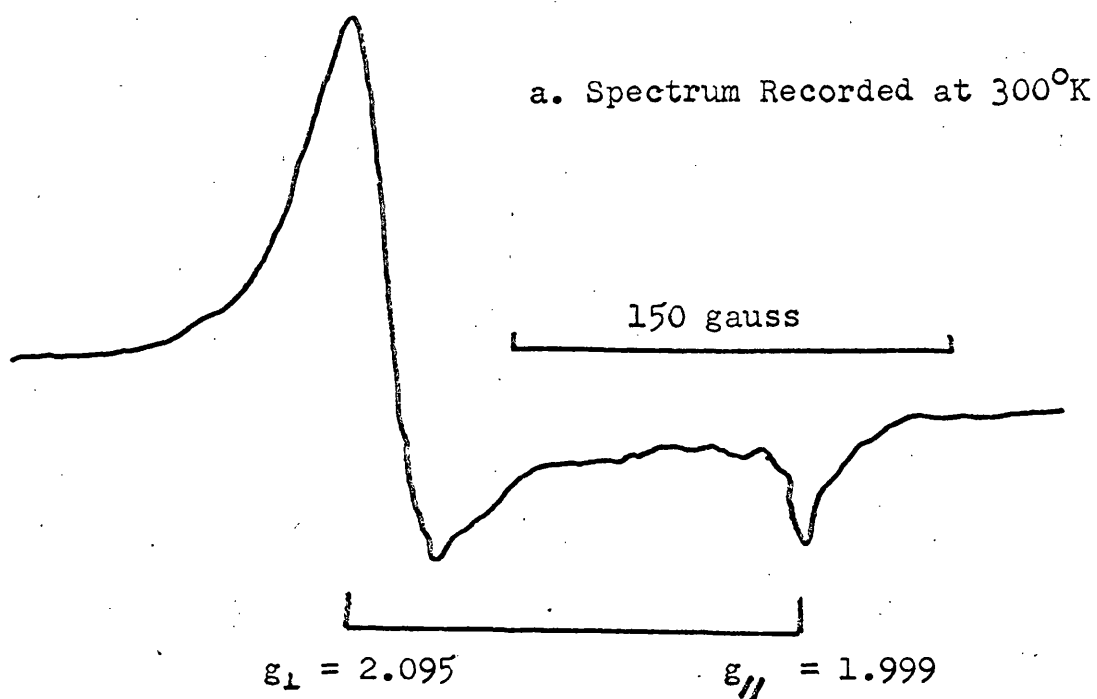
Fig. 5;12

E.S.R. Spectrum of $Fe(II)(CN)_6^{4-}$ in KCl after

24 Hours Irradiation   Recorded at $77^\circ K$

a. Low Gain

b. Higher Gain

10 gauss
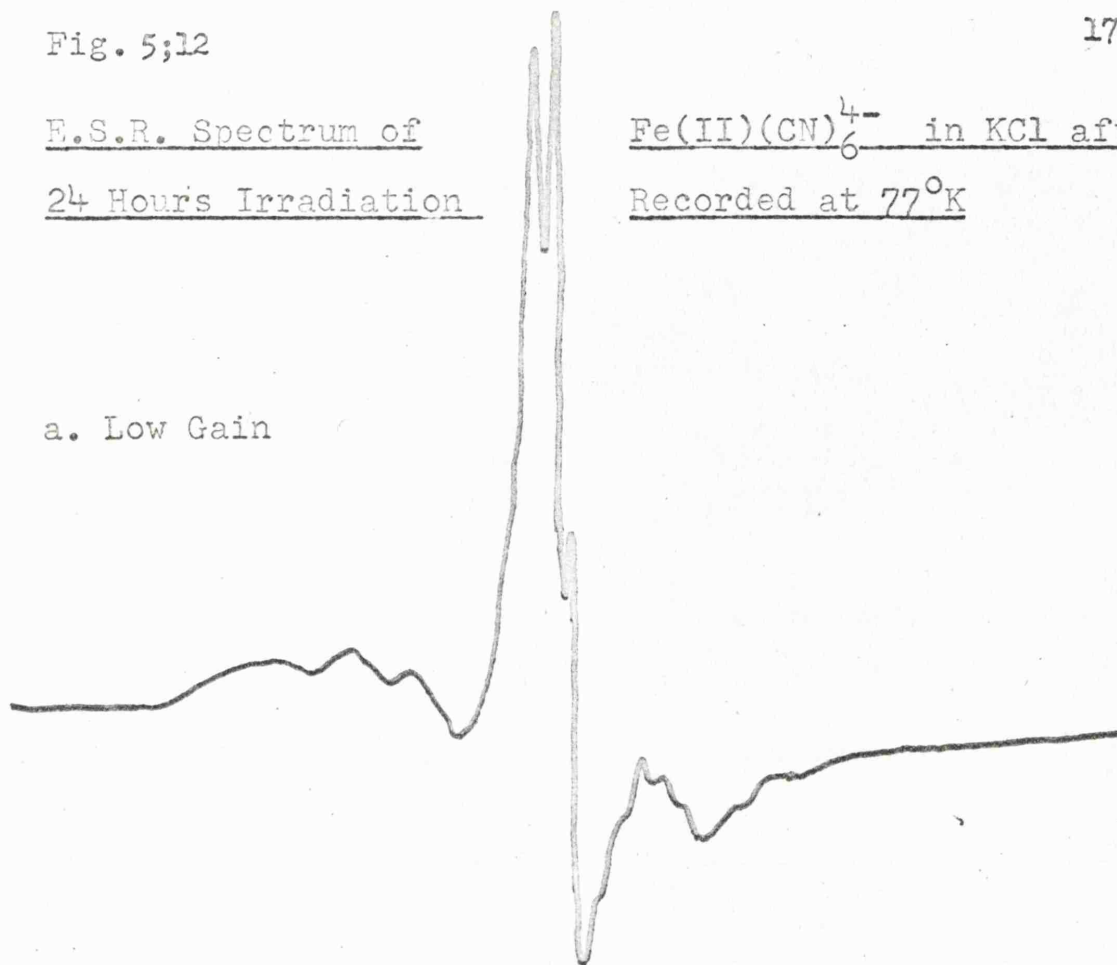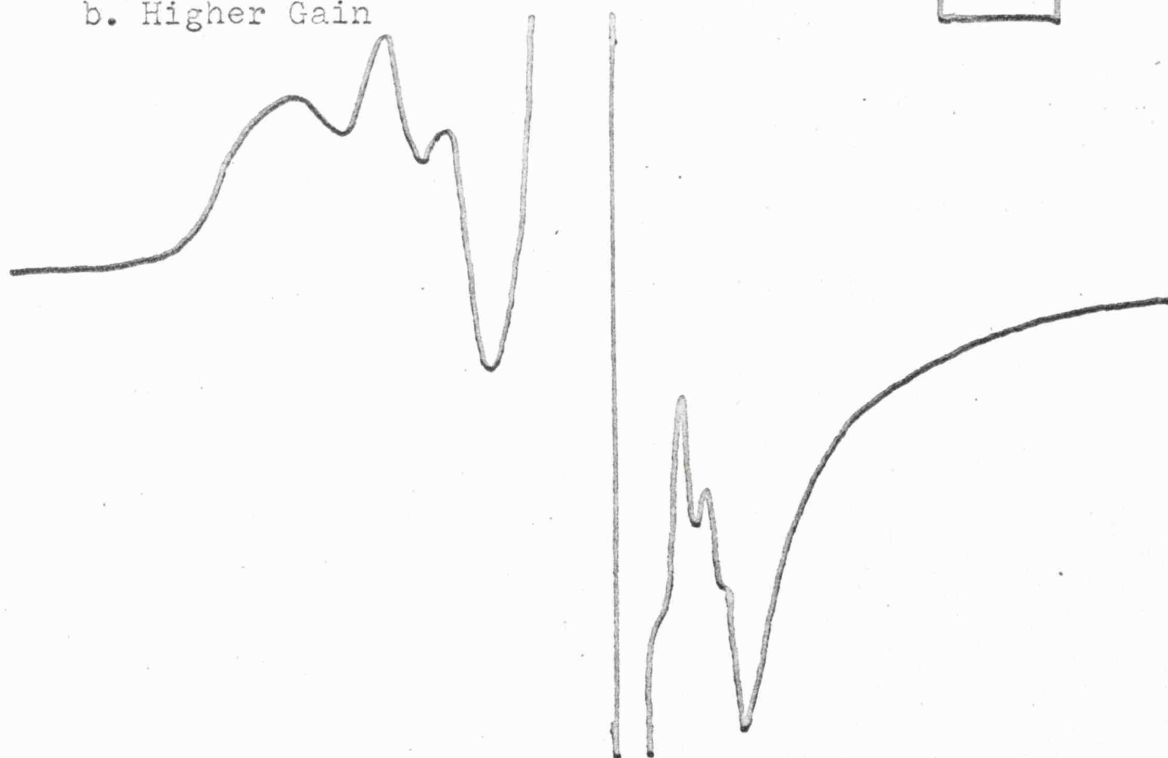
fig 5;13. The low field triplet is assigned to a perpendicular feature. This could also have been ascertained from the powder spectrum. The resolution of the perpendicular feature is lost after only 15° rotation from the perpendicular position. On rotation the line broadens from about 6 gauss at the perpendicular position to 11 gauss at the parallel.

The presence of only one triplet in the low field line was unexpected for a complex containing probably six cyanide ligands, and so the experiment was repeated using both sodium and potassium cyanide matrices. A powder spectrum of the potassium cyanide sample and a single crystal study of the sodium cyanide showed similar features at 77°K, but the perpendicular feature was not resolved into a triplet. This lack of resolution may be due to the change in crystal structure on cooling. The e.s.r; parameters are listed in table 5;5. Notably the value of $g_{\perp}$ increases with lattice size.

2._Ruthenium_hexacyanide_: The e.s.r. spectra of irradiated potassium chloride crystals containing $Ru(CN)_6^{4-}$ are similar to the ferrous case, except that the low field triplet has a larger splitting (Table 5;5). Again there are wing lines, but these do appear to form at the same rate as the triplet and may be due to coupling to ^{99}Ru and ^{101}Ru isotopes, both of which have a spin of 5/2 and 12.8 and 17.0 % abundance respectively. Some of these wing lines have a splitting close to that of the main triplet (3.6 gauss), but as overlapping lines are to be expected a value for the ruthenium splitting has not been obtained.

Fig 5;13

172

Angular Variation of E.S.R. Absorption Lines in γ-irradiated KCl
doped with $Fe(II)(CN)_6^{4-}$

g-value
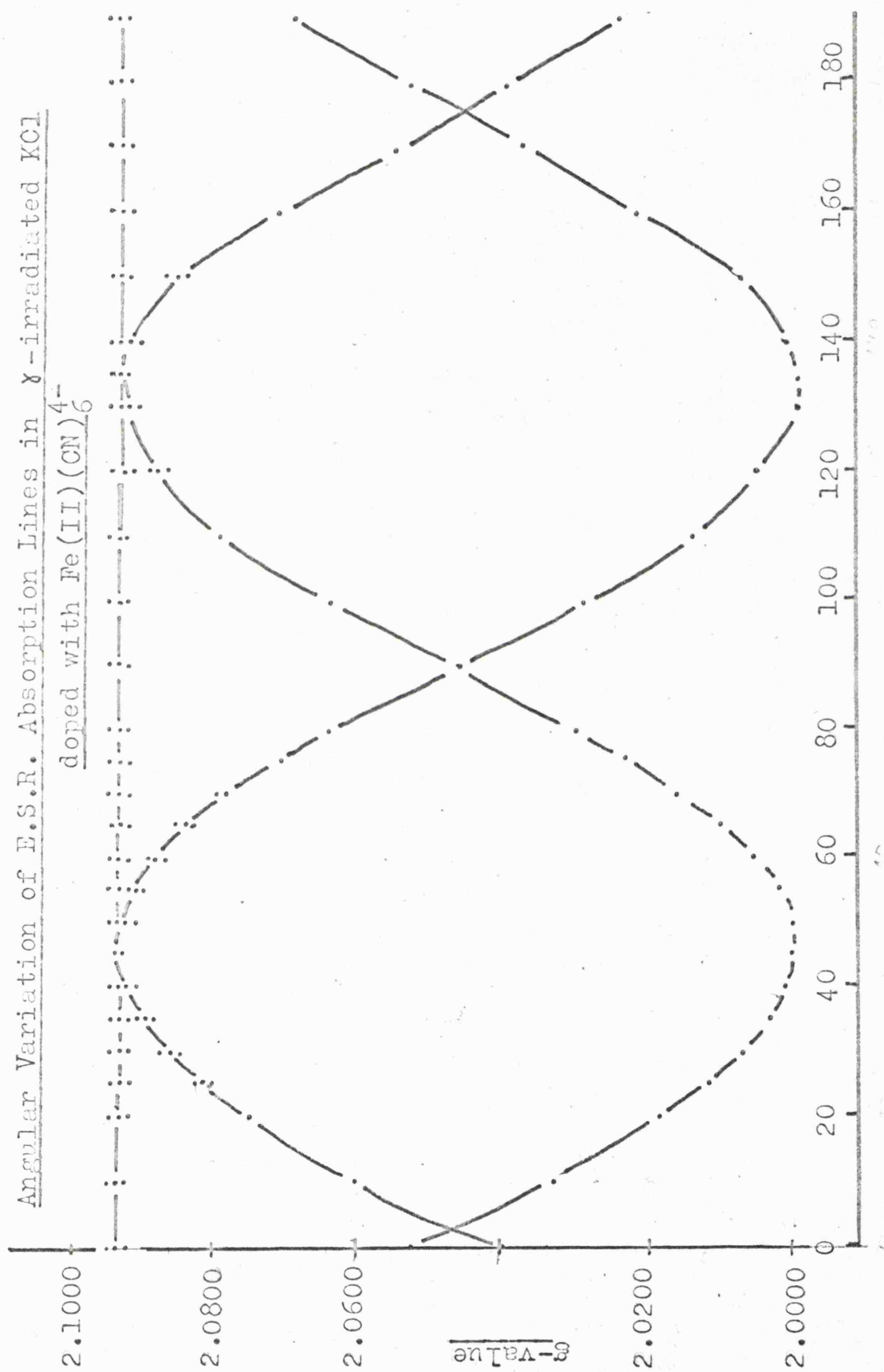
3._Other_Complexes_: The e.s.r. spectrum of potassium chloride

crystals containing $Co(III)(CN)_6^{3-}$ contains eight broad lines on γ-

irradiation, but these lines have no fine structure,

No e.s.r. signals were observed from the samples containing

the $Ag(CN)_2^-$, despite the possibility of Ag(0) having been formed.

Table 5:5

E.S.R. Parameters for the Irradiated Compec Cyanides in Ionic Lattices

a. $Fe(II)(CN)_6^{4-}$

Matrix	$g_{\perp}$	$g_{//}$	$A_{\perp}$(gauss)
KCl	2.0950	1.9998	1.95
NaCl	2.0766	2.0000	2^+
KBr	2.1035	1.9998	2.05
KCN	2.1010	x	++
RbBr	2.0951	1.9997	++
NaCN	2.0948	x	++

b. $Ru(II)(CN)_6^{4-}$ in potassium chloride

$g_{\perp}$ = 2.0815 $g_{//}$ = x $A_{\perp}$ = 3.65 gauss

c. $Co(III)(CN)_6^{3-}$ in potassium chloride

g = 2.0853   A = 34 gauss   (Both probably perpendicular
features)

x = obscured by other paramagnetic species

+ = poorly resolved

++ = not resolved

ii. Discussion

a. The Infra-red and Electronic Spectra

The new i.r. absorption bands which appear, on irradiation, at lower energy than the original complexs C-N stretching bands are attributed in all cases to lower oxidation state species of the transition metal complexes for the following reasons:-

1. The depression of the F-band formation when the metal complex is incorporated into the halide lattice indicates that the complex is acting as an electron trap.

2. Table 5;6 shows the position of the v_6 band for cyanide complexes in which the transition metal complex is in an oxidation state of III or II. The lower oxidation state can be stabilised by delocalization of electrons into the π -antibonding orbital on the cyanide ion. This delocalization has the effect of increasing v_7 and decreasing v_6. From table 5;6 it can be seen that cyanide complexes of oxidation state III have a main absorption at about 2120 cm^{-1}, and those of oxidation state II an absorption at about 2050 cm^{-1}. For oxidation state I an even lower energy absorption for v_6 would be expected.

3. The e.s.r. spectrum of the ferrous cyanide sample after irradiation is compatible with a d^7 Fe(I) complex and is discussed in the next section.

The value of 1947 cm^{-1} for the main absorption band in irradiated $Fe(CN)_6^{4-}$, which we attribute to $Fe(I)(CN)_6^{5-}$, is the lowest value reported for an octahedral complex cyanide v_6 (C-N)stretch. This

Table 5:6

The v_6 C-N Stretching Frequency for a number of Cyanides

Complex	v_6	Ref
$Mn(III)(CN)_6^{3-}$	2125	148
$Mn(II)(CN)_6^{4-}$	2060	148
$Mn(I)(CN)_6^{5-}$	2048	148
$Fe(III)(CN)_6^{3-}$	2125	142
$Fe(II)(CN)_6^{4-}$	2050	141
$Fe(III)(CN)_5H_2O^{2-}$	2120	149
$Fe(II)(CN)_5H_2O^{3-}$	2043	149
$Co(III)(CN)_5H_2O^{2-}$	2140	150
$Co(II)(CN)_5H_2O^{3-}$	2095	150

— — — — — — — — — — — — — — —

low value must reflect the instability of the complex, for as the extra electron has gone into an e_g orbital which is essentially a σ-antibonding orbital extensive delocalization via a t_{2g} antibonding mechanism was not expected. The σ-antibonding character of the extra electron is reflected in the lowering of the v_7 Fe-C stretch on irradiation despite the extra π-bonding. The spectrum of the irradiated potassium chloride crystals containing $Ru(II)(CN)_6^{4-}$ is very similar, but there is a general increase in the energies of all the absorption bands, compared with the $Fe(II)(CN)_6^{4-}$ complex and associated radiation products.

There are no stable octahedral complexes with more than 7 d-electrons. This may be due partly to the extra d-electrons weakening the M-C bond. This situation favours either the loss of two ligands to form a square planar complex, with the extra d-electrons in the

d_z2 orbital, or the formation of tetrahedral complexes. It may
therefore be significant that we have not been able to prepare the
d^8 Fe(O) or Ru(O) complexes. Further irradiation of the Fe(I) and
Ru(I) complexes yields the apparently uncoordinated cyanate ions in
quite large concentrations.

b. The Electron Spin Resonance Spectra

The e.s.r. spectra of the irradiated halides containing the
ferrous and ruthenium hexacyanides are all very strong, and hence
the concentration of the radicals must be high. The i.r. spectra
of the irradiated samples also contain strong bands, but due to the
relative insensitivity of the i.r. technique, the possibility of
examining the same paramagnetic species by i.r. and e.s.r. spectroscopy
is not usually considered. In this case, however, the i.r. bands
are very narrow, and the e.s.r. spectrum of the polycrystalline
material over 150 gauss wide.

The calculated number of paramagnetic species causing the e.s.r.
spectrum of the irradiated ferrous complex in potassium chloride is
of the order of 10^{18}. Samples of the doped potassium chloride
containing less than 0.1% of the complex gave peaks similar to the
weaker set of bands in fig 5;2. The pressed disc which is of
comparable weight to the.e.s.r. sample contains, in this case, about
10^{18} complex ions. To test these results further a paramagnetic
nitrosyl complex $(Cr(CN)_5NO^{4-})$ was incorporated into the potassium
chloride lattice. When the concentration was such that it yielded
similar strength cyanide stretching bands to those in fig 5;2 the

e.s.r. signal from the sample was similar to that from the irradiated

species under discussion. It would thus seem possible to observe

the same cyanide complex by e.s.r. and i.r. spectroscopy.

We thus assign the e.s.r. spectrum of the irradiated ferrous

complex to a Fe(I) complex and in ruthenium to Ru(I). The other

possibility, that of a d^5 M(III) complex is ruled out because the

g-tensor for these species is consistent with a d^7 and not a d^5

complex[151, 152].

In a purely octahedral d^7 complex the unpaired electron is in the

degenerate e_g orbitals (Fig 5;1). Unless there is some distortion of

the complex, which can lift this degeneracy, an e.s.r. spectrum would

not be observed above about 4°K. Since broad signals are observed

at room temperature a considerable distortion must occur. The

coupling to only one nitrogen atom, observed in the perpendicular

features of both the Fe and Ru cases, requires a distortion that will

produce one unique cyanide ligand. Since the triplet is observed in

both the iron and ruthenium complexes there may be a general method

of distortion of the molecule.

The g-tensor of the Fe(I) complex shows a positive shift of about

0.09 for $g_\perp$ and a small negative shift of about 0.0025 for $g_{//}$.

This is similar to that for $Fe(I)(CN)_5NO$ in irradiated sodium nitro-

prusside[151, 152], except that $\Delta g_\perp$ is larger. A simplified m.o.

diagram of an Fe(I) complex considering only the effects of the d-

orbitals is shown in fig 5;14. The effect of the π-bonding orbitals

on the cyanide ions is neglected, since these will not have much effect

d_{xz}, d_{yz} ——————— e

d_{xy} ——————— b_2

d_{z^2} ——————— a_1

$d_{x^2-y^2}$ ——————— b_1

d_{z^2} ——————— a_1

CN π^*

CN* π^*

3d ———————

$\Delta g_\perp > 0$

d_{xy} ——————— b_2

d_{xz}, d_{yz} ——————— e

CN* σ

CN σ

d_{z^2} ——————— a_1

$d_{x^2-y^2}$ ——————— b_1

d_{z^2} ——————— a_1
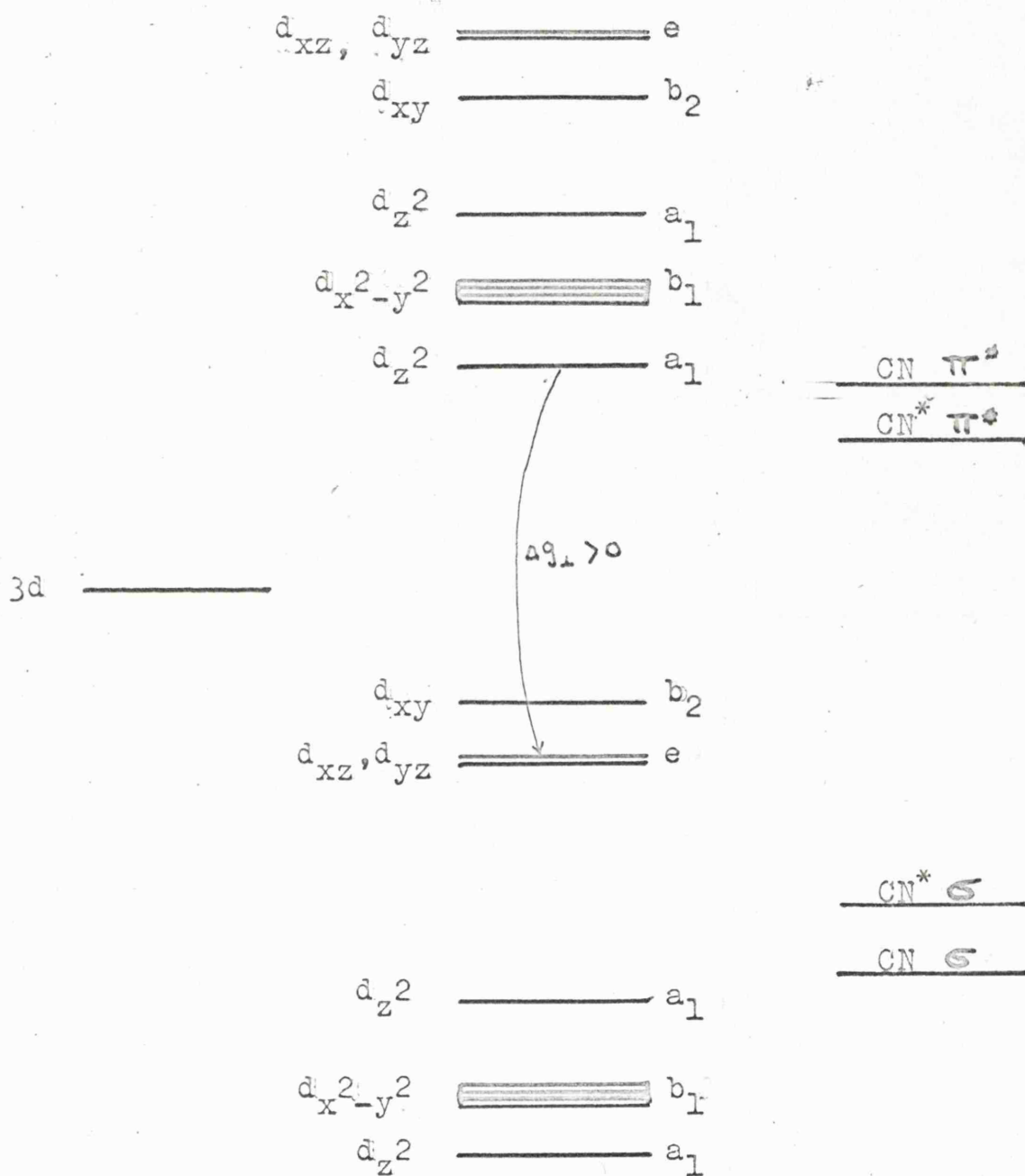
Simplified molecular orbital diagram for $M(I)(CN)_5(CN^*)$ complexes

on the energy levels in these low oxidation state complexes. In fig 4;14 one cyanide ion is different from the rest, (CN^x) and is assumed to have lower σ-donating, but better π-accepting properties than the normal cyanide ligands.

The e.s.r. spectrum can be explained satisfactorily with the electron in the d_z2 orbital. When the magnetic field is along the z-axis there are no orbitals which can mix with the d_z2 orbital which has a_1 symmetry (see product tables for C_{4v} group in appendix B). Thus there will be very little shift in $g_{\parallel}$ from the free spin value. When the field is perpendicular to the z-axis, however, there can be coupling with the filled e orbitals $(d_{xz},$ and $d_{yz})$. This should lead to a relatively large positive shift, as is observed. The shift in $g_{\perp}$ is greater than the shift found in $Fe(I)(CN)_5NO$. This may indicate that the effect of the π-antibonding orbitals, lowering the energies of the $d_{xy},$ d_{xz} and d_{yz} orbitals by back donation, is less in the case considered here than for the nitrosyl, where low energy π-antibonding orbitals are available on the nitrosyl ligand.

The loss of resolution on going to the parallel position may be due both to reduction in the coupling to the nucleus causing the perpendicular triplet and increase in the coupling to the other ligands in the complex.

Possible models for producing a unique cyanide ligand stem from a consideration of either the effect of charge compensating vacancies or protonation of one cyanide ion.

In the crystal near the $Fe(CN)_6^{4-}$ ion there must be a cation

vacancy, at one of the twelve nearest neighbour cation sites, to compensate for the charge on the ion. On irradiation an electron produced by ionisation of a halide ion is trapped at the complex, thus reducing the number of electrons available to form F-centres. This extra electron will go into the e_g orbitals, which are doubly degenerate, and hence a Jahn-Teller distortion is expected[153]. The distortion can stabilise either the d_{z^2} or the $d_{x^2-y^2}$ orbital depending on which bonds are lengthened or shortened. If there is a vacancy along an N-C-M-C-N direction then the complex can distort into the vacancy. The amount of the distortion would depend to some extent on the lattice size and so the $g_\perp$ value dependence on lattice size can be explained. Extension of the M-C bond into the vacancy would stabilise the d_{z^2} orbital relative to the $d_{x^2-y^2}$. With this mechanism for producing the distortion a marked effect is expected on cooling, as in fact found (Fig 5;11). The sharpening of the e.s.r. absorption bands is much more marked than in, for example, the $Fe(I)(CN)_5NO^{2-}$ ion where the distortion is due to substitution of a different ligand.

The second possibility, i.e. protonation, has been postulated recently to explain some results for nitrosyl complexes[154]. The formation of HCN$^-$ (Chapter 4) shows that hydrogen atoms are present in irradiated alkali halide crystals which have been grown from solution. The mechanism of attack might then involve attack of hydrogen atoms on the complex with the formation of the $Fe(CN)_5CNH^{4-}$ complex. To a first approximation the protonation of the ligand will not affect the π-system, but will lower the donating power of the

σ-system. The overall effect of protonation will thus be a weakening of the M-C bond. This bond will lengthen and so the d_z2 orbital will be stabilised, and the unpaired electron will be formally localized in a M-C antibonding orbital.

Both these mechanisms for distortion place the unpaired electron in the d_z2 orbital, and would give an uneven distribution between the M-C bonds in the z-direction. This distribution is such that the weaker M-C bond contains the greatest density of the unpaired electron. The unpaired electron is thus in a σ-orbital relative to the cyanide ion along the z-axis and so the nitrogen coupling can be explained by delocalization of the unpaired electron into the σ-system of the cyanide ligand by spin polarisation.

Despite the fact that the protonation of a cyanide ligand explains the e.s.r. spectra more readily than the distortion involving a neighbouring vacancy the protonation mechanism would appear unlikely from this preliminary investigation for a number of reasons:-

1. It does not easily explain the depression of the F-band formation.

2. The comparable rates of reduction of the complex ions by both γ- and ultra-violet irradiation are unlikely for a mechanism requiring the production of hydrogen atoms.

3. The rate of reduction of the complex is faster than the formation of hydrogen atoms trapped at vacancies in alkali halides[155].

Chapter 6

Radiation Damage in Solid Cyanides

In the preceding chapters only the spectra and structure of the paramagnetic species formed on irradiation of solids containing simple or complex cyanide ions have been considered. In this chapter the effect of irradiation is summarised and possible reaction schemes for the formation of these paramagnetic species discussed. Further i.r. studies on the effect of radiation on the simple cyanide ion incorporated into the alkali halide lattices have been performed. γ-irradiation of the cyanide ion doped halides produces relatively large concentrations of the cyanate ion, and an attempt has been made to explain the formation of the cyanate ion as well as the simple radicals containing the C-N group.

I. The Effect of Radiation on Solid Ionic Cyanides

The main paramagnetic species formed on γ-irradiation of sodium cyanide are the F- and V_k- centres. The simplest mechanism for the formation of these species is the ionisation of the cyanide ion, the electron being trapped at a vacancy and the cyanide radical reacting with a neighbouring cyanide ion to form the $(CN)_2^-$ ion.

The F-centre band in sodium cyanide is very weak, by comparison with the strong bands produced by irradiation of potassium chloride or bromide for similar lengths of time. The oscillator strength is probably similar for all F-centres and so this low band intensity is almost certainly due to smaller numbers of F-centres formed.

There is strong evidence[156] that the vacancies in alkali halides which are able to trap the F-electron are formed by the radiation. The vacancies which are present as thermodynamic defects[157] are in

some way unable to trap the electron. This may be due to aggregation of vacancies[68]. The actual mechanism for the formation of vacancies in alkali halides by irradiation has not been settled, but in all the proposed theories the affected halogen atom or ion migrates to either another lattice position or an interstitial site. Thus if the mechanism for forming F-centres in sodium cyanide is similar to that with the alkali halides then the cyanide radical must migrate, and it is unlikely to be as efficient at this as the single atomic halogen species. If the cyanide radical is near the generated vacancy it will inhibit the trapping of the electron, to form the F-centre, and this may be the reason for the lower concentration of F-centres in the cyanide lattice.

Some evidence for the radiation production of the F-centre vacancies in sodium cyanide is that on γ-irradiation of a newly bleached sample the F-centre is rapidly reformed.

The relative rates of F-centre production are also markedly dependent on the purity of the sample. Exposure to the atmosphere inhibits the production of the F-centre, as does the presence of transition metal impurities. It would appear that the F-centre formation in sodium cyanide is much more sensitive to impurities than the formation of these centres in the alkali halides.

II. The Effect of Radiation on Simple Cyanide Ions in Alkali Halides

i. Infra-red Study of the Effect of γ-irradiation on Cyanide Ions

a. Experimental Results

The alkali halides were doped with cyanide ions from aqueous

solution similar to the samples used for the work reported in chapter

4.   Samples obtained by a Stockbarger procedure contained strong

cyanate i.r. bands, despite stringent precautions to prevent the

formation of this ion.   The samples grown from solution contained

very little cyanate impurity.   In fact as the i.r. bands were very

broad (Fig 6;1) most of the cyanate did not appear to be incorporated

into the lattice.

On γ-irradiation for one hour a peak appears in the i.r. spectrum

at 2182 cm^{-1}, and on further irradiation other peaks at 1947 and 1920

cm^{-1} are observed.   Extended irradiation increases the intensity of

the absorption band at 2182 cm^{-1} and other peaks can also be observed

at 2171 and 2156 cm^{-1}(Fig 6;2).   The peak at 2156 cm^{-1} is not always

present, and so is due to a different species from that causing the

other peaks.   In similarly doped potassium bromide only two peaks

can be observed, a strong one at 2170 cm^{-1} and a weaker one at 2159 cm^{-1}.

Ultra-violet irradiation has only a minor effect on the i.r.

spectrum, but in potassium chloride matrices peaks can be observed at

2182, 2170 and 2156 cm^{-1}.   These peaks are never very strong even

after extensive irradiation and hence the ultra-violet irradiation

may only affect the surface of the samples.

If the unirradiated discs of the doped halide is heated, a broad

Effect of 5 hours γ-irradiation on I.R. Spectrum of

KCl Crystals Doped with Cyanide Ions

a. No irrad.

b. 5 hrs irrad.

2200   2100   2000   1900
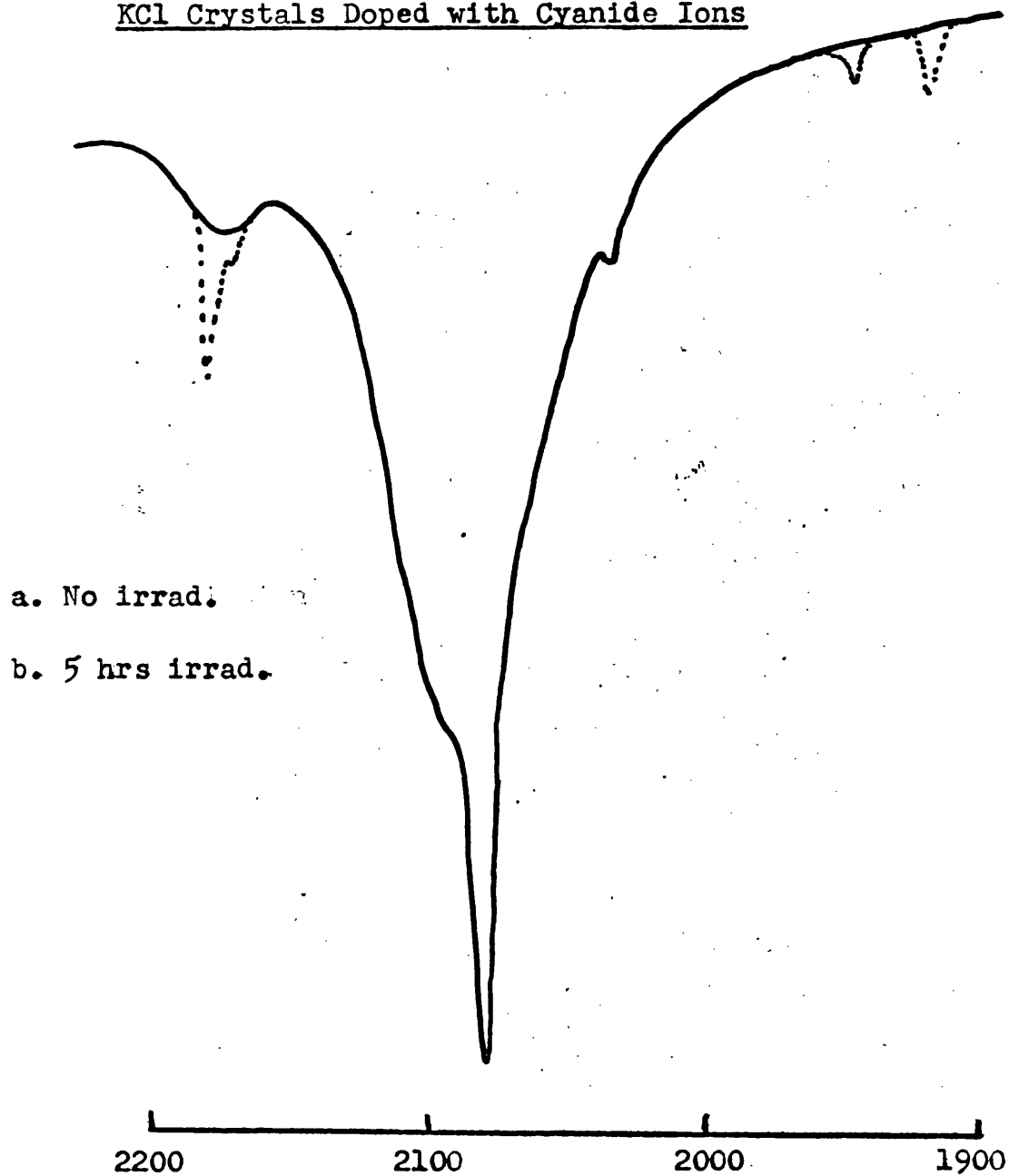
I.R. Spectrum of CNO⁻ Ion Formed by ɣ-irradiation of
Cyanide Doped KCl and KBr

a. KCl ——

b. KBr - - - -

2200   2180   2160   2140
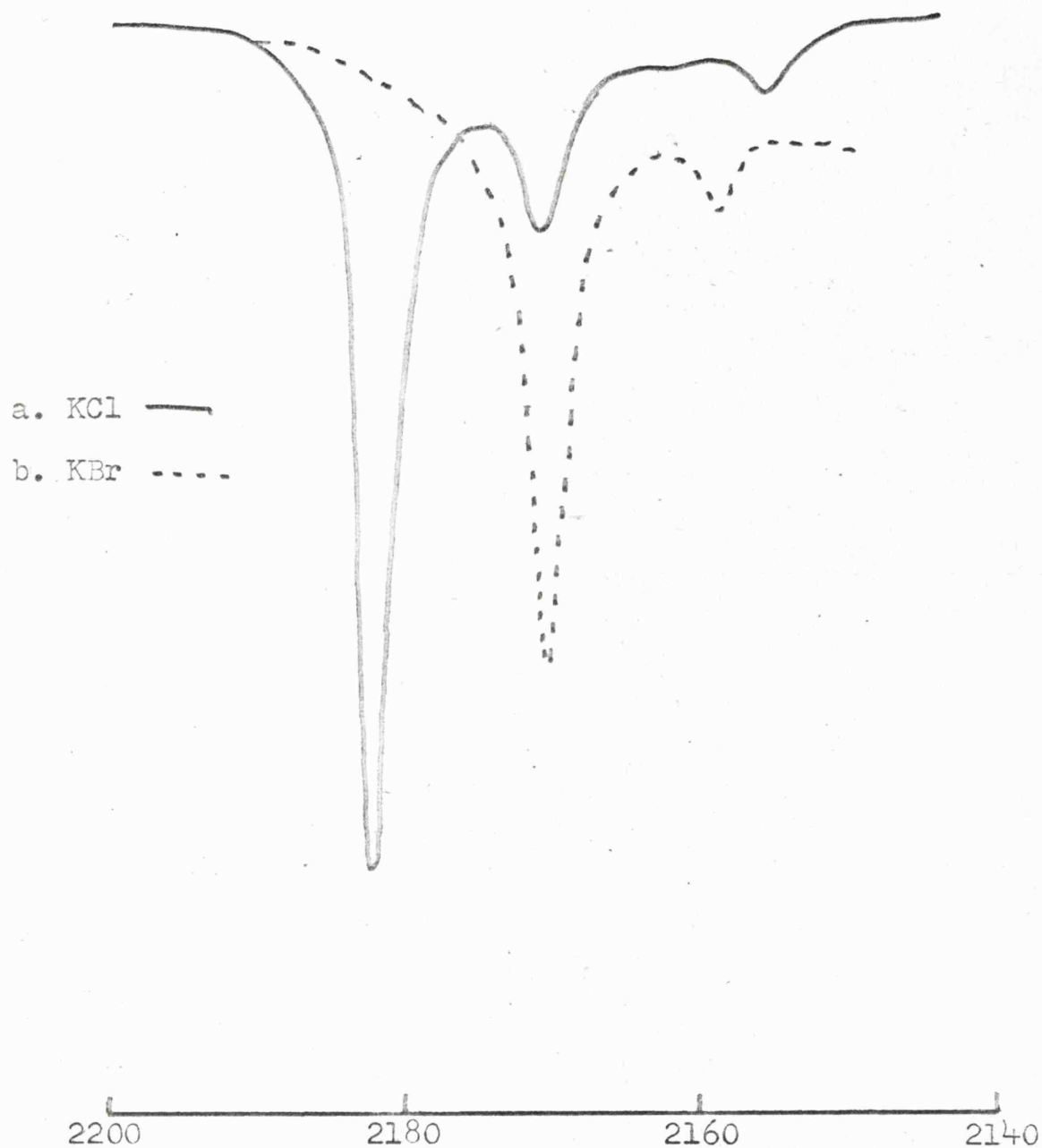
but weak absorption peak at about 2175 cm^{-1} is produced.

Table 6:1

Infra-red Absorption Bands Observed in Irradiated Alkali Halides Doped with cyanide

Lattice		(000) to (001)[c]	(010) to (011)[c]	(Other)
KCl	a.	2182	2171	2156
	b.	2181.2	2170.7	
KBr	a.	2170	2159	
	b.	2169.6	2158.6	

a. This Work.   b. Maki and Decius (146)   c. (v_1, v_2, v_3)

- - - - - - - - - - - - - - - - -

b. Discussion

The peaks which are formed at 2182 and 2171 cm^{-1} in the potassium chloride lattice are caused by the cyanate ion. These values agree well with the values quoted by Maki[146](Table 6;1) for this ion in potassium chloride, and the shift in the absorption on going to the potassium bromide lattice is characteristic for this ion. On cooling the sample the band at 2171 cm^{-1} (2159 cm^{-1} in KBr) is reduced in intensity and disappears at about 100°K. We thus follow Maki[146] in assigning this to the (0, 1, 0) to (0, 1, 1) transition, and the peak at 2182 cm^{-1} to the fundamental v_3 tansition, (0, 0, 0) to (0, 0, 1).

The peak at 1947 cm^{-1} is due to impurity $Fe(CN)_6^{4-}$ ion and the unassigned peaks at 2157 cm^{-1} and 1920 cm^{-1} may be due to other impurities.

ii. The Effect of Radiation on Alkali Halides Containing Cyanide Ions

At least three paramagnetic species have been identified from

their e.s.r. spectrum in irradiated potassium chloride doped with

cyanide ions. These are the cyanogen negative ion $(CN)_2^-$, the

hydrogen cyanide negative ion HCN^- and the methylene imino radical

H_2CN. The i.r. spectrum of the irradiated cyanide doped halide shows

that large amounts of cyanate ions are formed. The i.r. spectrum

also shows that the solution grown samples contain large amounts of

water and hydroxide ions. We now examine possible schemes for the

formation of the above radicals and for the cyanate ion.

a. The Formation of the Cyanogen Negative Ion $(CN)_2^-$

There are two possible methods of forming the $(CN)_2^-$ ion in alkali

halides. The first is identical with that previously described for

the formation of the ion in pure alkali cyanides. The other is via a

Cl_2^- intermediate. The Cl_2^- radical is observed in the low temperature

irradiated samples. On warming the sample, the Cl_2^- radical decomposes,

the electron hole becoming mobile, and is ultimately trapped at sites

containing cyanide ions. No e.s.r. signals which can be assigned to

CN. radicals or to radicals such as $ClCN^-$ have been observed. These

species might be expected from cyanogen radicals which do not have a

cyanide ion neighbour. Since, however, each anion has twelve nearest

neighbour anions there is a strong probability that the cyanide radical

will be adjacent to another cyanide ion (Fig 4;2 page 138).

The rate at which the $(CN)_2^-$ is formed in potassium chloride is

comparable with the rate in the pure cyanides, and hence a Cl_2^- or $Cl.$

intermediate is likely even with the irradiation at room temperature. The halide lattice has thus enhanced the formation of this electron deficient species.

The low temperature experiment is useful in all studies of this kind, for if the signal due to a certain species is enhanced on warming e.g. fig 4;19 (page 130) then this is indicative of an electron hole centre. Irradiation at room temperature will produce either an electron deficient or an electron excess centre depending on the relative depths of the electron traps in the crystal.

b. The Formation of the HCN⁻ and H_2CN Radicals

Gamma-irradiation of potassium chloride crystals grown from solution or doped with OH⁻ ions yields on irradiation trapped hydrogen atoms[155]. The hydrogen atoms can be trapped by a cyanide ion to form HCN⁻ radical. The neutral hydrogen atoms are small enough to be able to migrate through the crystal until they are trapped. The HCN⁻ radicals form rapidly, but it is impossible to build up large concentrations. The optimum irradiation time is approximately twenty minutes under our conditions. The radical decomposes fairly quickly, but the decomposition is minimised if the sample is kept in the dark, or cooled to 77°K. This may indicate that that the decomposition is related to the bleaching of the F-centres, which are also formed on irradiation.

The third radical formed in cyanide doped potassium chloride is H_2CN. This is much more stable than the HCN⁻ radical, and the concentration increases with irradiation time. The H_2CN radical

has also been prepared by photolysing a mixture of HI and HCN in an argon matrix[112]. Thus it is possible to prepare H_2CN by hydrogen atom attack on HCN. It is unlikely that there is much HCN in our samples initially, but this may be a product of the decomposition of HCN⁻. A possible scheme for the formation of HCN⁻ and H_2CN is given in fig 6;3.

<div align="center">

Fig 6:3

Possible Schemes for the Formation of HCN⁻ and H_2CN

</div>

HOH	$\xrightarrow{\gamma}$	H. +	.OH
OH⁻	$\xrightarrow{\gamma}$	H. +	.O⁻
OH⁻	$\xrightarrow{\gamma}$	HO. +	e
H. + CN⁻	$\longrightarrow$	HCN⁻	
HCN⁻	$\longrightarrow$	HCN +	e
H. + HCN	$\longrightarrow$	H_2CN	
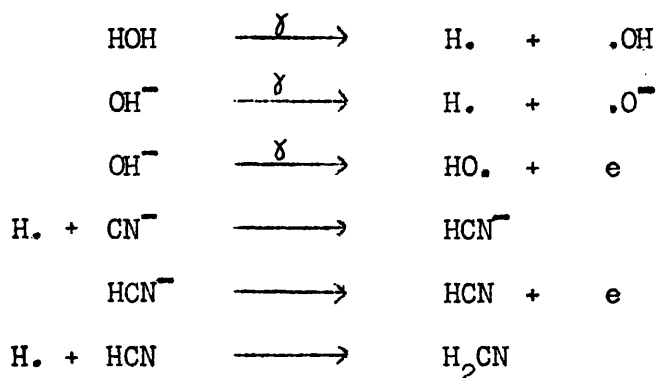
c. The Formation of the Cyanate Ions

Significantly larger concentrations of cyanate ions are formed on irradiation of the cyanide doped halides compared with the paramagnetic species discussed above. Indeed the cyanate ion is the major product of γ-irradiation of cyanide ion in alkali halide lattices. It is unfortunate that the only samples which are initially free from cyanate ions are those grown from aqueous solution. It is thus not possible to obtain samples free from water or OH⁻ ions and containing no cyanate ions. The radiation products of water or hydroxide ions postulated in fig 6;3 for the formation of HCN⁻ and H_2CN radicals are

thus also present in the lattice after irradiation and can be postulated for the oxidation of the cyanide ion. Two possible oxidants are the hydroxyl radical and the oxygen negative ion:

$$CN^- + .OH \longrightarrow HOCN^- \longrightarrow OCN^- + H.$$

$$CN^- + .O^- \longrightarrow OCN^{2-} \longrightarrow OCN^- + e$$
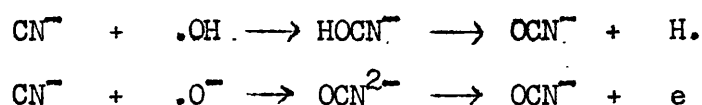
The inability of ultra-violet irradiation to produce large quantities of the cyanate ion may be due to only the surface layers receiving large enough quantities of radiation to form appreciable amounts of the oxidant. In the case of HCN^-, which could be formed by ultra-violet irradiation, the reactive species was the neutral hydrogen atom which can easily migrate through the crystal. Charged species will not be able to migrate as easily and so if formed near the surface they will not be able to react with cyanide ions in the body of the crystal.

CONCLUSION

This topic has proved a fruitful field of study, with regard to both the effect of radiation on ionic crystals containing simple and complex cyanide ions, and the new paramagnetic species observed. Further work with pure alkali cyanide crystals and with ^{13}C isotopically enriched complex and simple cyanide ions will no doubt lead to resolution of some of the unsolved problems in this work.

Appendices

Appendix A

Character Tables

A.1

$C_{\infty v}$	E	$2C^{\phi}$	...	σ_v		
A_1 Σ^+	1	1	...	1	z	x^2+y^2, z^2
A_2 Σ^-	1	1	...	-1	R_z	
E_1 Π	2	$2\cos\phi$	...	0	x, y; R_x,R_y;	xz; yz
E_2 Δ	2	$2\cos 2\phi$	...	0	x^2-y^2, xy	
E_3 Φ	2	$2\cos 3\phi$	...	0		

A.2

C_{4v}	E	$2C_4$	C_2	$2\sigma_v$	$2\sigma_d$		
A_1	1	1	1	1	1	z	x^2+y^2, z^2
A_2	1	1	1	-1	-1	R_z	
B_1	1	-1	1	1	-1	x^2-y^2	
B_2	1	-1	1	-1	1	xy	
E	2	0	-2	0	0	x, y; Rx, Ry; xz, yz.	

A.3

O_h	E	$8C_3$	$6C_2$	$6C_4$	$3C_2(C_4^2)$	i	$6S_4$	$8S_6$	$3\sigma_h$	$6\sigma_d$	
A_{1g}	1	1	1	1	1	1	1	1	1	1	$x^2+y^2+z^2$
A_{2g}	1	1	-1	-1	1	1	-1	1	1	-1	
E_g	2	-1	0	0	2	2	0	-1	2	0	$2z^2-x^2-y^2$, x^2-y^2
T_{1g}	3	0	-1	1	-1	3	1	0	-1	-1	R_x, R_y, R_z
T_{2g}	3	0	1	-1	-1	3	-1	0	-1	1	xz, yz, xy
A_{1u}	1	1	1	1	1	-1	-1	-1	-1	-1	
A_{2u}	1	1	-1	-1	1	-1	1	-1	-1	1	
E_u	2	-1	0	0	2	-2	0	1	-2	0	
T_{1u}	3	0	-1	1	-1	-3	-1	0	1	1	x, y, z
T_{2u}	3	0	1	-1	-1	-3	1	0	1	-1	

B.1

C_{4v}	A_1	A_2	B_1	B_2	E
A_1	A_1	A_2	B_1	B_2	E
A_2	A_2	A_1	B_2	B_1	E
B_1	B_1	B_2	A_1	A_2	E
B_2	B_2	B_1	A_2	A_1	E
E	E	E	E	E	$A_1+A_2+B_1+B_2$

B.2

C_{2v}	A_1	A_2	B_1	B_2
A_1	A_1	A_2	B_1	B_2
A_2	A_2	A_1	B_2	B_1
B_1	B_1	B_2	A_1	A_2
B_2	B_2	B_1	A_2	A_1

References

1. F. M. A. El-Sayed and R. K. Sheline   J. Inorg. Nucl. Chem. 1958, 6, 187

2. W. Low   "Paramagnetic Resonance in Solids"   Academic Press, New York   1960

3. H. A. Kramers "Quantum Mechanics"   North Holland Publ. Co., Amsterdam.   1957   p. 384

4. C. P. Slichter   "Magnetic Resonance"   Harper and Row, New York 1963

5. F. K. Kneubuhl   J. Chem. Phys.   1960, 33, 1074

6. J. W. Searl, R. C. Smith and S. J. Wyard   Proc. Phys. Soc. 1959, 74, 491

7. J. W. Searl, R. C. Smith and S. J. Wyard   Proc. Phys. Soc. 1961, 78, 1174

8. T. S. Johnston and H. G. Hecht   J. Mol. Spect.   1965, 17, 98

9. D. A. Gooding   Phys. Rev.   1961, 123, 1706

10. P. Kusch and V. W. Hughes,   Handbuch der Physik,   Vol 37 (1) Springer, Berlin.

11. J. S. M. Harvey   Proc. Roy. Soc.   1965, 285A, 581

12. V. Jaccarino and J. C. King   Phys. Rev.   1951, 83, 471

13. H. H. Brown and J. G. King   Phys. Rev.   1966, 142, 53

14. V. Jaccarino, J. G. King and R. A. Satten   Phys. Rev.   1954, 94, 1798

15. C. C. J. Roothaan and E. Clementi   Univ. of Chicago Rept.

16. R. E. Watson   and A. J. Freeman   Phys. Rev. 1961, 123, 521

17. M. Synek, A. E. Rainis and C. C. J. Roothaan   Phys. Rev. 1966, 141, 174

18. R. E. Watson and Freeman   Phys. Rev. 1961, 124, 1117

19. C. C. J. Roothaan, L. M. Sachs and A. M. Weiss Rev. Mod. Phys.
1960, 32, 186

20. E. Clementi and A. D. McLean Phys. Rev. 1964, 133A, 419

21. E. Clementi, C. C. J. Roothaan and M. Yoshimine Phys. Rev.
1962, 127, 1618

22. C. C. J. Roothaan and P. S. Kelly Phys. Rev. 1963, 131, 1177

23. E. B. Wilson, J. C. Decius and P. C. Cross "Molecular Vibrations"
McGraw-Hill New York 1955

24. F. A. Cotton "Chemical Applications of Group Theory" Interscience
New York 1963

25. R. S. Halford J. Chem. Phys. 1946, 14, 8

26. H. Winston and R. S. Halford J. Chem. Phys. 1949, 17, 607

27. A. Samakula "Molecular Science and Molecular Engineering"
John Wiley New York 1959

28. R. G. J. Miller (Ed.) "Laboratory Methods in I.R. Spectra"
Heyden and Son Ltd., London 1965

29. J. A. Brivati, N. Keen and M. C. R. Symons J. Chem. Soc. 1962,
237

30. J. H. de Boer Rec. Trav. chim. 1937, 56, 301

31. E. Mollwo Nachr. Ges. Wiss. Gottingen, Math.-phys. 1931 Kl 97

32. H. F. Ivey Phys. Rev. 1947, 72, 341

33. W. D. Compton and H. Rabin Solid State Phys. 1964, 16, 121

34. A. F. Kip, C. Kittel, R. A. Levy and A. M. Portis Phys. Rev.
1953, 91, 1066

35. H. Seidel Z. Physik 1961, 165, 218, 239

36. G. A. Noble J. Chem. Phys. 1959, 31, 931

37. W. C. Holton and H. Blum Phys. Rev. 1962, 125, 89

38. D. Schmid Phys. stat. sol. 1966, 18, 653

39. W. T. Doyle Phys. Rev. 1963, 131, 551

40. H. Seidel and H. C. Wolf Z. Physik 1963, 173, 455

41. H. C. Wolf and K. H. Hausser Naturwiss 1959, 46, 646

42. F. Hughes anf J. G. Allard Phys. Rev. 1962, 125, 173

43. J. Arends Phys. stat. sol. 1964, 7, 805

44. W. T. Doyle and W. L. Williams Phys. Rev. Lett. 1961, 6, 537

45. F. F. Carlson, G. J. King and B. S. Miller J. Chem. Phys. 1960, 33, 1266

46. G. Feher Phys. Rev. 1957, 105, 1122

47. H. Blum Phys. Rev. 1965, 140A, 1998

48. T. Inui and Y. Uemura Prog. Theor. Phys. 1950, 5, 252

49. T. Kojima J. Phys. Soc. Jap. 1957, 12, 908, 918

50. D. J. Greenslade Thesis 1965 Univ. of Leicester.

51. E. Clementi and D. L. Raimondi J. Chem. Phys. 1963, 38, 2686

52. J. E. Wertz, J. W. Orton and P. Auzins Disc. Farad. Soc. 1961, 31, 140

53. W. B. Lewis and F. E. Pretzel J. Phys. Chem. Solids 1961, 19, 139

54. T. G. Castner and W. Kanzig J. Phys. Chem. Solids 1957, 3, 178

55. C. E. Bailey Phys. Rev. 1964, 136, 1311

56. F. W. Patten and M. J. Murrone Phys. Rev. 1965, 142, 513

57. E. Boesman Thesis 1962 Univ. of Ghent

58. D. Schoemaker Phys. Rev. 1966, 149, 693

59. P. W. Atkins, N. Keen and M. C. R. Symons J. Chem. Soc 1962, 2873

60. G. Natta and L. Passerini Gazzetta 1931, 61, 191

61. C. E. Meiser and W. T. Zeigler J. Amer. Chem. Soc. 1941, 63, 2703

62. A. F. Wells "Structural Inorganic Chemistry" Oxford Univ. Press, 1962

63. L. Pauling Phys. Rev. 1930, 36, 430

64. J. Frenkel Acta Physicochim. U. R. S. S. 1935, 3,

65. C. K. Coogan and H. S. Gutowsky J. Chem. Phys. 1964, 40, 3419

66. G. Isetti and T. J. Neubert J. Chem. Phys. 1957, 26, 337

67. S. Susman Argonne Natl. Lab. Illinois Rept. 1963

68. J. H. Schulman and W. D. Compton "Colour Centres in Solids" Pergamon Oxford 1963

69. B. S. Miller J. Chem. Phys 1964, 40, 2371

70. H. Seidel Phys. Lett. 1963, 7, 27

71. A. D. Walsh J. Chem. Soc. 1953 2260, 2266, 2288, 2296, 2301, 2306

72. M. Born and J. R. Oppenheimer Ann. Physik 1927, 84, 457

73. J. W. Linnett "The Electronic Structure of Molecules" Methuen London 1964

74. M. J. S. Dewar "Hyperconjugation" Ronald Press New York 1962

75. G. W. Wheland J. Chem. Phys. 1934, 2, 474

76. L. Pauling, H. S. Springall and K. J. Palmer J. Amer. Chem. Soc. 1939, 61, 927

77. R. S. Mulliken J. Chem. Phys. 1939, 7, 339

78. J. W. Baker and W. S. Nathan J. Chem. Soc. 1935, 1844

79. J. Cassie Nature 1933, 131, 438

80. W. G. Penny and G. B. Sutherland   Proc. Roy. Soc. 1936, A156, 654

81. R. S. Mulliken   Rev. Mod. Phys. 1942, 14, 204

82. P. W. Atkins and M. C. R. Symons   "Structure of Simple Inorganic Radicals"   Elsevier   Amsterdam   1967

83. D. W. Ovenall and D. H. Whiffen   Mol. Phys. 1961, 4, 135

84. R. S. Mulliken   J. Amer. Chem. Soc. 1955, 77, 887

85. C. A. Coulson and A. H. Neilson   Disc. Farad. Soc. 1963, 35, 71

86. H. H. Schmidtke and H. Preuss   Z. Naturforsch. 1961, 16A, 790

87. M. Krauss   J. Res. Nat. Bur. Stand. 1964, 68A, 635

88. F. P. Boer, M. D. Newton and W. N. Lipscomb   Proc. Nat. Acad. Sci. 1964, 52, 890

89. J. C. Leclerc and J. C. Lorquet   Theoret. chim. Acta. 1966, 6, 91

90. F. O. Ellison and H. Schull   J. Chem. Phys. 1955, 23, 2348

91. H. M. McConnell   J. Chem. Phys. 1956, 24, 764

92. R. Bersohn   J. Chem. Phys. 1956, 24, 1066

93. S. I. Weissman   J. Chem. Phys. 1956, 25, 890

94. H. S. Jarrett   J. Chem. Phys. 1956, 25, 1289

95. H. M. McConnell and D. B. Chesnut   J. Chem. Phys. 1958, 28, 107

96. H. M. McConnell   J. Chem. Phys. 1958, 28, 1188

97. D. K. Ghosh and D. H. Whiffen   Mol. Phys. 1959, 2, 285

98. A. Carrington   Q. Rev. 1963, 17, 67

99. R. W. Fessendon and R. H. Schuler   J. Chem. Phys. 1963, 39, 2147

100. C. Heller and T. Cole   J. Chem. Phys. 1962, 37, 243

101. M. H. Hanna and H. M. McConnell   "Free Radicals in Biological Systems"   Academic Press   New York   1961   p. 133

102. J. P. Colpa and F. de Boer   Mol. Phys. 1964, 4, 333

103. D. B. Chesnut   J. Chem. Phys. 1958, 29, 43

104. A. D. McLauchlan   Mol. Phys.   1958, 1, 233

105. C. A. Coulson   "Valence"   Oxford Univ. Press   1961

106. D. Lazdins and M. Karplus   J. Chem. Phys. 1966, 44, 1600

107. M. C. R. Symons   J. Chem. Soc.   1959, 277

108. C. Heller and H. M. McConnell   J. Chem. Phys. 1960, 32, 1535

109. E. W. Stone and A. H. Maki   J. Chem. Phys. 1962, 37, 1325

110. M. C. R. Symons   Advances in Phys. Org. Chem.   1963, 1, 283

111. M. C. R. Symons   Tetrahedron   1962, 18, 333

112. E. L. Cochran, F. J. Adrian and V. A. Bowers   J. Chem. Phys. 1962, 36, 1938

113. C. Corvaja, G. Giacometti and P. Nordio   Theoret. chim. Acta 1963, 1, 393

114. F. J. Adrian and M. Karplus   J. Chem. Phys 1964, 41, 56

115. W. T. Dixon   Mol. Phys.   1965, 2, 201

116. J. A. Pople and D. B. Santry   Mol. Phys. 1964, 7, 269

117. D. A. Ramsay   J. Chem. Phys.   1953, 21, 960

118. G. Herzberg and D. A. Ramsay   Proc. Roy. Soc. 1955, A233, 34

119. J. W. C. Johns, S. H. Priddle and D. A. Ramsay   Disc. Farad. Soc. 1963, 35, 90

120. D. E. Milligan and M. E. Jacox   J. Chem. Phys. 1964, 41, 3032

121. G. E. Ewing, W. E. Thompson and G. C. Pimentel   J. Chem. Phys. 1960, 32, 927

122. G. Herzberg "I.R. and Raman Spectra" D. Van Nostrand New York 1945

123. W. G. Schneider and H. J. Bernstein Trans. Farad. Soc. 1954, 52, 13

124. J. C. Evans and H. J. Bernstein Canad. J. Chem. 1956, 34, 1083

125. L. J. Bellamy "Infra-red Spectra of Complex Molecules" Methuen London 1958

126. G. Herzberg "Spectra of Diatomic Molecules" D. Van Nostrand New York 1950

127. F. J. Adrian, E. L. Cochran and V. A. Bowers J. Chem. Phys 1962, 36, 1661

128. J. A. Brivati, N. Keen and M. C. R. Symons J. Chem. Soc. 1962, 237

129. E. L. Cochran, F. J. Adrian and V. A. Bowers J. Chem. Phys. 1966, 44, 4626

130. P. W. Atkins, N. Keen and M. C. R. Symons J. Chem. Soc. 1962, 2873

131. E. L. Cochran, F. J. Adrian and V. A. Bowers J. Chem. Phys. 1964, 40, 213

132. P. W. Atkins, N. Keen and M. C. R. Symons J. Chem. Soc. 1963, 250

133. J. Gendell, J. H. Freed and G. K. Fraenkel J. Chem. Phys. 1962, 37, 2832

134. L. Burnelle Theoret. chim. Acta 1964, 2, 177

135. E. Clementi and H. Clementi J. Chem Phys. 1962, 36, 2824

136. E. Clementi and A. D. McLean J. Chem. Phys. 1962, 36, 563

137. R. B. Horst, J. H. Anderson and D. E. Milligan Phys. Chem. Solids 1962, 23, 157

138. L. H. Jones   J. Chem. Phys.   1957, 26, 1579

139. W. P. Griffith   Q. Rev.   1962, 16, 188

140. I. Nakagawa and T. Shimanoushi   Spectrochim Acta   1962, 18, 101

141. G. B. Bonino and G. Fabbri   Lincei Rend sci. fis. mat. e nat.   1956, 20, 414

142. A. Hidalgo and J. P. Miellieu   Compte Rend   1959, 249, 233

143. V. Caglioti, G. Sartori and M. Scrocco   J. Inorg. Nucl. Chem.   1958, 8, 87

144. J. P. Miellieu and H. Poulet   Adv. Mol. Spect.   1962, Pergamon London.

145. L. H. Jones   Inorg. Chem.   1963, 2, 777

146. A. Maki and J. C. Decius   J. Chem. Phys.   1959, 31, 772

147. W. C. Price, W. F. Sherman and G. R. Wilkinson   Spectrochim. Acta   1960, 16, 663

148. V. Caglioti, G. Sartori and M. Scrocco   Lincei Rend sci. fis. mat. e nat.   1957, 22, 266

149. E. F. Herington and W. Kynaston   J. Chem. Soc.   1955, 3555

150. W. P. Griffith and G. Wilkinson   J. Chem. Soc.   1959, 2757

151. D. A. C. McNeil, J. B. Raynor and M. C. R. Symons   J. Chem. Soc.   1965, 410

152. J. Danon, R. P. A. Muniz and H. Panepucci   J. Chem. Phys.   1964, 41, 3651

153. H. A. Jahn and E. Teller   Proc. Roy. Soc.   1937, A161, 220

154. J. D. W. van Voorst and P. Hemmerich   J. Chem. Phys.   1966, 45, 3914

155. J. M. Spaeth   Z. Physik   1966, 192, 107

156. H. Rabin and C. C. Klick   Phys. Rev.   1960 117 1005

157. A. J. Dekker   "Solid State Physics"   MacMillan London 1963

BIBLIOGRAPHY

Electron Spin Resonance

"Paramagnetic Resonance", G. E. Pake, W. A. Benjamin, New York, 1962

"Paramagnetic Resonance in Solids", W. Low, Solid State Phys. Supp. 2
Academic Press, New York, 1962

"Principles of Magnetic Resonance", C. P. Slichter, Harper and Row,
New York, 1963

"The Structure of Inorganic Radicals", P. W. Atkins and M. C. R. Symons,
Elsevier, Amsterdam, 1967

"Principles of Magnetic Resonance", A. Carrington and A. D. McLachlan,
Harper and Row, New York, 1967

B. Bleaney and K. W. H. Stevens, Repts Progress of Phys. 1953, 16, 108

K. D. Bowers and J. Owen, Repts Progress of Phys. 1955, 18, 304

A. Carrington and H. C. Longuet-Higgins, Q. Rev. 1960, 14, 427

A. Carrington, Q. Rev. 1963, 17 67

M. C. R. Symons, Advances in Phys. Org. Chem. 1963, 1 284

Infra-red

"Molecular Vibrations" E. B. Wilson, J. P. Decius and P. C. Cross
McGraw Hill London 1955

"Molecular Spectra and Molecular Structure II" G. Herzberg, D. van
Nostrand New York, 1945

Colour Centres

"Colour Centres in Solids", J. H. Schulman and W. D. Compton,
Pergamon, London, 1963

B. S. Gourary and F. J. Adrian, Solid State Phys. 1960, 10, 127